universität wien

MASTERARBEIT /MASTER'S THESIS

Titel der Masterarbeit / Title of the Master's Thesis

Disease Modeling in Cerebral Organoids

verfasst von / submitted by

Daniel Reumann, Bsc

angestrebter akademischer Grad / in partial fulfilment of the requirements for the degree of

Master of Science (MSc)

Wien, 2017 / Vienna 2017

Studienkennzahl lt. Studienblatt / degree programme code as it appears on the student record sheet:	A 066 834
Studienrichtung lt. Studienblatt / degree programme as it appears on the student record sheet:	Molekulare Biologie/ Molecular Biology
Betreut von / Supervisor:	Prof. Dr. Jürgen Knoblich

Disease Modeling in Cerebral Organoids

By

Daniel Reumann

Table of Contents

Abstract German

Viele neurologische Erkrankungen können mit aktuellen *in vitro* und *in vivo* Modellen nicht zufriedenstellend beschrieben werden, da entweder die komplexe 3D-Struktur eines Organs, oder der menschliche genetische Hintergrund nicht vorhanden sind. In dieser Arbeit werden krankheitsrelevante Mechanismen in zerebralen Organoiden beschrieben, dreidimensionale gehirnähnliche *in vitro*-Gewebe, die in zukünftigen Studien bei der Forschung an neurologischen Erkrankungen helfen können. Wir fokussieren uns auf die entwicklungsbiologischen Aspekte der Migration von Interneuronen und der Neuralrohrfaltung, bei denen zerebrale Organoide einen Vorteil gegenüber anderen Modellsystemen haben können. Außerdem wird die Entwicklung einer skalierbaren Plattform für das Wachstum von zerebralen Organoiden präsentiert.

Neocorticale Interneurone haben eine wichtige regulatorische Funktion, da sie das inhibitorische Potential im Gehirn modellieren. Kommt es zu einer Beeinträchtigung von bestimmten Interneuronen-Subtypen, kann dies zu der Entwicklung von neurologischen Erkrankungen wie Schizophrenie und Epilepsie führen. Während der Entwicklung des Neocortex haben Interneurone eine komplexe Entwicklung, da sie von ihrem Entstehungsort im ventralen Prosencephalon tangential über lange Strecken migrieren, bevor sie sich im dorsalen Prosencephalon in neuronale Schaltkreise integrieren. Durch die Fusion von zwei unterschiedlich differenzierten zerebralen Organoiden, die das ventrale und das dorsale Prosencephalon präsentieren, konnten wir eine ventral-dorsale Achse in zerebralen Organoiden darstellen, an der Interneuronen von dem ventralen in den dorsalen Bereich migrieren. Mithilfe von Immunfärbungen konnten verschiedene Interneuron-Subtypen nachgewiesen werden, welche typische Migrationseigenschaften zeigten.
Dieses Interneuronen-Modell kann dazu benutzt werden, krankheitsrelevante Aspekte bei der Entstehung, der Migration und der Integration von Interneuronen zu untersuchen. Außerdem können Drug Screens für potentielle therapeutische Substanzen ausgeführt werden.

In einem zweiten Projekt wurden die Elemente der Neurulation und des Neuralrohrs in neuronalen Rosetten von zerebralen Organoiden untersucht. Fehlbildungen des Neuralrohrs können zu tödlichen oder stark beeinträchtigenden Effekten auf den entstehenden Embryo führen. Allerdings gibt es signifikante Unterschiede in der Faltung des Neuralrohrs in menschlichen Embryos im Vergleich zu den meisten eingesetzten Modellsystemen. Darum wäre ein Modellsystem mit menschlichem genetischem Hintergrund von Interesse. Wir analysieren Ähnlichkeiten der Entwicklung des Neuronalrohrs zwischen zerebralen Organoiden und der Neuralrohrentwicklung. Wir konnten zeigen, dass die Zellen der frühen Entwicklung von neuronalen Rosetten in zerebralen von ähnlicher Identität sind wie das Neuroepithelium. Außerdem präsentieren wir zwei modifizierte zerebrale Organoid-Protokolle, die die Beobachtung von a) früh entwickelnden, struktur-stabilen neuronalen Rosetten, und

b) faltungsähnlichen Strukturen erlaubt. Wir schlussfolgern aus diesen Ergebnissen, dass man in zerebralen Organoiden einige, aber nicht alle Elemente eines Neuralrohrs beobachten kann.

Zuletzt werden die ersten Entwicklungsschritte eines Projektes diskutiert, welches Upscaling des zerebralen Organoid-Protokolls erlauben soll. Das aktuelle Protokoll erfordert einen hohen Arbeitsaufwand, weswegen ein vereinfachtes Protokoll auf einer all-in-one Plattform von großem Nutzen wäre. In dieser Arbeit präsentieren wir Ergebnisse die zeigen, dass das Wachstum der initialen Entwicklungsschritte von zerebralen Organoiden auf diesen Plattformen bereits möglich ist.
Wir hoffen, dass diese Plattform in späteren Entwicklungsschritten zu einem reduzierten Arbeitsaufwand und zur automatisierten Produktion von zerebralen Organoiden führen wird.

Abstract English

Using current *in vitro* 2D and *in vivo* systems, many human neurological diseases cannot be investigated in a satisfactory level, as either the complex 3D structure or the human genetic background are missing. In this work, we study two disease-relevant developmental aspects in cerebral organoids which could address some of these limitations. Additionally, we present an approach to upscale cerebral organoid growth, which could help in large scale-screens.

Forebrain interneurons have a major function in the human brain as the main inhibitory source for excitatory neurons and impairments of interneuron function are strongly associated with psychiatric diseases such as Epilepsy and Schizophrenia. One aspect of forebrain interneuron impairment is their complex emergence during human brain development and their long-distance migration from ventral into dorsal forebrain, which may be impaired in the named neurological disorders. Using cerebral organoids, we tried a novel approach and fused 2 distinct brain region organoids, depicting the ventral and the dorsal forebrain, together in one organoid "fusion" to generate a ventral-dorsal axis. We could observe robust and targeted migration of interneurons from the ventral into the dorsal cerebral tissue and further characterized multiple different interneuron subtypes in our model. With this interneuron migration assay, disease relevant studies of the emergence, migration and integration of interneurons in early human brain development could be addressed in future studies, and drug screens could be applied for testing potential therapeutic compounds against neurological diseases.

We also investigated whether cerebral organoids can be used to study the neural tube and neural tube closure. Neural tube closure defects can have severe to even fatal consequences on developing embryos and neural tube closure in humans and mice differs significantly, thus a human model system could be useful in understanding neural tube closure defects. We investigated several components of neural tube, from cell identity to morphological characterizations, and describe modified cerebral organoid protocols where we could observe a) the emergence of temporally stable neural rosettes in

early embryoid body (EB) formation and b) could observe a folding event of neural rosettes in cerebral organoids. We conclude that these experiments show the usability of cerebral organoids for the analysis of neural tube elements in cerebral organoids.

We also discuss the initial steps of a project which addresses the upscaling of the cerebral organoid method. The organoid method is labor intensive, so a simplified protocol with the potential of automatization would help tremendously in using the cerebral organoids in large scales. We currently engineer an all-in-one platform for cerebral organoid growth which targets the initial development of cerebral organoids. As intermediate results, we present a simplified generation step of EB for cerebral organoid growth. We hope that the design of this platform will help in the future to make the cerebral organoid protocol less time-consuming and allow upscaling as well as automatization of the growth of cerebral organoids.

Publication Statement

The content of chapter one is part of the publication “Fused cerebral organoids model interactions between brain regions” in Nature Methods (Bagley et al. 2017). Content of chapter one is therefore congruent with the original publication and figures where the author was contributing were adapted from this publication.

Introduction

The early developing human neocortex

Around day 17 post conception in humans, the developing human brain consists of a small sheet of pseudostratified, neuroepithelial cells (Bear et al. 2007). This neural plate, which emerges out of parts of the outer of the three germ layers, the ectoderm, is of epithelial identity (Figure 1A). For the process of neural tube formation, the neural plate starts to invaginate, and forms a neural groove (Figure 1A). The neural groove will start to close until the neural tube forms- a structure, which will give rise to the central nervous system. Notably, the neural tube consists of neuroepithelia with a lumen on the apical inside of the tube (Figure 1B). With the event of neurulation, the very early steps of the human brain development are set (Bear et al. 2007). The dorso-ventral and the rostro-caudal (=anterior-posterior in early development) axis are determined and a temporally and spatially varying composition of morphogenic signaling factors set the further fate of the neural stem cells in the neural tube (ibid., 2007). Initially, the anterior-posterior axis of the neural tube is determined (Harland & Gerhart 1997; Hikasa & Sokol 2017). Anterior-posterior axis segmentation is defined by a broad range of patterning factors and morphogens differ strongly over distance and time.

The posterior/caudal regions of the neural tube will form the spinal cord, the rostral end forms the brain. Dorsal-ventral (DV) axis patterning of the neural tube is regulated by a gradient of three main signaling molecule classes (Le Dréau & Martí 2012). First, Wnt and BMP families are produced from the roof plate and overlying ectoderm and pattern spatially close cells of the neural tube towards dorsal fate (Figure 1B) (Dennis & Bradshaw 2011; Le Dréau & Martí 2012). In contrast, the notochord, which lies ventral of the neural tube, will produce sonic hedgehog (SHH), which creates a ventralizing gradient onto the neural tube (Le Dréau & Martí 2012).

The rostral neural tube at day 28 post conception consists of the three primary brain vesicles; the prosencephalon, the mesencephalon, and the rhombencephalon (Figure 1C) (Bear et al. 2007; Brady et al. 2012). These 3 vesicles develop further, and on day 42 two additional vesicles can be observed: the prosencephalon (forebrain) splits into telencephalon and diencephalon, and the rhombencephalon undergoes a division into metencephalon and myelencephalon (ibid, 2007, ibid, 2012). While the more caudal regions of these structures are phylogenetically relatively old, the expanding prosencephalon is a newer invention of evolution and its complexity increased tremendously over a comparable short time span (Florio & Huttner 2014a). The telencephalon develops into the biggest structure of our nervous system: the two hemispheres of the cerebrum (Figure 1C, D) (Bear et al. 2007; Brady et al. 2012).

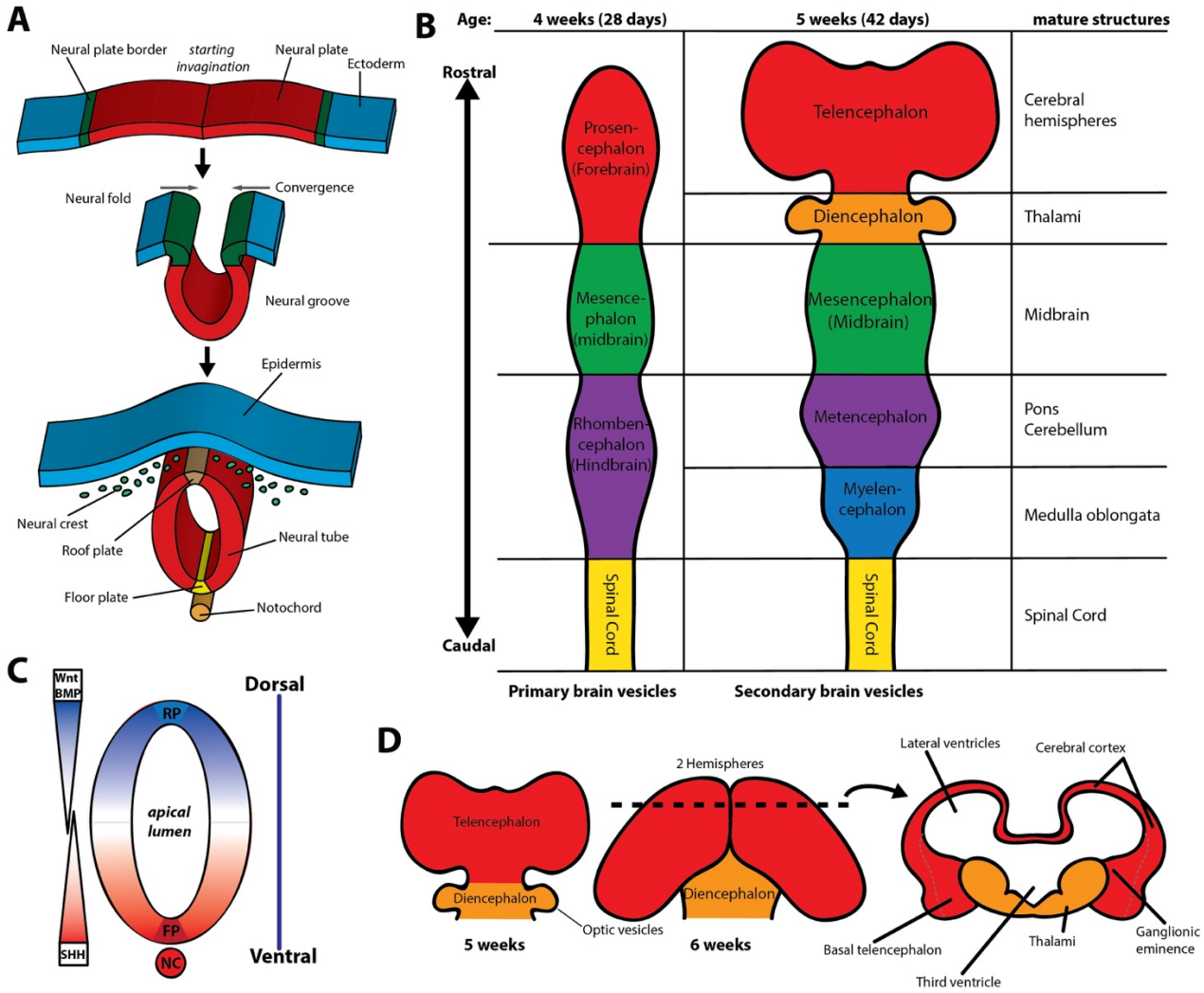

Figure 1: The early steps of corticogenesis
(A) Primary neurulation in humans. The neural plate invaginates to a neural groove, which subsequently will close completely and forms the neural tube. Dorso-ventral signaling centers are the roof plate, the floor plate and the notochord. Neural crest cells emerge in the dorsal area from the cells of the neural plate border. (B) Rostral ventral-dorsal patterning of the neural tube. RP=roof plate, FP=Floor plate, NC=Notochord. Dorsalizing Wnt and BMP gradient are indicated in blue, ventralizing SHH signaling is indicated in red. Note that Wnt also has an anteriorizing patterning effect. (C) Early CNS development (Rostro-caudal view) of human primary and secondary brain vesicles and their corresponding mature CNS structures. (D) Development of the forebrain (dorso-ventral view) from 5 to 6 weeks including a coronal section schematic on week 6.

The tremendous expansion of the of the mammalian prosencephalon is mediated by the production of transient amplifying neural stem cells which, by symmetric and asymmetric division, enlarge the pool of radial glia on the one hand, and the pool of neurons on the other hand (Figure 2A, B) (Florio & Huttner 2014a). Initially, neuroepithelial cells (NEC) develop from ectoderm and form the neural plate (Fernández et al. 2016). NECs further develop into radial glia cells, which give rise to the developing cortex (Florio & Huttner 2014a). Initial radial glia, also termed apical radial glia (aRG) as they are connected to the apical side of the structure (the lumen), are initially having processes from the

ventricle (the apical side) to the cell body (ibid, 2014). The cell body sits in the ventricular zone, and from there another process goes into the marginal zone (MZ), which is the basal ending of the developing human brain (Figure 2A) (Florio & Huttner 2014a; Fernández et al. 2016). Along these processes, early born neurons migrate through the subventricular zone into the developing cortical plate (Tamamaki 2002; Florio & Huttner 2014a). On arrival, they integrate and form the remaining cortical layers 4-6 in an inside-out manner (Rakic 2009; Mota & Herculano-Houzel 2012; Sun & Hevner 2014). During evolution to a more complex and expanded neocortex, e.g. in humans, the basic process of neuronal differentiation got amplified through several steps. It is very well described now in humans, that the initial population of aRG cells can give rise to so called basal radial glia (bRG), also called outer radial glia (oRG) cells, which have the same symmetric and asymmetric division capacities as aRG cells and further amplify the pool of newborn neurons (Sun & Hevner 2014; Fernández et al. 2016). Additionally, intermediate progenitors (IP) are produced, which are located in the subventricular zone and again can divide symmetrically or asymmetrically (Sun & Hevner 2014). New studies also show different pools of IPs, namely the short radial IPs in the ventricular zone and the multipolar IPs in the subventricular zone (Kowalczyk *et al.*, 2009; Florio and Huttner, 2014). The short radial IPs are in contact with the apical surface, but do not show projections to the MZ, whereas the multipolar IPs are located in the SVZ and do not have any organized directional projections. Together, the aRG, bRG, aIP and bIP form a, compared to the aRG based neural expansion only, tremendously increased population of amplifying neuron progenitors and are thought to be one of the key reasons for the expanded human neocortex (Figure 2B) (Sun & Hevner 2014; Fernández et al. 2016).

The locally emerging neurons in the human forebrain are mostly of excitatory nature and integrate through a short radial migration in the developing cortical layers (Marín et al. 2010). During the development of the human forebrain, a big subset of cells is not locally emerging through radial migration, but through long-distance, tangential migration (Marín & Rubenstein 2001; Britanova et al. 2006; Sun et al. 2015; Barber & Pierani 2015). These tangentially migrating neurons are of multiple sources, such as cortical projection neurons (Britanova et al. 2006), Cajal Retzius cells which create a Reelin scaffold for radial migration in the MZ (Barber & Pierani 2015) and a larger population of interneurons (Marín & Rubenstein 2001). These interneurons represent 20-30% of the neurons of the human brain and are regulatory, usually locally active neurons (Markram et al. 2004).

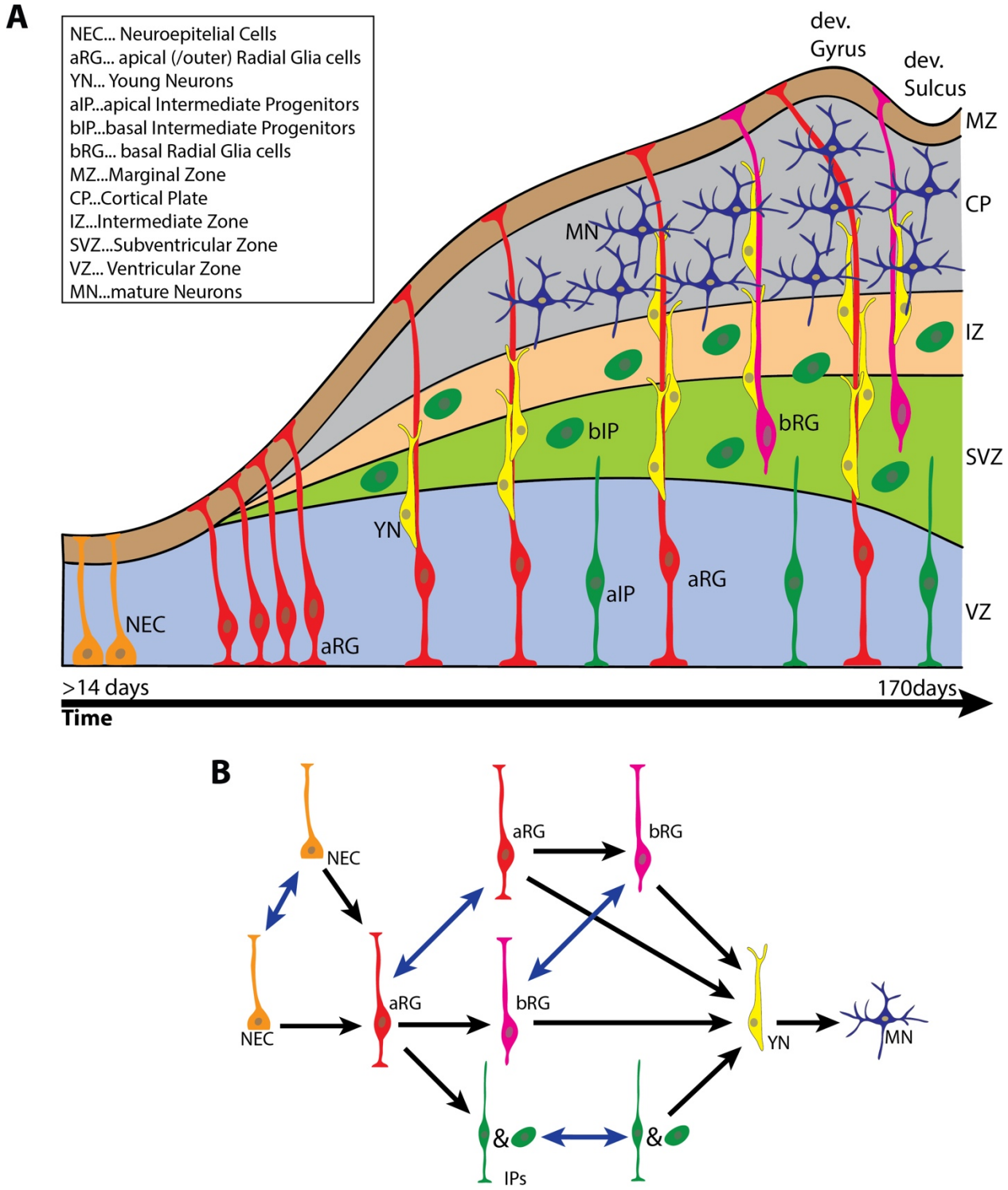

Figure 2: The expanding human brain on a cellular level.
A) Amplification schematic of the developing human cortex. Neuroepithelial stem cells give rise to apical radial glia cells. These proliferate in symmetrical and asymmetric manner, producing more aRG cells and young, early born neurons. Additionally, the neuron producing capacities of the developing brain can get amplified by the production of basal radial glia cells and apical& basal intermediate progenitors, which have symmetric and asymmetric division capacities as well. Together, these four sources of young born neurons generate an increasing pool of mature neurons. In later development, folding of the human developing brain layers occurs, giving rise to Gyrus and Sulcus structures of the whole cortical layer from VZ to MZ. B) Schematic of different progenitor populations and their abilities of symmetric and asymmetric cell divisions for further expansion of the neocortex.

Interneurons in the CNS

Inhibitory signaling in the human CNS is largely mediated by the activity of locally active, GABAergic neurons, so called interneurons (Gelman et al. 2012; Markram et al. 2004; Le Magueresse & Monyer 2013). Interneurons are a diverse class of neurons which generally regulates the firing capacities of target neurons and can almost solely be found in the central nervous system (Bear et al. 2007). Target neurons can be both of excitatory and inhibitory nature, thus allowing complex regulatory circuits in the human brain (Woodruff & Yuste 2008; Kepecs & Fishell 2014). Generally, the function of interneurons is the balancing of excitatory signaling (excitatory/inhibitory balance) for controlled communication in the brain (Haider et al. 2006; Turrigiano 2011). Interneurons usually sit in close proximity of their target neuron, however some cases of long distance projections of GABAergic cells has been observed as well (Brown et al. 2012; Wu et al. 2015). Axons of interneurons in the forebrain usually arborize within a cortical column, however they can also laterally interact with proximate columns (Markram et al. 2004).

Emergence

Forebrain interneurons have an elaborate way of emergence, as they are not produced in proximal distance to their target destination, thus making it necessary for interneuron progenitors to migrate to their target destination over a far distance. Interneuron progenitors are emerging in the proliferative ventricular zone (VZ) of the ventral telencephalon in the so called ganglionic eminences (GE), which emerge from the ventral regions of the rostral tube (Figure 3A). In the GEs, they undergo a first maturation step and subsequently start to tangentially migrate either through the lateral GE (LGE) subventricular zone (SVZ) or the marginal zone (MZ) into the developing dorsal forebrain (Figure 4 B, C) (Kelsom & Lu 2013; Sultan et al. 2013).

The GEs can be split up in three distinct regions which contribute to interneuron emergence: the caudal, medial and lateral ganglionic eminences (CGE, MGE and LGE) (Figure 3B). The MGE and CGE are contributing the highest quantities of interneurons which populate the forebrain (Wonders & Anderson 2006). The third region of the GE, the lateral ganglionic eminence (LGE), was often reported to be not participating to the number of interneurons in the neocortex, but is responsible for interneurons which will populate the striatum and olfactory bulb (Sussel et al. 1999; Stenman et al. 2003; Lledo et al. 2008). However, experimentally this was so far hard to screen, as the MGE- and CGE-derived interneurons will pass the LGE during migration in the forebrain and thus a contribution of the LGE to the cortical interneuron pool may still be possible (Rudy et al. 2010; Sultan et al. 2013). Additionally, LGE has no defined border to the CGE and MGE and shares common properties with the CGE (Rudy

et al. 2010; Sultan et al. 2013). Thus, the dorsal LGE and dorsal CGE are often combined as a discrete source of neocortical interneurons (Ma et al. 2013).

After production through asymmetrical cell division, MGE-derived interneuron progenitors first disperse laterally and then migrate tangentially throughout the cortex (Sultan et al. 2013). In contrast, CGE-derived interneuron progenitors will migrate tangentially through caudal migratory streams (Yozu et al. 2008). Depending on the timepoint of migration, interneurons in rodents migrate through the preplate (E12.5) and subsequently through the developing intermediate zone (IZ) (Figure 4C). Later, two main migration streams can be observed: one in the marginal zone (MZ) and one in the lower intermediate zone (IZ) and subventricular zone (SVZ) (Figure 4C), with some reports on interneuron migration in the subplate as well (Kelsom & Lu 2013). After migrating tangentially, the populations of CGE and MGE-derived interneurons will start radial migration into the developing human neocortex and integrate in the cortical circuitry (Figure 4C) (Marín & Rubenstein 2001; Guo & Anton 2014).

Immunolabeling of interneuron subtype markers Calretinin, Calbindin and GABA showed that from about gestation week 5 in humans, first interneurons could be found (Zecevic et al. 2012). While the MGE and its pre-/initial migrating interneurons broadly express the transcription factors Nkx2.1 and Dlx1/2/5/6, these MGE origin dependent transcription factors become deactivated over migration and other transcription factors like Lhx6 and Sox6 become upregulated, which regulate cortical integration of interneurons (Gelman et al. 2012; Kelsom & Lu 2013; Kessaris et al. 2014). The CGE expresses a divergent set of markers. Dlx1/2 is expressed as in the MGE, but Sox6 and Lhx6 seem not to be activated in CGE-derived interneurons (ibid, 2012, ibid, 2013). However, COUP-TFI and COUP-TFII, also known as NR2F1 and NR2F2, get highly activated and can be used for identifying migrating, CGE-derived interneurons. Additionally, Gsx1 and Gsx2 seem to be required for the specification of the LGE and CGE (Gelman et al. 2012).

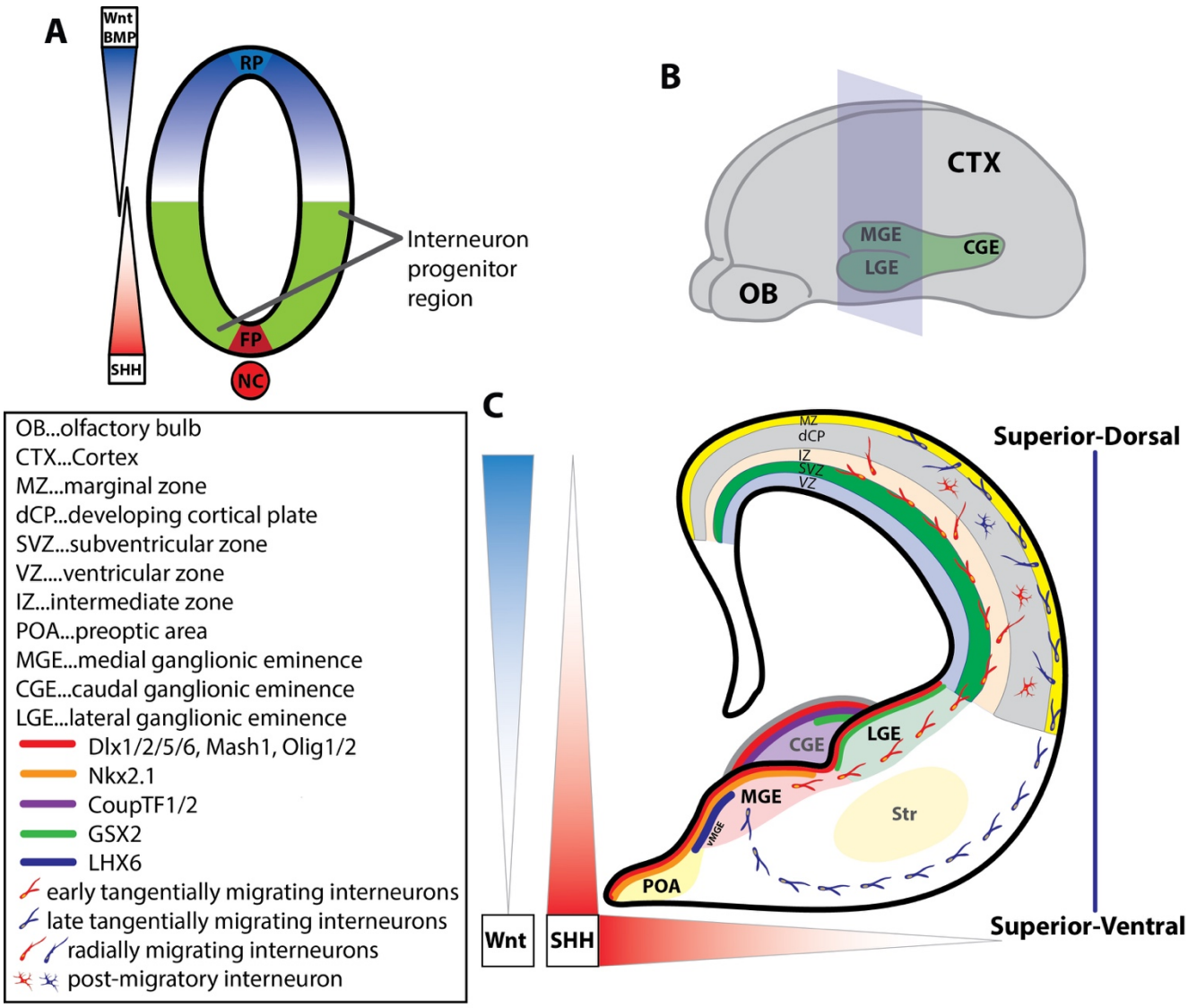

Figure 3: Emergence and migration routes of interneurons in the developing human telencephalon
A) Patterning of the anterior neural tube through Wnt, BMP and SHH induces a dorsal-ventral gradient with interneurons emerging from the ventral areas. B) Schematic of a coronal cut of a developing human brain, indicating the ventral derived ganglionic eminences. C) Model of a coronal section of a developing forebrain. Different GEs can be distinguished using alternative marker expression. Interneurons emerge in the MGE and CGE/LGE and start tangential migration through the SVZ and MZ. At their target destination, they start radial migration into the developing cortical plate (dCP) (Guo & Anton 2014; Wonders & Anderson 2006; Sultan et al. 2013).

A broad range of chemoattractants and chemorepellents may be used for the initial guidance of interneurons into the cortical plate (CP). Interneurons which express neurophilins and thus are determined to migrate into the CP, get strongly repelled by a family of ligands called semaphorins. Exemplarily, Sema3A and 3F are expressed in the striatal mantle, prohibiting migration of interneurons which are not determined as striatum interneurons into the striatal area (Marín & Rubenstein 2001; Flames et al. 2004). Other early chemorepellents are Slit1, which is expressed in the VZ and SVZ of the GEs and in the POA and repels interneurons from these regions, and Ephrins. Together, both Slit1 and Ephrins repel post-mitotic, matured interneurons which develop sensitivity to its repellent function; thus Slit1 and Ephrins seem to be initial driving forces for interneurons to start migration (Kelsom & Lu 2013).

While the initial start of tangential migration is strongly dependent on proper function of chemorepellents on maturing interneurons, the later tangential migration is more defined through a concert of chemoattractants in the cortical plate (ibid., 2013). Starting with the LGE, which is the permissive area of many MGE and CGE-derived interneurons, it was found that a membrane bound form of Neuregulin-1 (Nrg1), Nrg1-CRD, is highly expressed throughout the LGE. This creates a permissive corridor for MGE-derived interneurons which express the Nrg1-binding receptors ErbB-4 and ErbB-3 (Flames et al. 2004). This permissive corridor is thought to create a window for migrating interneurons to enter the cortex. Additionally, a secreted version of Nrg1, Nrg1-Ig, is expressed in the CP and acts as a diffusible chemoattractant to MGE-derived interneurons (ibid., 2004), hence attracting them to the pallium (dorsal telencephalon). Other chemoattractants from the pallium are chemokines such as CXCL12 (also known as SDF-1), which attracts interneurons expressing the receptors CXCR4 and CXCR7. CXCL12 mainly targets MGE-derived interneurons in rodents and is mainly expressed in the SVZ and MZ. CXCL12 is known to mediate the switch from tangential to radial migration, and a knockout of CXCL12 was reported to lead to the accumulation of interneurons in the ventral pallium (Sultan et al. 2013). Additionally to secreted chemoattractants, neural cell adhesion molecules like TAG-1, expressed in axons of the developing corticofugal system, may be necessary for migration of a subpopulation of interneurons (Denaxa et al. 2001).

Another important integration mechanism is the ability of migrating interneurons to sense GABA and Glutamate levels (Bartolini et al. 2013). Higher levels of both GABA and Glutamate induce depolarization of the membrane of migrating interneurons and stimulate the production of calcium transients, which enhances neural migration. It was also reported that using GABA and Glutamate sensing, migrating interneurons can predict the onset of synaptogenesis and thus allow controlled migration behavior (ibid, 2013). When maturing, the effects of GABA on interneurons changes from depolarization to hyperpolarization- a process known as GABA switch (Bortone & Polleux 2009;

Bartolini et al. 2013). By hyperpolarizing the membrane, GABA becomes a stop migration signal for migratory interneurons (ibid., 2009, ibid. 2013).

However, interneuron migration is still a field of heavy research and several mechanisms of migration may still be unknown. For instance, migration mechanisms of interneurons from the CGE are barely unraveled. Furthermore, it is thought that dorsal radial glia cells can also give rise to interneurons of the human brain (Yu & Zecevic 2011).

Diversity

Forebrain interneurons are a heterogeneous, complex group of neurons and it is estimated that more than 20 different subtypes of interneurons may exist in the human neocortex (Kelsom & Lu 2013). Interneuron subtypes have been characterized by their morphological properties (including axon targeting) first, followed by marker expression, electrophysiological properties and broader connectome analysis (Markram et al. 2004; Kessaris et al. 2014; Rudy et al. 2010; Kelsom & Lu 2013). However, as overlaps in different markers can frequently be observed, it is under discussion whether interneuron subtypes should be seen as precisely defined subgroups or can be seen as a continuum between different flavors which may be dependent on different demands of inhibitory potential (Sultan et al. 2013).

Briefly addressing the morphological properties, the most occurring interneurons have basket cell, chandelier cell or bi-tufted cell morphology, with deviations into double bouquet and bipolar shapes (Figure 3A) (Markram et al. 2004). Interneurons were also characterized by subtype-dependent markers and their intrinsic firing properties, which on the one hand complemented the morphological specifications, but also broadly enlarged the pool of subtypes (Kepecs & Fishell 2014). For *in vitro* assays, marker expression is the most frequently used characterization approach, as the *in vitro* existing morphology of interneurons as well as electrophysiological properties can be diverging from *in vitro*. Almost all neocortical interneurons express either the markers parvalbumin (PV), somatostatin (SOM) or 5HT3aR (Figure 4A) (Rudy et al. 2010). Parvalbumin is a Ca^{2+} binding protein and is expressed in approximately 40% of all interneurons, the neuropeptide SST is expressed in approximately 30% of interneurons, and the ionotropic serotonin receptor 5HT3aR is expressed in the remaining 30% (Lee et al. 2010; Rudy et al. 2010). By analyzing marker expression, the interneuron subtypes can partially be traced back to their morphology (Figure 4B).

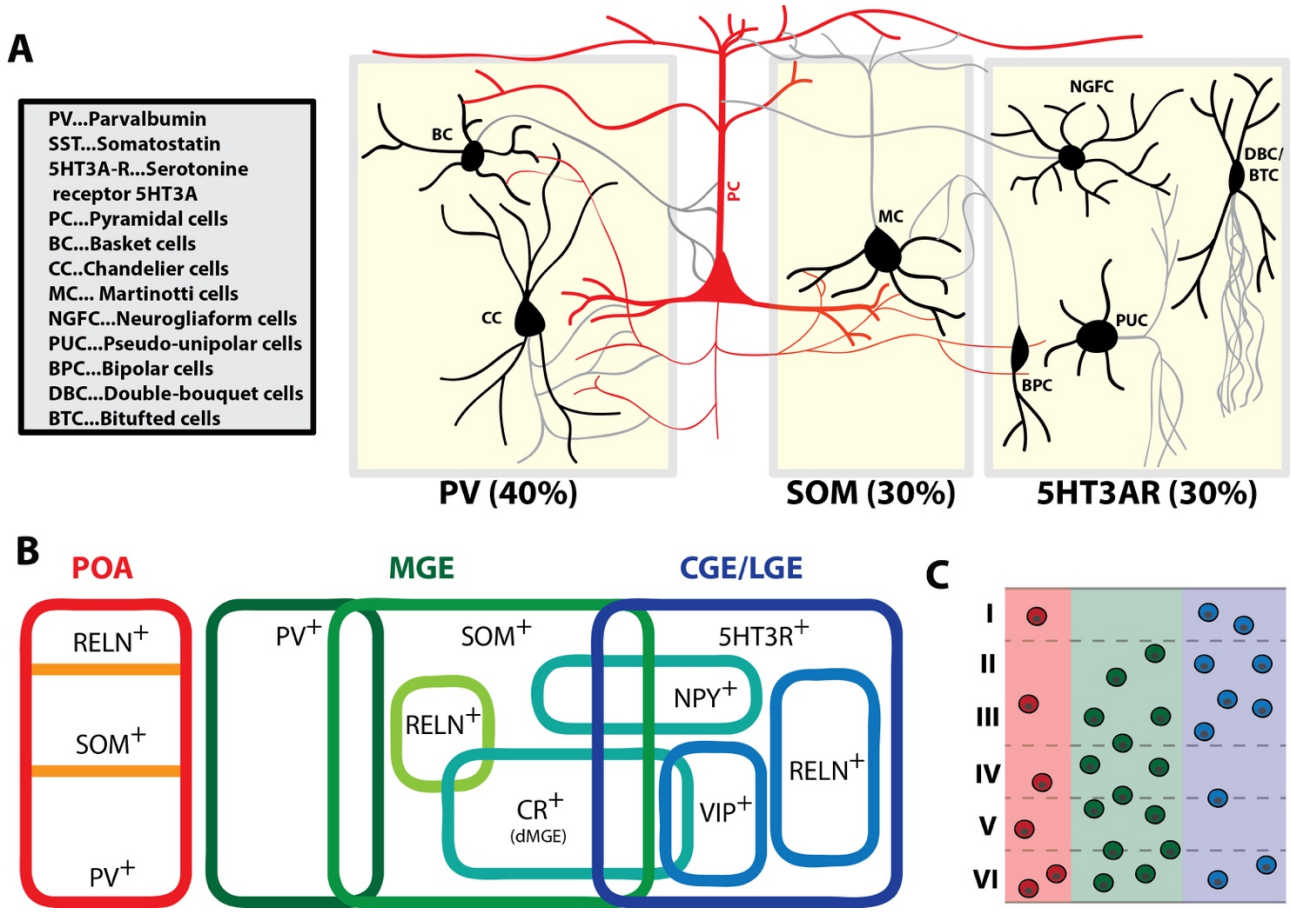

Figure 4: Interneuron subtypes according to morphology, marker expression and cortical distribution
A) PV, SOM and 5HT3AR depict almost all interneuron subtypes in the neocortex and subdivide interneurons in different groups. Morphological characteristics can strongly be correlated to 3 main interneuron markers (Sultan et al. 2013). Basket cells can be further subdivided in large basket cells, nest basket cells and small basket cells, which vary in morphology and axon targeting. B: Interneurons express source-dependent markers. Dependent on the different ganglionic eminences (MGE, CGE) origin of interneurons, interneurons will express GE-dependent markers. Combined information from (Wonders & Anderson 2006; Kessaris et al. 2014; Cauli et al. 2014). C: The distribution of interneurons in the cortical layers is origin-dependent and thus also subtype-dependent.

The three main subtypes of interneurons can be further divided in different classes which are derived from different origins of emergence, the MGE and the CGE, with the potentially contributing LGE (Figure (Figure 4B). Additionally, a small subset of interneurons may be derived from the preoptic area (POA) (Figure 4B) (Wonders & Anderson 2006). Generally, PV^+ interneurons are derived from the MGE, together with a subpopulation of SOM^+ which may also express Calretinin (CR), neuropeptide Y (NPY) or Reelin (Figure 3B). It was also found that a subset of PV^+ interneurons may be positive for SOM (Rudy et al. 2010). CGE-derived interneuron subtypes express Reelin (RELN), vasoactive intestinal peptide (VIP), Calretinin (CR), or SOM, whereas POA derived interneurons express RELN, SOM and PV (Wonders & Anderson 2006; Kessaris et al. 2014; Cauli et al. 2014).

Interestingly, the origin of interneurons is also determining its distribution in the cortical layers (Figure 3C) (Kessaris et al. 2014). Whereas MGE derived interneurons can be found in higher numbers in the earlier produced layers, CGE interneurons can be found in increased numbers in the more superficial layers (Miyoshi et al. 2010; Kessaris et al. 2014). Thus, while it is thought that MGE-derived interneurons populate the cortical layers in an inside-out manner, the CGE seems to preferentially populate the superficial layers. This is consistent with the observation of deviating migration timings in rodents, where MGE derived interneurons start to migrate earlier than CGE derived interneurons (E9.5 vs. E12.5) (Miyoshi et al. 2007; Miyoshi et al. 2010). Additionally, several subtypes of interneurons are strictly restricted to certain layers: Martinotti cells can particularly be found in layers V and VI and are almost absent in layer IV, and few can be found in layer II and III (Bartolini et al. 2013). Contrary, PV+ interneurons can only be found in layer 2-6 and chandelier cells are strongly correlated with layers II and V in rodents (Ibid, 2013). Thus, the laminar distribution of interneurons depicts a remarkable degree of organization, which suggests that its precise distribution has an important function in the brain.

Function

Interneurons regulate the global balance of excitatory signaling by modulating signaling propagation on a local level (Vogels & Abbott 2009). The decision of processing of a signal or blocking it is a complex process, however the executive unit for the inhibition of a signal is GABAergic interneuron signaling (Markram et al. 2004). Interneuron activity, and thus inhibitory levels, are regulated by a concert of self-regulation, regulation by encompassed excitatory (long-range and local) and inhibitory neurons, and neuromodulators (Kepecs & Fishell 2014). Initially, the principal understanding of interneurons was their role in the guidance of neuronal networks against runaway excitation (Douglas et al. 1995).

However, understanding of interneurons tremendously increased over time, and it recently has been stated that there are at least as many inhibitory circuit motifs as there are cell types "it has become clear that there are at least as many inhibitory circuit motifs as there are cell types" (Kepecs and Fishell, 2014, p322). An interesting example of collecting inhibitory capacities are VIP-expressing interneurons. VIP^+ interneurons collect long-range and local inputs as well as neuromodulatory inputs and process these information further on SST^+ and PV^+ interneurons, which then modulate excitatory capacities of pyramidal cells (ibid, 2014). Other examples are Basket cells, which target the dendrites of pyramidal neurons, whereas Chandelier cells normally target the axonal segments of pyramidal cells (see also Figure 3A). However, as impressively shown in (Kepecs & Fishell 2014), the connections of interneurons are of multidimensional diversity, thus neither marker expression, connectivity or intrinsic firing properties can give a distinct characterization of the remaining criteria of an interneuron.

While interneurons are essential for proper local inhibition, subgroups of interneurons also give rise to neuronal oscillations in the human brain. While PV^+ interneurons are reported to be stimulating in the gamma-frequency range (30-80hz), SST-interneurons are stimulating in the beta-frequency (15-30hz) (Buzsáki & Draguhn 2004).

Interneurons in diseases

The modulation and balance of excitatory/inhibitory signaling has essential functions for proper communication and data processing in the human brain, and imbalances in both excitatory and inhibitory firing or sensitivity towards this signaling can have detrimental effects (Marin 2012). Indeed, many subtypes of neuropsychiatric diseases are strongly correlated with the number and activity of interneurons in the human cortex (Marin 2012; Lewis et al. 2005; Olivetti & Noebels 2012; Selby et al. 2007; Seshadri et al. 2015). Dependent on affected interneuron subtype, brain area and type of impairment, the phenotype can be very similar even though the underlying mechanisms are quite different, or vice versa. In most cases, the regulatory capacity of excitatory signaling is impaired, leading to hyperexcitability in the corresponding cortical areas (Marin 2012). Corresponding to altered inhibitory levels, also a correlation between changes in neural oscillations and epilepsy (Zijlmans et al. 2012) and schizophrenia (Liddle et al. 2016; Hong et al. 2012) could be observed, which is another indicator for excitatory/inhibitory imbalance.

Interneurons are a target of extensive research, as many features of interneurons are still unknown and may be impaired in a broad range of diseases (Marin 2012). Additionally, the inhibitory system in humans may vary tremendously compared to the rodent system. For example, interneuron emergence and migration in humans seems to take place long after birth, which has so far not been reported to exist in rodents (Paredes et al. 2016). However, human studies are strongly restricted because of the lack of an *in vitro* model which encompasses the high complexity of the interneuron system and are mostly based on post mortem tissue analysis and brain section cultivation. Thus, no genetically modifiable system with human genetic background for interneuron analysis exists. In contrast, 2D differentiation approaches for receiving interneurons were developed, but are strongly limited in complexity compared to the system which is observable *in vivo* (Maroof et al. 2013; Nicholas et al. 2013; Liu et al. 2013).

Cerebral organoids

Organoids are defined as stem cell derived, 3D tissues which are often being characterized by a) containing more than one cell type of the organ they model, b) exhibiting organ specific functions and c) having a similar structural component as the organ they depict (Lancaster & Knoblich 2014). Besides the in this work used cerebral organoids, a broad range of emerging organoids, such as optic cup organoids, gut organoids, liver organoids and lung organoids exist, expanding the available tissues for research purposes further and further (Huch & Koo 2015; Clevers 2016).

Cerebral organoids are *in vitro* 3D brain-like structures derived from human embryonic stem cells (hESCs) or induced pluripotent stem cells (iPSCs) (Lancaster et al. 2013). They reassemble the early steps of human brain development and produce structures very similar to the ventricular zone, the inner and outer subventricular zone, intermediate zone and early cortical plate, containing early born $CTIP2^+$ and late born $SATB2^+$ neurons ((Bershteyn et al. 2017; Lancaster et al. 2013). Recent studies also indicate that the event of folding of the cortical plate in cerebral organoids may be within reach (Li et al. 2017).

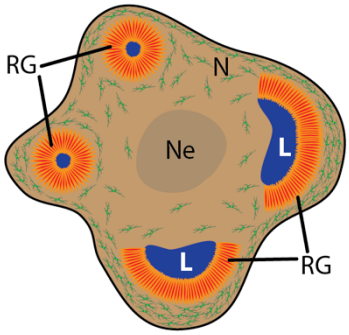

Schematic of a cerebral organoid.
RG…Radial glia neuronal rosettes
N…Neurons
L…Lumen
Ne…Necrotic/apoptotic core

Cerebral organoids can be cultured for up to one year and thus can be used particularly for questions targeting the early developmental steps of the human brain development (Lancaster & Knoblich 2014).
While many human diseases can be modeled appropriately in other model systems, the human brain has always been a restricted subject to study, as there is no corresponding model system available which would fulfill its high complexity and differentiation (Bershteyn et al. 2017; Kadoshima et al. 2014). Thus, studies investigating diseases or development of the human brain were restricted to other species, post mortem tissue and 2D cell culture (Busskamp et al. 2014). With cerebral organoids, it was first possible to observe human developing neurons in an *in vivo*-like, 3D environment in a more complex cellular environment, thus allowing modifiable, screenable systems which are more alike to the developing conditions in human embryos (Huch & Koo 2015).

Development of a cerebral organoid

The development of cerebral organoids is, on a cellular and transcriptomic level, relatively comparable to the early developmental steps of the human brain (Lancaster et al. 2013; Camp et al. 2015a). Generally, neural rosette structures form in the early steps of organoid formation (Lancaster et al. 2013). The initial formation of these rosettes in cerebral organoids is rather poorly described and characterized, however in later stages these rosettes show high similarities to human corticogenesis: They give rise to bigger rosette structures, consisting of apical radial glia (aRG) and its produced neurons

(comparable to Figure 2A, B), reassembling the early emerging deeper-layer neurons of the cortical plate (Lancaster et al. 2013; Kadoshima et al. 2014). So far, the production of apical radial glia cells ($PAX6^+$), intermediate progenitors ($TBR2^+$), basal radial glia ($HOPX^+$), early born neurons ($CTIP2^+$), late-born superficial layer neurons ($SATB2^+$) and interneurons have been reported to exist in forebrain cerebral organoids (Lancaster et al. 2013; Bershteyn et al. 2017; Li et al. 2017; Kadoshima et al. 2014). However, by the continuous growth of the system, cells in the organoid core will turn necrotic or apoptotic (Lancaster et al. 2013), limiting the usability of the organoids to approximately 100 days so far. Outside neurons will proceed to exist, however the neural progenitor population will decrease over time. This can partially be avoided by cutting the organoid into smaller parts (Kadoshima et al. 2014), but a general solution to thicker 3D tissue development is still outstanding.

Through intrinsic differentiation, cerebral organoids can form many different tissues from the human brain, such as dorsal and ventral forebrain, hippocampus, choroid plexus, retina, and prefrontal lobe (Lancaster et al. 2013). However, multiple approaches exist using small molecules or patterning factors for targeted differentiation into cerebellum (Muguruma et al. 2015), choroid plexus, pallium (both Sakaguchi et al. 2015), midbrain (Jo et al. 2016; Qian et al. 2016), optic cup (Nakano et al. 2012) and hypothalamus (Qian et al. 2016). These patterning and growth factors, such as sonic hedgehog or retinoic acid, must be applied in a certain developmental window, as fate commitment in cells is occurring relatively time-sensitive. Thus, all above mentioned differentiation protocols use different windows and media compositions for achieving their goal, too late applied patterning factors may have no effect or the wrong effect, and a too early application may alter the output cells tremendously.

One current limitation of the cerebral organoids is the lack of nutrients and oxygen in the centers of the organoids, as well as further developmental stages due to the first named limitations. While some protocols include the cutting of the organoids once they reach a certain age (Kadoshima et al. 2014; Sakaguchi et al. 2015), alternative approaches work on the introduction of a vasculature into the organoid (“cerebrovascular organoid”) including micro pumps, thus allowing medium flux into the deeper tissues of an organoid (unpublished data, e.g.: Church 2017) or the study of more complex cellular interaction of different tissues.

The cerebral organoid method

The original protocol was published first published by Lancaster et al. 2013 and was routinely used for growing organoids in this thesis. However, for organoid improvements, several steps of the protocol have been targeted in the second chapter of this thesis, thus the protocol will be briefly discussed here. For further details, a comprehensive protocol can be found in the Material& Methods section of this thesis and in Madeline A Lancaster & Knoblich 2014.

Generally, cerebral organoids can be grown out of any pluripotent stem cell line, either hES or iPSC cells, which allows differentiation towards neuroectoderm. Routinely in our lab, H9 cells and an iPSC cell line were used for growth of cerebral organoids. Initially, 9000 cells are used for the formation of an EB in human embryonic stem cell (hES) medium in a low attachment 96well plate. The EBs are transferred to 24 well low attachment plates and to a neural induction (NI) medium on day 5-7 when the EBs reach a certain size of 500 to 600µm and fed every other day by the addition to the already existing medium. Alternatively, they can be kept in 96well plates with every day feedings (unpublished data). The EBs are then cultivated in neural induction (NI) medium until day 10-13, where they start to show a bright, stratified ring of neuroepithelia on the outside of the EB (Lancaster & Knoblich 2014). Subsequently, the EBs get embedded in Matrigel, an ECM-like environment, and are transferred to a 6cm or 10cm dish. After one feeding round, the dishes are kept on an orbital shaker for better nutrition supply and are fed every 3 days (6cm plates) to 7 days (10cm plates).

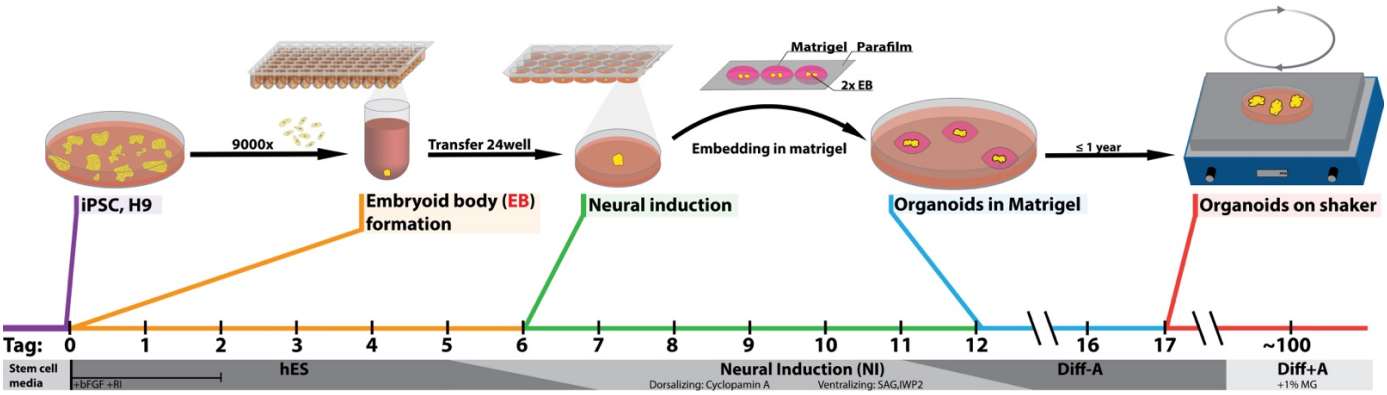

Figure 5: Cerebral organoid generation from iPSC and hES cells
iPSC or H9 derived EBs are grown in hES medium in low attachment 96well plates and then transferred on low attachment 24well plates with neural induction medium. On day 10-13, EBs are embedded into Matrigel and transferred on a 6cm or 10cm dish with differentiation medium. After one feeding, EBs are transferred on an orbital shaker.

Disease modeling in cerebral organoids

Cerebral organoids in general can be used for insights into early neural development, disease modeling of early emerging diseases and drug screenings (Clevers 2016; Huch & Koo 2015; Fatehullah et al. 2016; M A Lancaster & Knoblich 2014; Sasai 2013; Astashkina & Grainger 2014; Bershteyn et al. 2017; Li et al. 2017). As many of the early steps of cortical neurogenesis, from neural stem cells to early born mature neurons, are depicted in the organoids, the underlying differential mechanisms and available cells can be targets of scientific questions. Cerebral organoids have already been used in the research of fundamental mechanisms in, amongst others, Microcephaly (Lancaster et al. 2013), Zika virus infection (Qian et al. 2016), Lissencephaly (Bershteyn et al. 2017) and Macrocephaly (Li et al. 2017). Additionally, projects target early glioblastoma emergence in organoids (unpublished data), and the question of interneuron migration and diseases will be addressed in this work. Thus, more and more knowledge in early developmental impairments is generated through the usage of cerebral organoids.

Bioengineering cerebral organoids

Another important part in the organoid field is the further development in two aspects of the protocol. With all its complexity, the cerebral organoids still lack later developmental timepoints of brain development, and a proper development of all cortical layers has not been observed yet (Lancaster et al. 2013; Kadoshima et al. 2014). Additionally, all published organoid methods have in common, that they are very time consuming and upscaling is hard to achieve. Addressing these two questions will be a challenge in the future of the organoids and will very likely be solved using bioengineering scaffolds, which could be tremendously useful for upscaling and genesis of cerebral organoids. First attempts in this direction were the generation of microvessels for upscaled EB formation (Sato et al. 2016) and the rising field of chemically defined hydrogels as Matrigel alternatives (Lindborg et al. 2016; Gjorevski et al. 2016). However, these strategies so far have not been addressed for cerebral organoids but other organoid systems and are still limited in usability so far.

Aim of this work

The aim of this work is to use cerebral organoids to study interneuron migration related diseases in a human genetic background. We want to use these organoids for the recreation of interneuron emergence regions, the ganglionic eminences, and their targets of tangential migration, the dorsal forebrain. With this system, we want to observe migratory interneurons and characterize the model system, which will be described in chapter I.

Additionally, the elements of neural tube (formation) in cerebral organoids of the Lancaster et al. 2013 protocol have been studied to generate an overview which elements of neural tube closure we can observe in cerebral organoids. The results of this can be found in chapter II.

Furthermore, a project which uses hydrogel plates for further upscaling and easier handling of the cerebral organoids will be discussed briefly in chapter III.

Chapter I: Development of an interneuron migration assay

Author contributions

I collaborated closely with Dr. Joshua Bagley for the development of the fusion assay and its subsequent characterization. The initial idea of the project and the patterning of organoids (including Figure 6) was worked out by Dr. Bagley. The author participated in the initial fusion attempts and grew the labeled fused organoids used in the published article, screened them for migration of cells and did the IHC characterization as well as parts of the quantifications for migratory cells. Dr. Shan Bian and Julie Lévi-Strauss helped with the IHC quantifications.

Introduction

Human GABAergic forebrain interneurons have crucial function in the developing brain, however their functional description and way of emergence are still under investigation, as there may be intricate differences compared to model systems like rodents, where interneuron migration is well described. One of the limiting steps in studying emerging human interneurons is the low availability of research material: for studying alive human interneurons, researchers are dependent on fetal brain slice cultures (Paredes et al. 2016). Additionally, fixed tissue can be used for characterizations, but is further limited in usability as no live cells can be studied. Furthermore, both sources have an additional limitation: the system is hardly modifiable. Viral vectors may label region specific cells, but the applicability is limited as tissue survivability is limited and reproducibility in a significant matter is hard to achieve due to limited tissue availability. Much research has been done in rodents for fundamental characterization of interneurons, and without this research not much would be known about interneurons at all. However, the limitations in rodent interneuron emergence compared to primates are numerous and range from a shorter developmental timeline over a reduced complexity of subtypes towards reduced complexity in emergence, as well as a lower relative number of interneurons in the cortex (Jones 2009). Thus, our tools to study interneuron emergence, migration and function are limited in many considerations. In this work, we want to present a new tool to study interneurons in a highly modifiable 3D culture with genetic background, developed using either human embryonic stem cells or induced pluripotent stem cells. We focus particularly on the migration of interneurons as a readout and present data indicating that we can get a broad range of different interneurons which show directed migration and integration into dorsal forebrain-like cerebral organoid tissue.

Results

Patterning of organoids

Cerebral organoids have intrinsic self-patterning and can produce many different regions of the human brain (Lancaster et al. 2013). This shows the tremendous capacities of the cerebral organoid method, but it makes studies on certain brain regions difficult, as numbers of these regions may vary considerably. Interestingly, the tissue identity of dorsal forebrain seems to be the default state of EB derived neurons when lacking morphogenic patterning (Elkabetz et al. 2008). Morphogenic signaling may in a cell and passage dependent manner occur spontaneously in cerebral organoids, indicated by the multiple regions observable in cerebral organoids, but could also be useful in modulating the cerebral organoids towards regions of interest.

Focusing on ventral and dorsal forebrain regions in 3D cultures, it was Kadoshima et al. 2014 which first reported targeted patterning of ventralized organoids using different levels of the hedgehog agonist SAG (smoothened agonist). And indeed, initial experiments indicated that small molecules which interfere with sonic hedgehog signaling and Wnt signaling can be used as well in our cerebral organoid protocol for generation of differently patterned forebrain regions when used in the right time window, namely throughout the NI medium step until Matrigel embedding (Figure 6A, C-E).

Modulating shh and Wnt signaling based on recently published 2D (Maroof et al. 2013; Nicholas et al. 2013; Liu et al. 2013) and one 3D protocol (Kadoshima et al. 2014) , it was possible to grow both "dorsalized" and "ventralized" forebrain organoids. For shh activation and thus ventral forebrain localization of the neural tube, the small molecule SAG (Millipore, cat.566660) at 100nM was used. Additionally, the Wnt inhibitor IWP2 (Sigma, cat. I0536) at 2.5µM was used for creation of more anterior ventral regions. For dorsal organoids, initially untreated iPSC derived organoids were used. However, it was reported that SHH inhibition by the small molecule Cyclopamine A (CycA) (Calbiochem, cat. 239803) at 5µM in 2D neuronal differentiation approaches can enhance dorsal patterning (Vazin et al. 2014), we used that condition for further dorsal differentiated organoids. These ventral, dorsal^{unt} and dorsal^{CycA} patterned organoids depicted either ventral or dorsal forebrain in many, but not all regions, indicating residual patterning effects (Figure 6D, E for ventral and dorsal^{unt}, dorsal^{CycA}: data not shown). However, as a general trend ventralized organoids showed strongly increased levels in ventral markers in qPCR and IHC and a decrease in dorsal marker expression levels of dorsal markers (Figure 6C). It has to be mentioned that untreated control cerebral organoids which were derived from the iPSC cell line used in that work, as ground state produced dorsal regions at high chance (labeled "dorsal^{unt}") (Bagley et al. 2017). A schematic of the patterning protocol can be found in figure 6A.

Ventralization and dorsalization was tested using qPCR and IHC. A schematic of the localizational identity of the used qPCR markers can be found in figure 6B. Generally, both ventralized and dorsalized organoids depicted high levels of FOXG1 expression in both qPCR and IHC, thus indicating forebrain identity (Figure 6C, D). While in the ventralized organoids, the ventral markers DLX2, GSX2, NKX2.1 and LHX6 were upregulated and the dorsal marker TBR1 was downregulated, the inverse expression pattern could be observed with the control organoids; IHC confirmed this trend (Figure 6C-E).

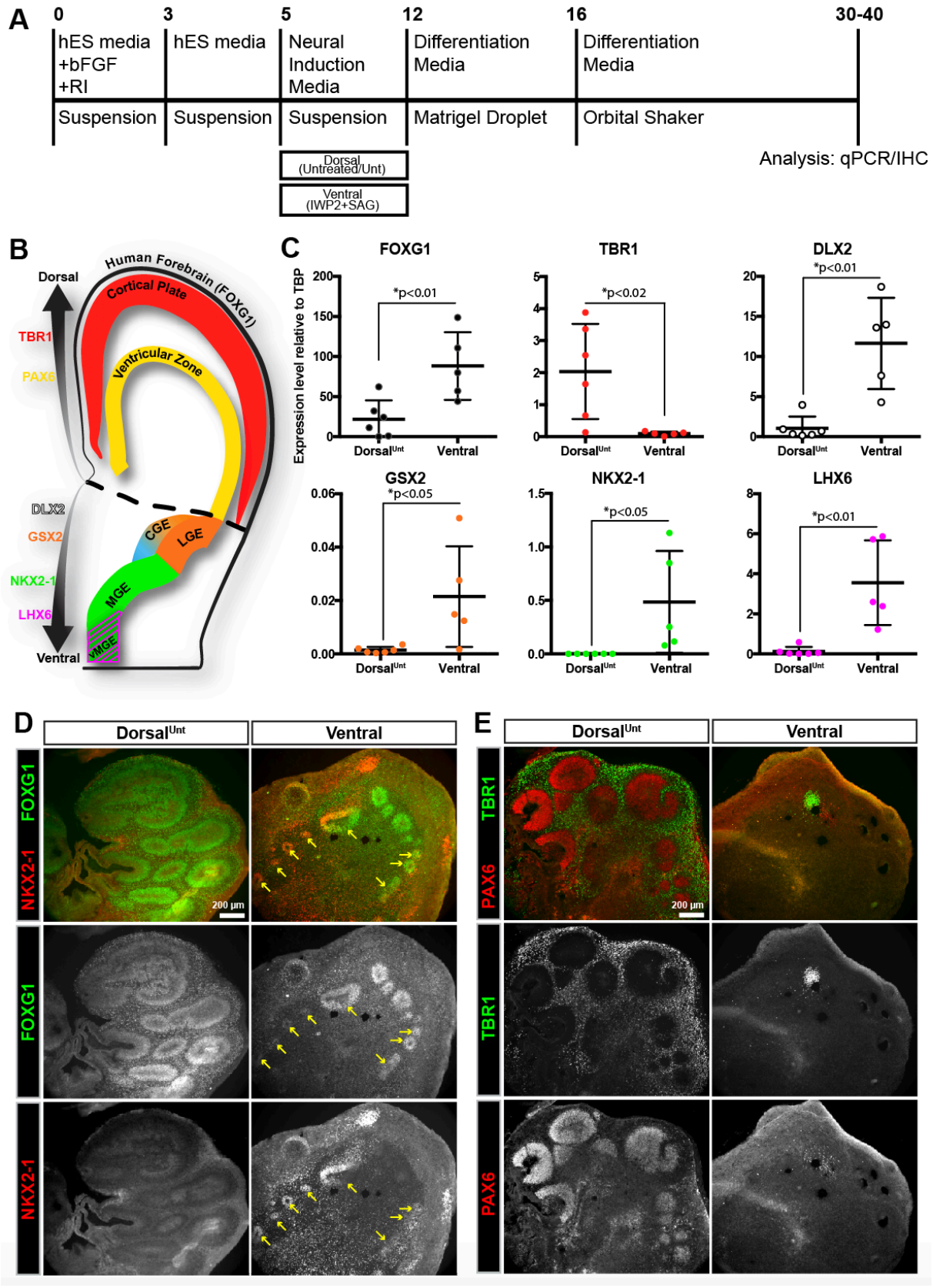

Figure 6: Patterning of ventralized and dorsalized cerebral organoids.
A) Schematic of the patterning protocol of cerebral organoids for dorsal (untreated) and ventral (2.5µM IWP2+ 100nM SAG). B) Schematic of a coronal slice of a developing human brain, indicating important markers for qPCR/IHC analysis of dorsal and ventral organoids. C) qPCR expression analysis of dorsal (untreated) and

ventralized organoids. Values are relative expression level ($2^{-\Delta Ct}$) to TBP. Each data point represents an independent batch of 8-10 organoids. Data is presented as ±s.d. and statistical significance was tested using the Student's t-test (df=9) for dorsal (untreated) (n=6 batches) versus ventral (n=5 batches). D), E) Widefield images of dorsal (untreated) and ventralized cerebral organoids immunostained for forebrain (FOXG1), MGE (Nkx2.1) and dorsal forebrain (PAX6, TBR1) markers. Scale bars are 200µm. Figure adapted from (Bagley et al. 2017).

Fusion of differently patterned organoids recreates a dorsal-ventral axis and shows increasing levels of migrated of cells from ventral into dorsal areas over time

The ventral forebrain gives rise to interneuron progenitors, which then subsequently migrate tangentially into the dorsal forebrain and integrate in the developing cortical plate through radial migration. Interneurons and its progenitor regions were reported to exist in cerebral forebrain organoids or neurospheres before (Kadoshima et al. 2014; Renner et al. 2017; Birey et al. 2017) and should be highly enriched in ventralized forebrain organoids, whereas dorsalized forebrain organoids should depict the target region of migrating interneurons. We therefore next addressed the question how to put the two different regions together in a controllable and modifiable manner, with the aim to hopefully see migrating interneurons. We tried a novel approach in fusing a ventralized and a dorsalized organoid during the step of Matrigel embedding, termed organoid "fusion", thus allowing the two organoids to grow together to one fused organoid over time (Figure 7A).

In a first attempt, the fusion of unlabeled, ventral or dorsal patterned organoids was performed to assess feasibility and efficiency of the fusions. Indeed, the organoids fused efficiently and remained fused to a very high extent (>90% of a batch of ~100 fusions) (data not shown). Secondly, an EF1α-GFP^+ and an EF1α-$tdtomato^+$ iPSC cell line (Bagley et al. 2017) was used for labeling different cerebral organoids and the fusions were repeated (Figure 7B). Immunofluorescent stainings for the ventral (MGE) marker Nkx2-1 and the dorsal marker TBR1 in a ventral-dorsal fusion indicated that the patterning can work similarly in juxtaposed and subsequently fused organoids (Figure 7C). Interestingly, levels of migrating cells were observable at high levels from ventral into the dorsal organoid, but not vice versa (Figure 7D). Additionally, we could often observe GFP^+ migration streams on the outside of the dorsalized organoid, whose cells in later organoid development seem to spread through the whole organoid (Figure 6D). While VZ-like regions could be observed in fusion organoids up to day 60, particularly in the dorsalized part of the fusion, VZ-like structures could not be observed any more in day 80 old organoids (supplemental Figure 1). This observation is in consistency with the initial organoid protocol, which did also not show VZ-like structures in older organoids (Lancaster et al. 2013).

To assess the time course of migrating cells, we collected tissue from day 32, 46, 58 and day 80 and analyzed the density of GFP^+ migrated cells in dorsal regions over time (Figure 7E, F). At day 32, very few cells were migrating into the ventral organoid, however on day 46 we could observe a tremendous increase in density of migrated cells. When analyzing the cell density on day 58 and day 80, the density

of cells did not significantly increase further, however we could observe a by trend more equal distribution of GFP^+ cells in the dorsal organoid. Since organoid size increases in time, the constant density of GFP^+ cells is an indicator for proceeding migration of GFP^+ cells to maintain similar density levels, particularly as the migrated cells were mostly post-mitotic, as indicated by very low numbers of cells which express the mitotic marker Ki67 (≤1%, supplemental Figure 2). Notably, rosettes were observable at day 60 in IHC slices, but could not be observed in later organoids >80 days of age (supplemental Figure 1).

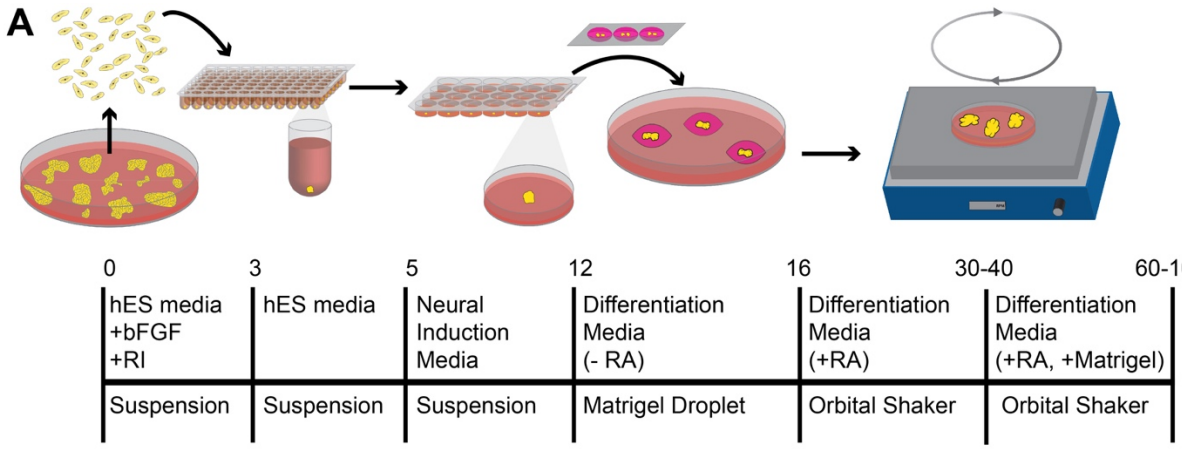
A
0
3
5
12
16
30-40
60-1
hES media +bFGF +RI
hES media
Neural Induction Media
Differentiation Media (- RA)
Differentiation Media (+RA)
Differentiation Media (+RA, +Matrigel)
Suspension
Suspension
Suspension
Matrigel Droplet
Orbital Shaker
Orbital Shaker

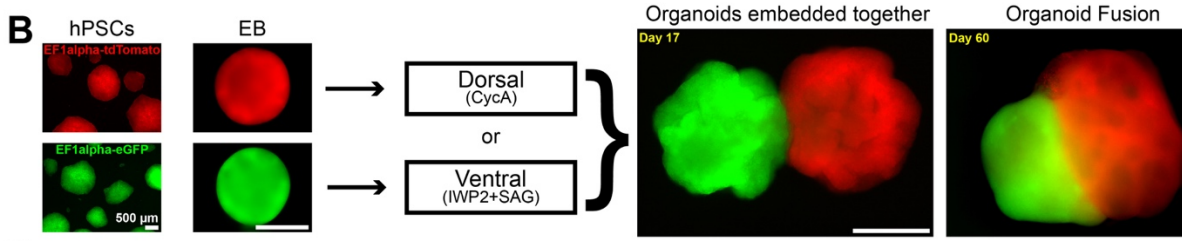
B
hPSCs
EB
EF1alpha-tdTomato
EF1alpha-eGFP
500 µm
Dorsal (CycA)
or
Ventral (IWP2+SAG)
Organoids embedded together
Organoid Fusion
Day 17
Day 60

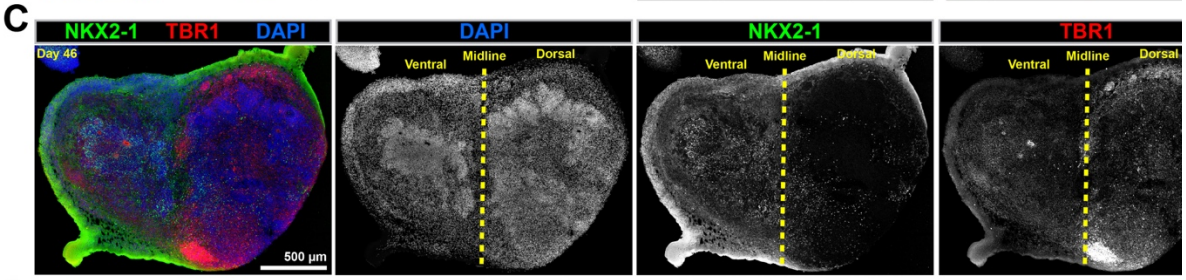
C
NKX2-1 TBR1 DAPI
DAPI
NKX2-1
TBR1
Day 46
Ventral
Midline
Dorsal
500 µm

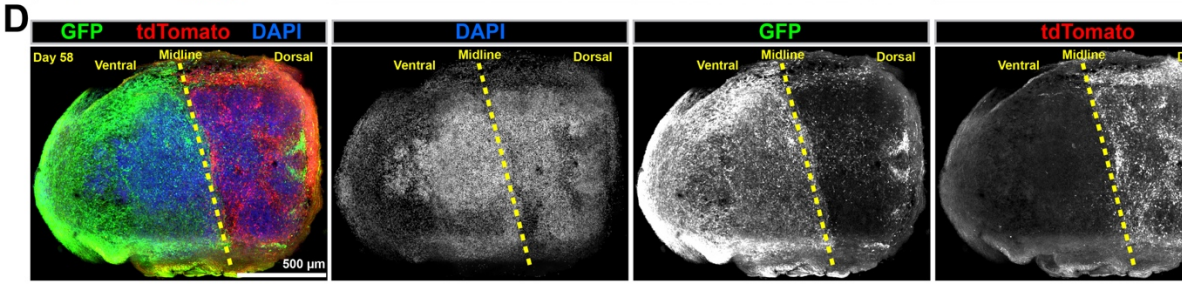
D
GFP tdTomato DAPI
DAPI
GFP
tdTomato
Day 58
Ventral
Midline
Dorsal
500 µm

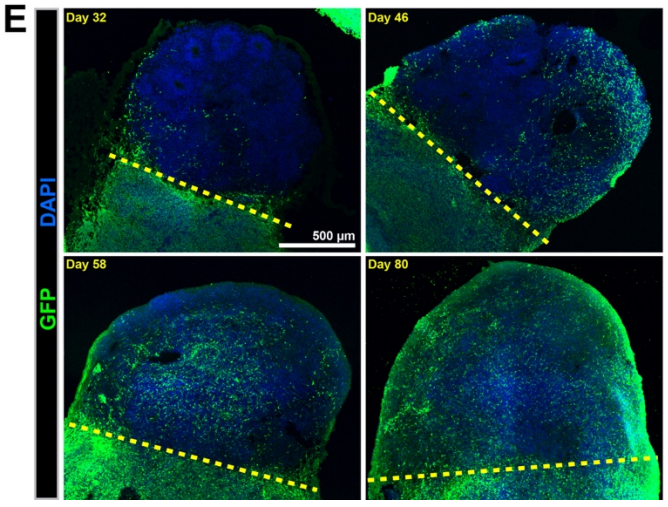
E
DAPI
GFP
Day 32
Day 46
Day 58
Day 80
500 µm

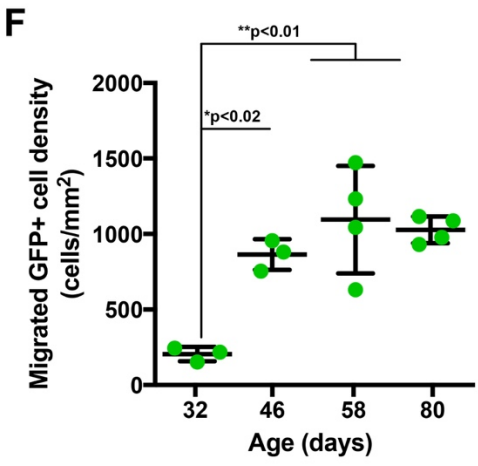
F
**p<0.01
*p<0.02
Migrated GFP+ cell density (cells/mm2)
2000
1500
1000
500
0
32
46
58
80
Age (days)

Figure 7: Fusion of cerebral organoids with different patterning is possible and cells migrate between ventral and dorsal organoids.
A) Experimental outline of the organoid fusion. The protocol of Lancaster et al (2013) was used, with the modification of juxtaposing 2 differently patterned EBs in close proximity during Matrigel embedding. B) Representative widefield images of tdtomato^{+} and GFP^{+} iPSC colonies and embryoid bodies (EBs) before, 5 days after and 48 days after fusion. Note that the organoids fuse together but still depict a recognizable border. C) The ventral patterned, GFP^{+} organoids express the ventral forebrain marker Nkx2-1, the dorsal patterned, tdtomato^{+} organoid expressed the dorsal forebrain marker TBR1. D) IHC stained ventral-dorsal fusions show increased migration of cells from ventral (GFP^{+}) into dorsal tissue in a time-dependent manner. Samples were taken on day 32, 46, 58 and 80. E) GFP^{+} cells were quantified in representative sections from 32 (n=3 organoids), 46 (n=3) 58 (n=4) and 80 (n=4) day old organoids. Data is presented as mean±SD and statistical significance was tested using an one-way ANOVA [$F(3,10)=12.59$, $p=0.0010$] with posthoc Turkey's test for groups comparisons. Scale bars are 500µm. Figure adapted from (Bagley et al. 2017).

Migration of cells from one organoid to the other is origin and target specific

To systematically assess if migration of the cells occurs in a directed manner comparable to *in vivo*, or randomly happens when two organoids of same or different identity become fused, several fusion groups of differently patterned organoids were grown and analyzed. We investigated cell migration in Ventral-Dorsal^{Unt} (VD^{Unt}), Ventral-Dorsal^{CycA} (VD^{CycA}), Dorsal^{Unt}-Dorsal^{Unt} (D^{Unt}D^{Unt}), and Dorsal^{CycA}-Dorsal^{CycA} (D^{CycA}D^{CycA}) fusions, where Dorsal^{Unt} corresponds to wildtype organoids without applied patterning. Ventral-Ventral fusions were not investigated. One of the organoids was consistently labeled using a GFP^{+} iPSC line, whereas the other organoid was labeled using a tdtomato^{+} iPSC line. Whole-mount imaging of these fusions on day 60 (data not shown) and day 81 (Figure 8A) indicated the occurrence of GFP^{+} spots in the tdtomato^{+} organoid in VD^{CycA} and in more variable levels in VD^{Unt} in a reproducible manner, but not in the other control groups D^{Unt}D^{Unt} and D^{CycA}D^{CycA}. More strikingly, IHC based GFP^{+} cell density quantifications in the target organoid revealed significant differences between the groups (VD^{Unt} and VD^{CycA}) and the control groups D^{Unt}D^{Unt} and D^{CycA}D^{CycA} (Figure 7B, C). Interestingly the VD^{CycA} fusion seemed to have a more consistent level of migration compared to the VC^{Unt} fusions, which may be due to increased levels of different patterning in some regions of the D^{Unt} organoid, depicting other regions than dorsal forebrain. Concluding, this experiment shows that the VD^{CycA} group had the most robust levels of migration between both organoids, thus it was used further for characterizations and was termed "ventral-dorsal".

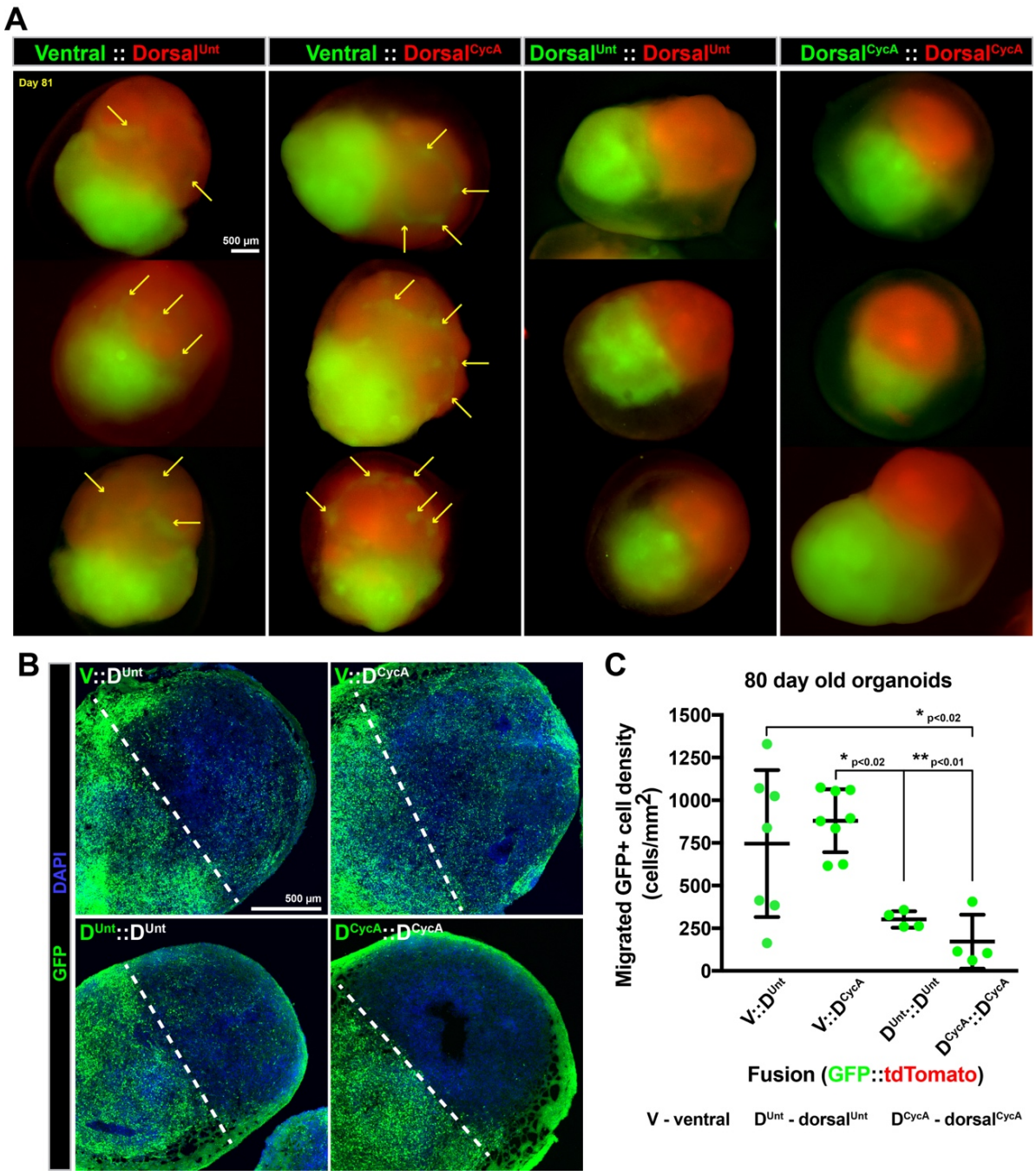

Figure 8: Mixing different patterned organoids together shows most robust migration in ventral-dorsal fusions. A) Cerebral organoid fusions were created using ventral, dorsal+CycA and non-patterned (dorsal-untreated) organoids. Whole-mount imaging of VD^{Unt} and VD^{CycA} fusions showed observable green spots in the tdtomato^{+} organoid on day 81. B) Tile-scan confocal images of 80 day old immunostained organoid fusions show migration of GFP^{+} cells across the midline (dashed line) into the other organoid. C) Quantification of GFP^{+} cell density in target organoid, counted from IHC tissue sections. Each data point= 1 individual organoid fusion. Data is represented as mean±SD with statistical significance testing using one-way ANOVA [$F(3,19)=8.214$, $p=0.0010$] with posthoc Tukey's test for group comparisons. The VD^{Unt} (n=7) and VD^{CycA} (n=8) fusions show the most migration of GFP^{+} cells compared to $D^{Unt}D^{Unt}$ (n=4) and $D^{CycA}D^{CycA}$ (n=4) fusions. Scale bars are 500µm. Figure adapted from (Bagley et al. 2017).

Migratory cells express interneuron markers and show signs of maturation

We next addressed the question of cellular identity of migrating cells using immunofluorescent labeling of established interneuron markers. One of the key enzymes in GABA production is GAD1 (Glutamate Decarboxylase 1), which catalyzes the decarboxylation of glutamate to GABA and CO_2 and is expressed in interneurons (Erlander et al. 1991; Le Magueresse & Monyer 2013). IHC stainings revealed that the GFP^+ positive cells which migrated from the ventral into the dorsal organoid broadly expressed GAD1 (Figure 9A-C). Interestingly, GAD1 was expressed in a similar pattern to the GFP^+ migratory cells (Figure 9A) and the expression of GAD1 seemed to be stronger in regions further away from the ventral organoid (Figure 9B).

Another population of tangentially migrating cells in the human developing brain are Cajal-Retzius cells which express the protein Reelin, (Hevner et al. 2003). However, while many cells were positive for Reelin-expression in the dorsal organoid, none of the migrated GFP^+ cells were positive for Reelin (supplemental Figure 3). Thus, we did not have Cajal-Retzius cells in the migratory cell population, but we did also not have interneuron species which express Reelin.

All migratory cells expressed the pan-neuronal marker HuC/D (Figure 9D) and a small subset also expressed the early MGE interneuron marker Nkx2-1, (Figure 9E). Quantifications showed that all migratory, GFP^+ cells expressed HuC/D, ~60% of all migratory cells expressed GAD1, and ~20% expressed Nkx2-1. Additionally, we analyzed the expression of the pan-neuronal marker DCX and the mature neuron marker NeuN and MAP2 and found that the majority of GFP^+ migrating cells were positive for DCX and a small subset also expressed NeuN or MAP2 (Supplemental Figure 4A, B). We could observe both GFP^+ cells with a more mature morphology, having branching processes in multiple directions, and cells with typical interneuron migratory morphology with elongated cell body, a branched leading process and a trailing process (supplemental Figure 5).

In summary, we could show that a population of migrated cells were migratory interneurons. They broadly expressed immature neuronal markers and a subset also expressed mature neuronal markers.

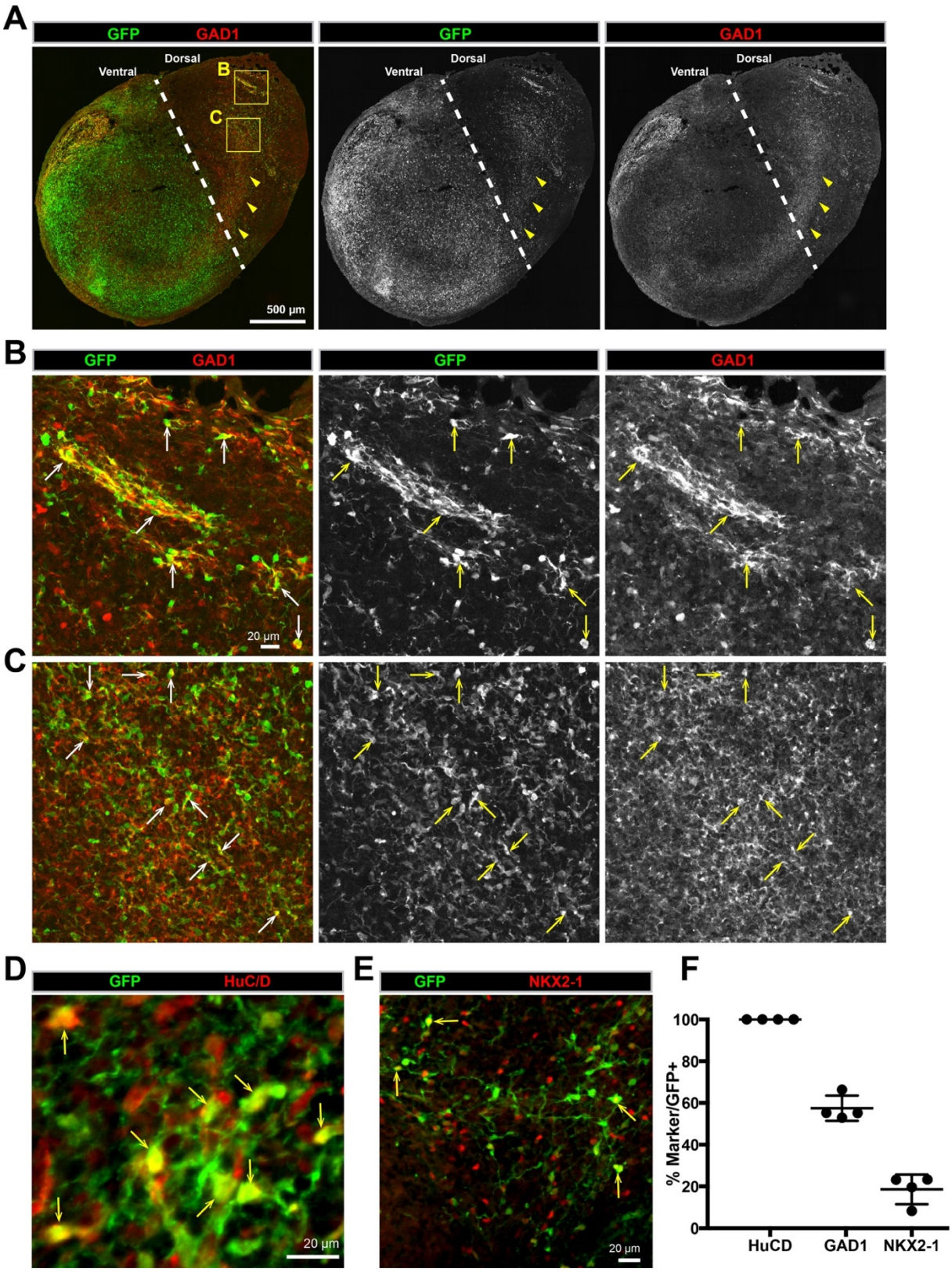
A
GFP
GAD1
Ventral
Dorsal
B
C
500 µm
GFP
GAD1
Ventral
Dorsal
GFP
GAD1
Ventral
Dorsal
B
GFP
GAD1
20 µm
GFP
GAD1
C
D
GFP
HuC/D
20 µm
E
GFP
NKX2-1
20 µm
F
% Marker/GFP+
100
80
60
40
20
0
HuCD
GAD1
NKX2-1

Figure 9: GABAergic interneurons migrate between fused dorsal-ventral cerebral organoids and show signs of maturation
A) Whole organoid confocal tile-scan of an immunostained 80day old ventral-dorsal fusion cryosection. GFP^+ cells migrate across the fusion midline (dashed line) from the ventral (GFP^+) into the dorsal (GFP^-) organoid. GAD1 expression can be observed in a similar pattern as the GFP migration route (arrowheads). B) and C) Magnification of the whole organoid scan from panel A from a peripheral region (B) and internal region (C). GFP^+ GAD^+ positive cells can be observed throughout the organoid and are indicated with an arrowhead in the exemplarily regions. D) Confocal image of GFP, HuC/D immunostaining in the dorsal region of an 80day old ventral-dorsal organoid fusion cryosection. All GFP^+ cells were also HuC/D positive. Yellow arrows point out double positive cells in the in-focus z-section. E) Confocal image of GFP-Nkx2-1 immunostaining in the dorsal region of an 80 day old ventral-dorsal organoid fusion cryosection showing that migrating GFP^+ cells at low levels also express Nkx2-1 (yellow arrows). (F) Percentage (mean ±SD) of GFP^+ cells migrated into the dorsal organoid which express HuC/D (100 ± 0%, 1427 cells counted from representative sections of n=4 organoids), GAD1 (57.5 ± 3%, 1879cells counted from repr. sections from n=4 organoids) and Nkx2.1 (18.6 ± 3.6%, 3067 cells counted from repr. sections from n=4 organoids). Scale bars are: A)500µm, (B-E) 20µm. Figure modified from (Bagley et al., 2017).

Various interneuron subtypes can be found in the population of migrated cells

Interneurons are a very heterogeneous population and can migrate from different subregions of the ganglionic eminences (GE) in a temporal and spatially different manner into the dorsal forebrain (Sultan et al. 2013, see also Figure 3). In this work, we focus on an initial determination of the interneuron subtypes in the fused ventral-dorsal organoids, based on alternative marker expression. In humans, the majority of interneurons are emerging from $Nkx2\text{-}1^+$ regions of the MGE (Gelman et al. 2012). These regions and its derived migrated interneurons express the transcription factor SOX6 (Batista-Brito et al. 2009; Kessaris et al. 2014). We could observe ~40% of migrated cells which were GFP^+ $GAD1^+$ and $SOX6^+$, thus being MGE-like derived interneurons (Figure 10A, I). Further characterization of mature subtypes of MGE-derived interneurons indicated that ~6% of GFP^+, GAD^+ migrated cells were positive for Somatostatin (SOM) (Figure 10B, I), ~6% for Neuropeptide Y (NPY) (Figure 10C, I), ~20% for Calbindin D-28k (CB) (Figure 10D, I), and ~5% were positive for Parvalbumin (PV) (Figure 10E, I). Additionally, ~4% of migrated cells which were positive for GFP, VGAT were also positive for Calretinin (Figure 10H, J).

Another group of cortical forebrain interneurons is derived from the CGE, with unknown LGE contribution. CGE-derived interneurons do not express SOX6, but they broadly express the transcription factors COUP-TFII/NR2F2 and SP8 (Yozu et al. 2008; Sultan et al. 2013). We could observe that both SP8 and COUP-TFII were expressed in some of the migrated cells together with GFP and GAD1 or VGAT (Figure 10F, G) thus being derived from CGE-like regions. Both markers were expressed in approximately 30-40% of all migrated cells. Reportedly, CGE-derived interneurons may also express NPY, SOM, CR, RELN and VIP (Wonders & Anderson 2006; Cauli et al. 2014; Kessaris et al. 2014). However, migrated VIP^+, GFP^+ and $GAD1^+$ cells were not observed, and the same was true for Reelin-expressing cells, as already indicated before (Figure S4).

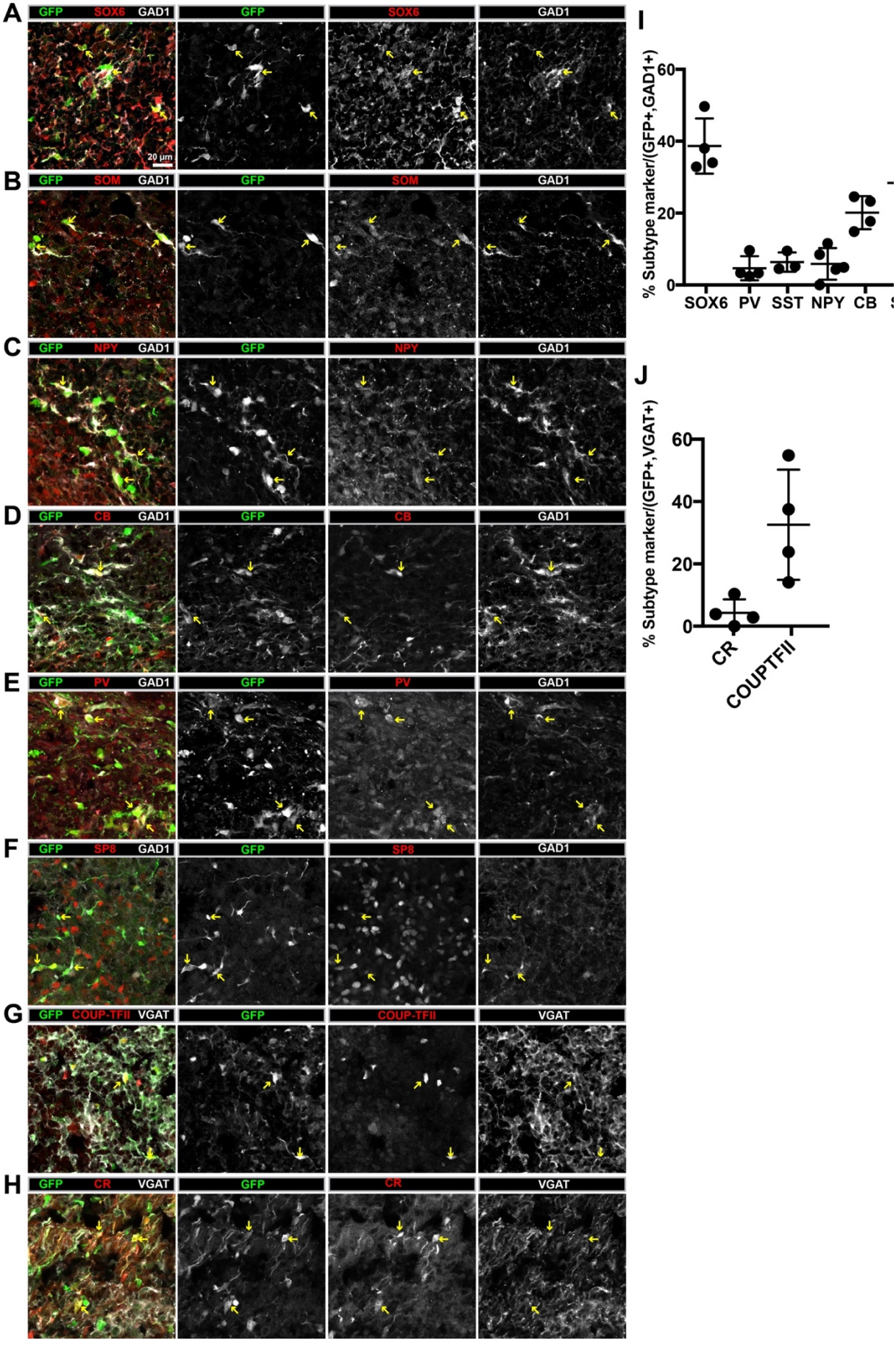
A
GFP SOX6 GAD1
GFP
SOX6
GAD1
20 μm
B
GFP SOM GAD1
GFP
SOM
GAD1
C
GFP NPY GAD1
GFP
NPY
GAD1
D
GFP CB GAD1
GFP
CB
GAD1
E
GFP PV GAD1
GFP
PV
GAD1
F
GFP SP8 GAD1
GFP
SP8
GAD1
G
GFP COUP-TFII VGAT
GFP
COUP-TFII
VGAT
H
GFP CR VGAT
GFP
CR
VGAT
I
% Subtype marker/(GFP+,GAD1+)
60
40
20
0
SOX6
PV
SST
NPY
CB
J
% Subtype marker/(GFP+,VGAT+)
60
40
20
0
CR
COUPTFII

Figure 10: Migrating interneurons express a broad range of interneuron subtype markers
(A-H) Confocal images from IHC stained cryosections in day 80 old ventral-dorsal fusions. For interneuron identity, either GAD1 or VGAT staining was used, together with GFP and a corresponding subtype staining. Examples for cells positive for GFP, GAD/VGAT and subtype marker are indicated with an arrow. SOX6, indicating MGE derived interneurons (A), was expressed with a set of MGE-derived interneuron subtypes, namely SOM (B), NPY (C), CB (D) and PV (E). Another subset of GFP^+, $GAD^+/VGAT^+$ cells expressed the CGE-derived interneuron markers SP8 (F), COUP-TFII (G) and the CGE-derived interneuron subtype marker CR (H). Scale bars are 20µm. (I) Quantification of the percentage (mean ± SD of GFP^+, GAD^+ double positive migrating interneurons in the dorsal region of organoid fusions for the expression of different interneuron subtype markers. SOX6 (38.7 ± 3.9%; 1,002 cells counted from n = 4 organoids), PV (4.7 ± 1.7%; 1,879 cells; n = 4 organoids), SST (6.4 ± 1.5%; 818 cells; n = 3 organoids), NPY (5.9 ± 2.0%; 748 cells; n = 5 organoids), CB (20.1 ± 2.3%; 1,114 cells; n = 4 organoids), SP8 (33.0 ± 5.2%; 620 cells; n = 4 organoids). (J) Quantification of the percentage (mean ± SD of GFP^+, $VGAT^+$ double positive migrating interneurons in the dorsal region of organoid fusions for the expression of interneuron subtype markers CR and COUP-TFII. CR (4.3 ± 2.2%; 898 cells; n = 4 organoids), COUPTFII (38.7 ± 7.8%;781 cells; n = 4 organoids). Scale bars are 20 µm. Figure adapted from (Bagley et al. 2017).

Discussion

With the organoid fusion of defined brain areas, we developed a cell-migration assay using a similar concept as classical co-culture experiments. Through the fusion of V-D fusions, we could introduce robust cell migration from ventral to dorsal forebrain regions in cerebral organoids, and we could demonstrate that the migratory cells expressed interneuron markers GAD1 and VGAT to a high extent. We additionally could show that the migrated cells expressed markers of different interneuron populations. Additionally to the work presented in this thesis, time-lapse recordings of migrating interneurons were performed and showed stereotypic morphology of migrating interneurons (Bagley et al., 2017). The inhibition of CXCR4, a receptor known for its function in interneuron migration, resulted in drastically reduced levels of interneurons (ibid., 2017).

One interesting phenomenon was the expression of Nkx2.1 by the migrating interneurons. In mice, the expression of Nkx2.1 becomes downregulated in interneurons after they leave the GE (Nóbrega-pereira et al. 2008). In humans, Nkx2.1 positive cells could be observed within the dorsal forebrain as well, and it was speculated that this could mean the production of interneurons also from dorsal forebrain radial glia cells. Alternatively, Nkx2.1 expression in humans could be maintained, which would be a hypothesis supported by our observations on Nkx2.1 expression.
Two experiments which were not described in this work, but were part of this research project, were time-lapse recordings from interneurons which migrate into the dorsal organoid, and a drug treatment of organoid fusions with AMD3100, an CXCR4 antagonist.

The interneuron migration assay will be a valuable tool for many scientific questions in the future. First, it can be used to better understand interneuron migration in a human genetic background, and together with that, how early onset neurological diseases are emerging. Particularly of interest here is, that the migration assay allows modifications on both interneuron origin region and migration target region with all tools stem cell culture work provides. Further studies could imply genetically modified

brain region organoids fused with healthy brain region organoid, which allow further discrimination between effect and causalities of e.g. a migratory defect. For this, a pipeline for disease studies in cerebral organoids could look as followed: Find a phenotype and its genotype in the literature, re-grow the particular system which is thought to be impaired in cerebral organoids, and use either embryonic stem cells with genetically modified genotype or use patient-derived iPSC-cells and screen for a phenotype. Downstream applications of this could then be part of personalized medicine, such as replacing miss-functional elements in the human brain, or selectively target these systems. One candidate for such a screen could be ERB-B4, an important receptor for interneuron migration. ERB-B4 is a receptor for the ligand Nrg1, an chemoattractant molecule produced in the forebrain, and mutations in both ERB-B4 and Nrg1 are highly associated with Schizophrenia (Walsh et al. 2008; Marin 2012). For studying the complex interactions between both Erb-B4 and Nrg1, the fusion assay would be an ideal tool, as both origin and target region can separately be modified and the migration behavior of multiple interneuron subtypes could be analyzed. An additional candidate could be ARX, which is an transcription factor which is upregulated in interneurons, and where increased pA repeats are strongly associated with Epilepsy (Olivetti & Noebels 2012; Marques et al. 2015).

Another approach for this interneuron migration assay would be drug screenings. As initial experiments with the CXCR4 inhibitor AMD3100 indicated, interneuron migration in cerebral organoid fusions could be impaired by inhibiting chemotaxis mechanisms. That on the one hand could help as a tool in screening medicaments for whether they are applicable on pregnant woman, but could also be a tool in finding new therapies which target interneuron migration.

While in this work the interaction of two specific brain parts was investigated, the fundamental concept of organoid fusion could be extended to any region of the human brain. The interaction of different parts of the brain is not limited to the migration of cells, but could probably also be extended onto other migratory cells, or neuronal projections into different parts of the brain.

Chapter II: Elements of neural tube formation – a question of orientation?

Author contributions

I independently performed the experiments of the following project. The iPSC EBs which were tested in the following experiments were a kind gift from Dr. Shan Bian. qPCR on additional NI-derived organoid batches was performed on organoids grown by Dr. Joshua Bagley.

Introduction

The event of neural tube closure has implications in many diseases, which range from deadly diseases such as Anencephaly with the prosencephalic end never to be closed to mild, but impairing diseases such as Spinal dysraphism and Spina bifida with partially open spinal cord. As neural tube closure in humans varies significantly from mouse and other neural tube model systems (Copp et al. 2014), a human model for neural tube closure would be of interest.

So far, all reported cerebral organoid protocols use an embryoid body (EB) as a basic for further organoid growth. EBs are 3D tissue aggregates of pluripotent stem cells which show varying differentiation levels towards the early three germ layers and beyond (Martin 1981; ten Berge et al. 2008; Pekkanen-Mattila et al. 2010). Through their reassembly of all germ layers, EBs were extensively used for differentiations into various tissues, but particularly neural differentiations (Schulz et al. 2003; Dhara & Stice 2008; Abranches et al. 2009; Zhang et al. 2013). The common principle amongst these strategies is the plating of EBs to a 2.5D-structure which subsequently starts to develop neuronal rosettes, which reassemble pseudostratified structures of early embryonic stem cells. These neuronal rosettes commonly depict population of neurons which is normally not reassembling the complete neural tube, but shows discrete identities of neurons with only primitive ventral-dorsal or apical-basal axis (Wilson & Stice 2006; Meinhardt et al. 2014). While the identity of neural epithelia of these rosettes is discrete, the general morphology of the neural rosettes with a pseudostratified layer and an apical lumen as well as an outside-basal polarity at high levels reassembles the cellular structure of a neural tube (Elkabetz et al. 2008; Meinhardt et al. 2014). However, the emergence of these rosettes in EB based neuronal differentiation protocols as well as in cerebral organoids is poorly investigated and descriptions focus on already existing neural rosettes and further differentiated neurons.

The initial question of this project was, whether morphogenic elements of neural tube closure could lead to the rosettes observed in cerebral organoids. RNAseq indicates the appropriate identity of forebrain neural tube neuroepithelia (Camp et al. 2015b), and reconstructions of Lancaster et al. 2013 - derived cerebral organoid rosettes revealed elongated lumen of neuroepithelia (Renner et al. 2017), indicating that bigger lumen in cerebral organoids are possible. However, while an organoid protocol published by Kadoshima et al. 2014 indicated that a rounding morphogenesis of neuroepithelia could

occur in cerebral organoids, such an event was to date not observed in organoids published by Lancaster et al., 2013.

Results

Neuroepithelia dynamics in iPSC and H9 derived EBs during Matrigel embedding

Comparing the later neuronal rosettes derived by the Lancaster et al. 2013 and 2014 protocol ("Lancaster et al.") reveal several differences compared to another published organoid method by Kadoshima et al. 2014. One of the most striking differences was the apical orientation of the rosettes, which was generally lying in the inside of the organoids in the lumen of the neuronal rosettes in Lancaster et al. protocol. Conversely, the method by Kadoshima et al. 2014 showed initial formation of rosettes with their apical side oriented towards the outside in some, but not all rosettes (Figure 11A). The apical-outside rosettes described by Kadoshima et al. 2014 allowed some interesting folding of the rosettes which was not observed in organoids derived by the Lancaster et al. method or in EB-derived 2D neural rosette protocols. It was therefore interesting to study the intrinsic formation of early rosettes in cerebral organoids to find out more about their emergence and to compare it to the organoids from Kadoshima et al. 2014.

One of the quality control steps in the Lancaster et al. organoid protocol is the observation of a pseudostratified neuroepithelial structure on the outside of the EB at the late stages before Matrigel embedding (Figure 11B), which in brightfield microscopes corresponds to the transparent layer on the outside of the EBs. However, the organoids undergo a tremendous shift of morphology within the first days after Matrigel embedding, resulting in the observable neural rosette formation on the outer layers of the EB and the loss of the pseudostratified layer (Figure 11B). Initial 3D time-lapse movies of iPSC and H9 derived, Matrigel-embedded EBs with 5% GFP^+ labeled stem cells over 80 hours indicated a tremendous shift in the orientation of cells after Matrigel embedding (Figure 11C, D).

Within only several hours, the structure of an emerging neural rosette was determined and the radially organized cells proliferated in a symmetrical manner (Figure 11D). We therefore focused on a characterization of the morphological changes of EBs using IHC on cryosectioned EBs before and 24h after Matrigel embedding, where the morphological changes would already have been determined according to the initial time-lapse movies. The initial morphological analysis was performed in both iPSCs and H9-derived EBs, with the interest of cell line independent comparability.

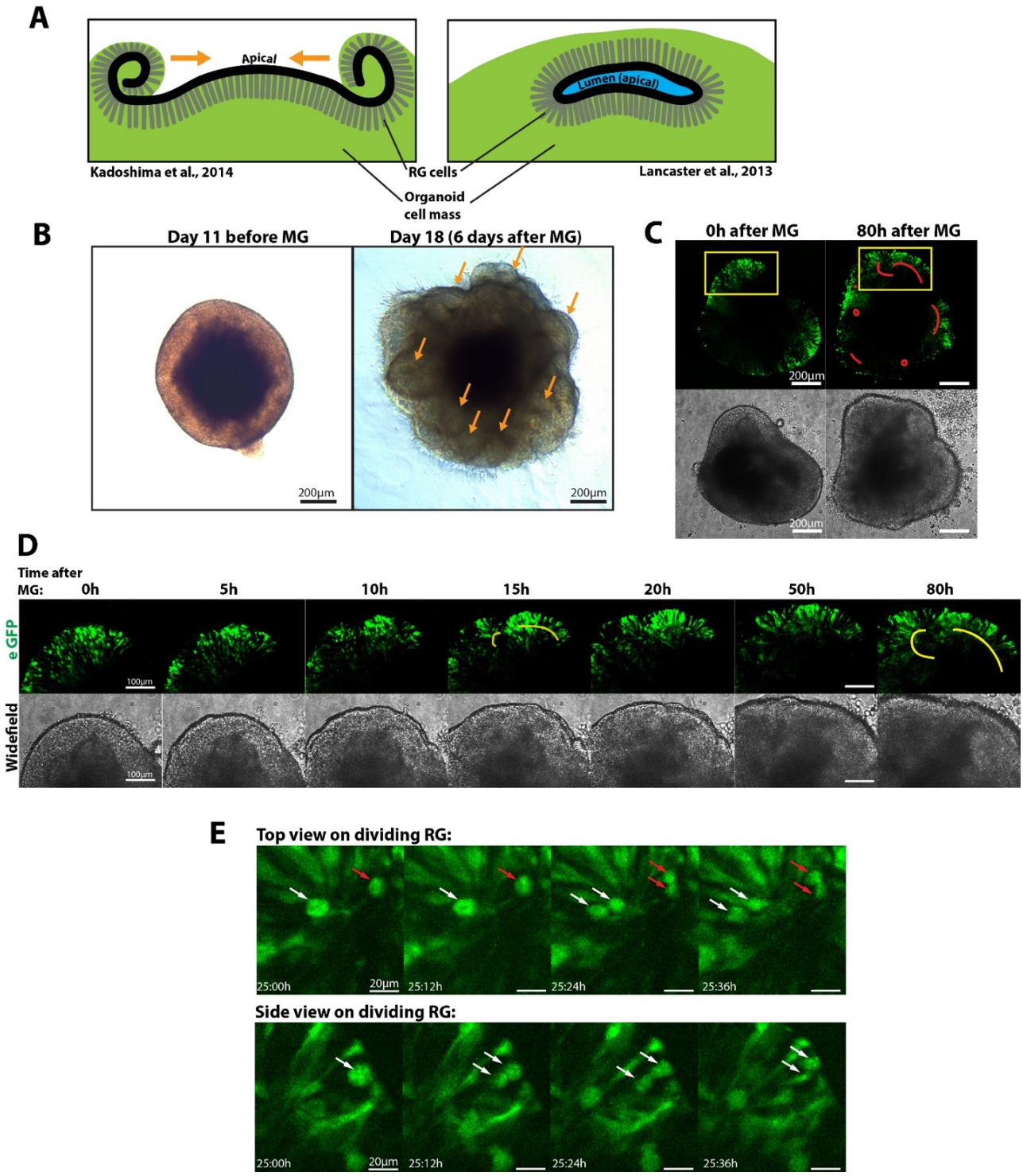

Figure 11: Morphogenesis of EBs after Matrigel embedding
A) Schematic of different rosette origin in Kadoshima et al. 2014 versus Lancaster et al., 2013. The incurling neural rosettes in Kadoshima et al.-derived organoids invaginate further together along the orange arrows and subsequently close the neural rosette. B) A 11 day old EB before Matrigel embedding vs. a day 18 old cerebral organoid which has been embedded for 6 days. By visual inspection, the bright ring on the outside of the day 11 old EB shows a radial structure. The 18 day old organoid did not show this structure any more, but showed the emerging of neuronal rosettes on the organoid (orange arrows). C) Whole organoid 3D time-lapse recordings (fluorescent and brightfield) of an EB with 5% GFP^{+} cells directly after Matrigel embedding and 80h after Matrigel embedding. Developing orientation centers of neuroepithelial cells are indicated by red lines. n=16 organoids from 3 different replicates in both H9 and iPSC derived EBs. D) Focus on the emergence of 2 different neuronal rosettes (yellow box in panel C). The re-orientation of cells takes

place within hours after Matrigel embedding. Lumen of developing neuronal rosettes indicated by red lines 15h after MG and 80h after MG. E) Cells of in panel D described rosettes show symmetrical dividing neuroepithelial/ radial glia cells (white and red arrows). Scale bars are 200µm (B, C), 100µm (D) and 20µm (E).

Neuroectodermal orientation in iPSC and H9 derived EBs before Matrigel embedding

Investigating the morphology of EBs before Matrigel embedding first, we could observe a strongly positive, pseudostratified ring of cells positive for the neuronal markers Nestin (Oikari et al. 2016), n-Cadherin (Théveneau et al. 2007) and the cell adhesion molecule β-Catenin (Sineva & Pospelov 2014) on the outside of both iPSC and H9 derived EBs (Figure 12A, B, Supplemental Figure 6C). Inside of this ring, tissue was often partially positive for these three markers, but the remarkable degree of orientation of the outside ring was absent. Stainings for the apical marker aPKCζ indicated that the apical orientation of the pseudostratified layer was oriented towards the outside (Figure 12A, Supplemental Figure 6C). Conversely, the inside Nestin^{+}, N-Cadherin^{+}, β-Catenin^{+} tissue did mostly not show apical structures. However, sometimes formation of some small, "internal" rosettes could be observed. These internal rosettes were observable in higher prevalence in the iPSC derived EBs (Supplemental Figure 6C) and were not frequently found in H9 derived EBs. Interestingly, aPKCζ stainings also revealed breakings of the outer apical layer of EBs already before MG embedding, resulting in an infolding-like structure (Figure 12C).

Stainings for the mesodermal marker Brachyury/T indicated that the EBs on day 10 did not show high levels of mesoderm (no expression: Figure 12B, biased representation of Brachyury^{+} EBs: Supplemental Figure 7). As NI medium promote neuroepithelia growth (Lancaster et al. 2013), other germ layer tissues in an EB will probably not further proliferate or even undergo cell death, and it cannot be excluded that higher levels of Brachyury positive cells exist in earlier EB development. Consistent with this theory, inner regions of the organoids in DAPI stainings showed nuclear fragmentation and nuclear condensation, both signs of cells which underwent either apoptosis or necrosis (Figure 12D) (Cummings et al. 2004).

SOX10 was used as a neural crest marker, as the orientation of neural crest was speculated to reveal the orientation of a neural tube-like structure (Figure 1A). The migratory neural crest marker SOX10 indicated different levels of positive cells across multiple batches of H9 derived organoids, however the SOX10^{+} cells were situated in the inside of the EB (Figure 12A) or in the buds on the outside of the EBs. EBs, which had external tissue buds growing outside of the pseudostratified layer showed high SOX10 expression within these buds, indicating that these buds are of neural crest origin (Supplemental Figure 7D). However, few buds were also positive for Brachyury/T (Supplemental Figure 7E), indicating different origins of external tissue buds of EBs.

Summing up, both H9 and iPSC derived organoids, using the organoid protocol of Lancaster et al. 2013, showed a pseudostratified layer of neural stem cells on the outside of the EB, and a varying level of neural stem cells in the inside of the EB. Additionally, neuronal rosette structures were observed in the inside of some EBs. Neural crest, if existent, was situated in the inside of the EB or in buds on the outside of the EB. Thus, the expanded rosette structures which were later reported in cerebral organoids could not be observed in EBs before Matrigel embedding.

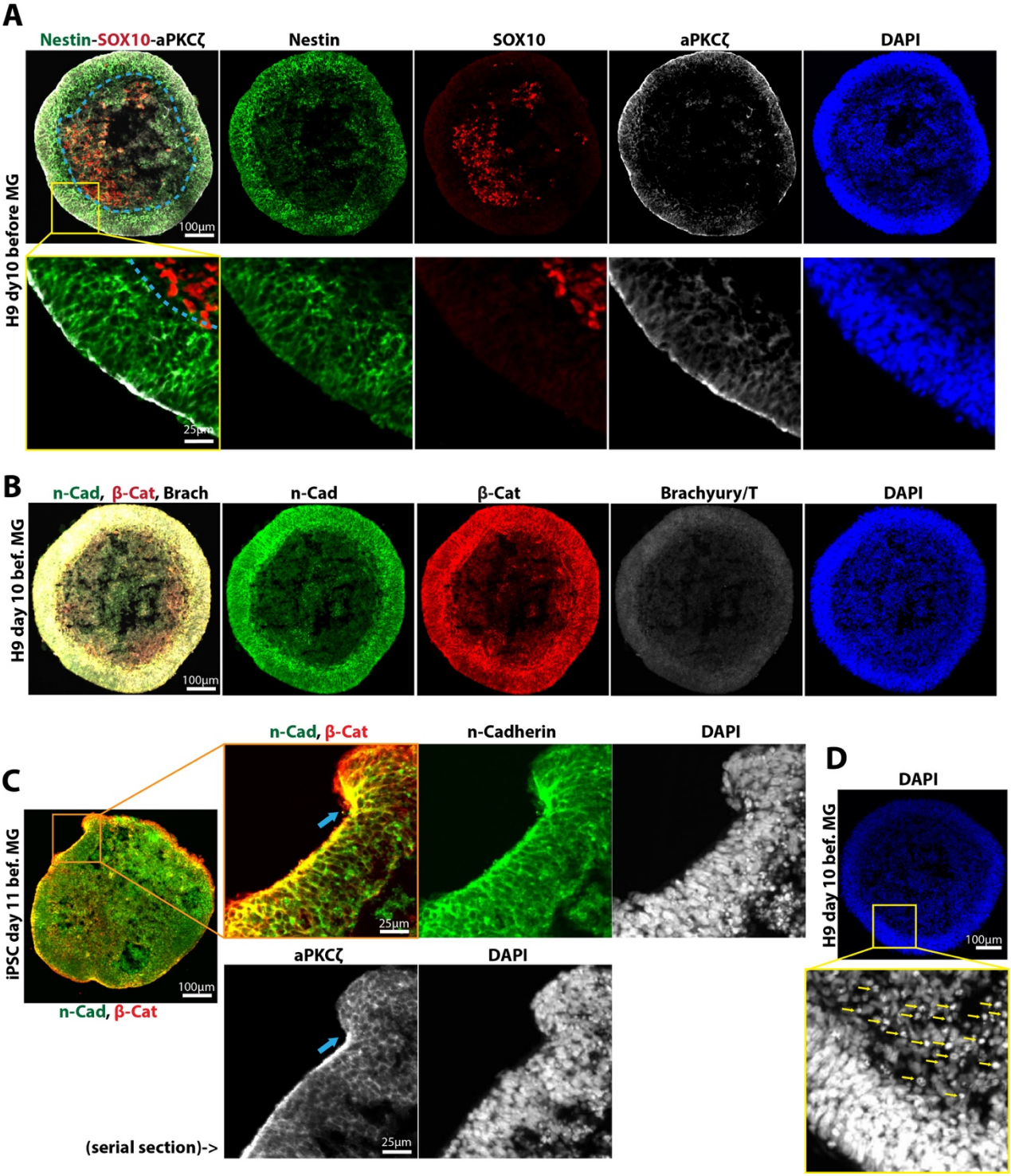

Figure 12: Morphology of EBs before Matrigel embedding
A)-E) Confocal spinning disk images of IHC labeled cryosections of H9 EBs on day 10 before Matrigel embedding. A), B): N>20 EBs of 2 independent replicates in H9. A) Staining for Nestin, SOX10, aPKCζ and DAPI. Nestin staining indicates a pseudostratified ring of neuronal stem cells on the outside of the EB (see also magnification below, and dashed turquois line). aPKCζ stainings indicate an apical orientation of this neural epithelium towards the outside of the EB. SOX10 indicates migratory neural crest in the inside of the EB, next to the necrotic/apoptotic core. DAPI stainings of the Nestin^{+} ring indicate an increased cell density. B) n-Cadherin and β-Catenin stainings confirm the structure of neuroepithelia. The shown EB did not show Brachyury/T positive cells. C) IHC of an iPSC EB for n-Cadherin, β-Catenin and DAPI in one, and aPKCζ+ DAPI staining in a serial section. Note the folding-like structure on one side of the neuroepithelia (blue arrow). D) Magnification of a DAPI-stained section of an EB. The nuclei marked with an arrow showed signs of nuclear fragmentation and nuclear condensation, both signs of cell death. Scale bars are 100µm (A, B, C, D) and 25µm (A).

Neuroectodermal orientation in iPSC and H9 derived EBs 24h after Matrigel embedding

Extracellular matrices such as Matrigel *in vivo* reassemble the basal side of tissues and thus probably provide basal signaling onto the cells. We were therefore interested in the effect of Matrigel embedding onto the initially apical-outside structured sheet of neuroepithelia. To look at the Matrigel-derived morphological changes on EBs which were embedded in Matrigel for 24 hours, we applied the same marker set as on EBs before Matrigel embedding.

Nestin, n-Cadherin and β-catenin stainings revealed tremendous morphological changes as the initially uniform, pseudostratified layer of neural stem cells underwent a complete re-orientation (Figure 13A, B, supplemental Figure 6D). As an overall structure, the layer of neuroectoderm can still be found, however the previous radial, pseudostratified structure to the outside was gone, and the cells developed neuronal rosettes. The newly created neuronal rosettes were sometimes of elongated structure (Figure 13A), but could also be more punctual (Figure 13B). Consistent with the reorientation observation, aPKCζ stainings reveal that the apical orientation on the outside of the EB was completely gone, and new, aPKCζ positive apical centers approximately in the middle of the previous pseudostratified layer emerged (Figure 13A). These reorientation centers are the onset of the formation of bigger neural rosettes in the organoids and determine the starting point of lumen formation in cerebral organoids, as can easily be detected by brightfield imaging: they can be observed as "neuronal buds" in post-embedded, developing cerebral organoids, which strongly develop into the droplet of Matrigel (Figure 13C). Breakings of the aPKCζ^{+} ring outside of the EB which was observed in few EBs before MG embedding (Figure 12C) could also not be observed any more. While Brachyury levels in EBs after Matrigel embedding were consequentially non-existent or very low (Figure 13B), SOX10 stainings indicated that the cells inside of the organoids had a lower SOX10 expression level than before (data not shown). Additionally, no SOX10^{+} buds on the outside of the Matrigel were observed any more.

The initial SOX10^{+} identity is not just important for the neural crest characterization of these buds. In quality controls, organoids with many depictable tissue buds on the outside are considered as a negative implication. As can be seen in supplemental Figure 7A-C, these migratory buds as well as migratory cells from the inside of an EB can apply strong mechanical forces onto the developing organoid in their attempt to migrate into the Matrigel. Dependent on the size of the neural crest buds, the buds can separate from the organoid and migrate further into the Matrigel, or, if they are big enough, the organoid can be torn in the direction of migration. Both behaviors could be observed repeatedly in time-lapse movies and brightfield images of emerging organoids and can be considered as negative implications for appropriate organoid development.

Summarizing, the pseudostratified neural stem cell layer on the outside of the EB completely breaks up after Matrigel embedding and induces the formation of expanded neuronal rosettes. In this process, the apical orientation of the cells becomes drastically re-oriented towards the newly emerging

rosette lumen which are situated close to the middle of the previously existing pseudostratified neuroepithelia. While inside, sparsely spread neural crest cells do not seem to have any effect on the organoid morphogenesis, however high levels of migratory cells in the inner mass of an EB or the outside neural crest buds may have negative effects on the formation of the organoid (Supplemental Figure 7C). $SOX10^{+}$ neural crest cells for not further investigated reasons reduce SOX10 expression after Matrigel embedding and outside tissue buds start to migrate into the Matrigel.

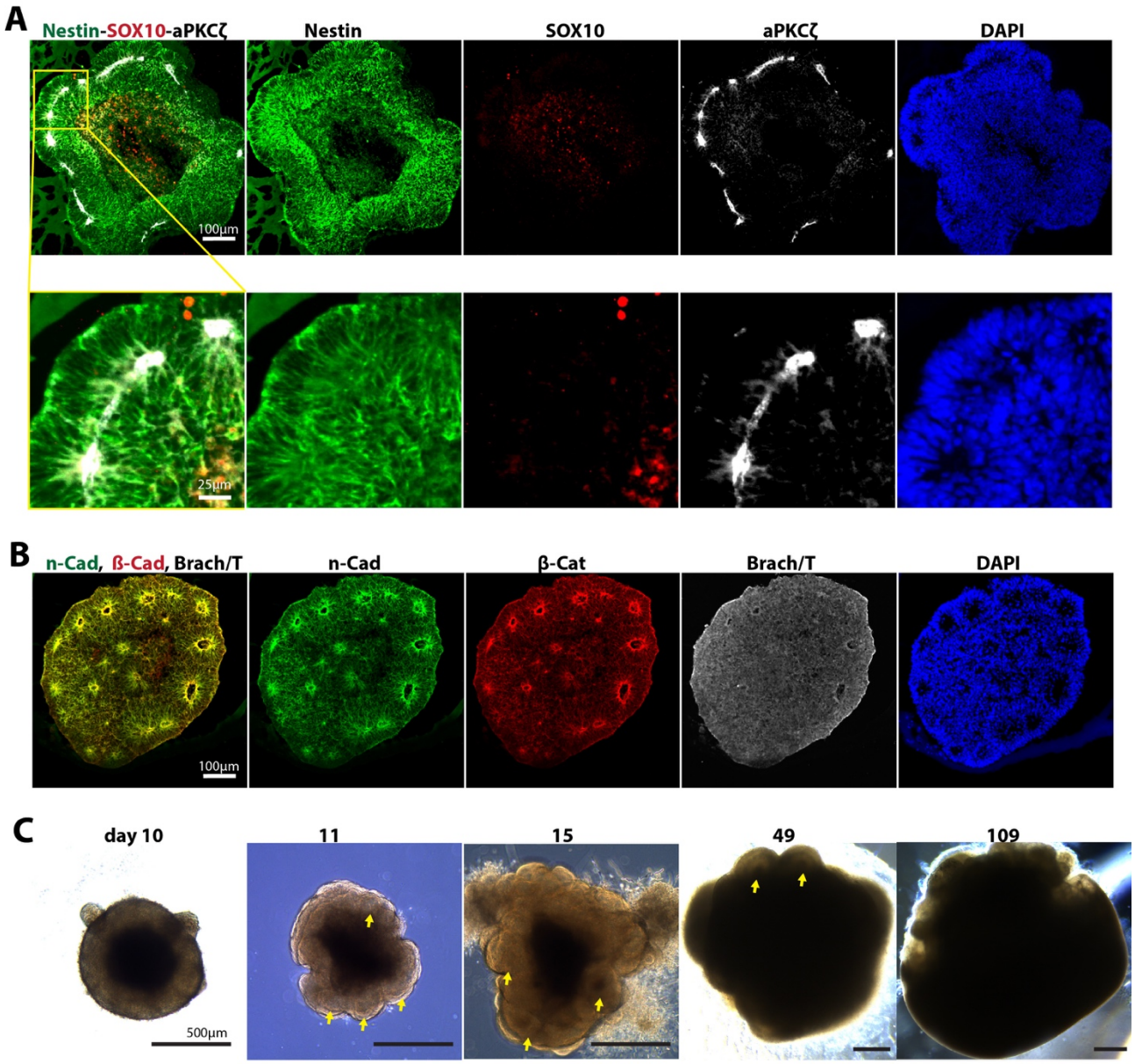

Figure 13: Morphology of EBs 24h after Matrigel embedding

A), B) Confocal spinning disk images of IHC labeled cryosections of H9 EBs on day 11, 24 hours after Matrigel embedding. Stainings were the neuronal marker Nestin, and n-Cadherin, the neural crest marker SOX10, the apical marker aPKCζ, the structural marker β-catenin and the mesoderm marker Brachyury/T. N>20 EBs of 2 independent replicates. A) Immunostaining for Nestin-SOX10-aPKCζ-DAPI. Nestin staining indicates the breakup of the radial structure and a reorientation of the cells towards approximately the middle of the previously radial neuroepithelia. aPKCζ stainings indicate the complete reorientation of apical orientation of the neuroepithelia. $SOX10^{+}$ cells can be observed, but a reduction in expression levels was observed. DAPI together with aPKCζ indicates the emergence of lumen on the apical reorientation centers. Magnifications below show the strong reorientation of the neuroepithelia. B) IHC for n-Cadherin and β-catenin confirm the structural re-orientation towards neural rosettes. Brachyury/T stainings did not show detectable mesodermal cells. Note that organoids did not always show an expanded $aPKC\zeta^{+}$ lumen as in panel A, but could also show discrete rosettes. C) Representative development of an organoid from day 10 to day 109. After Matrigel embedding on day 11, neural rosettes emerge and develop further (yellow arrows). On day 100, the produced superficial early and late born neurons cover the neuronal rosettes, thus a rosette/ cortical plate structure cannot be observed any more.
Scale bars are 100µm (A, B) 25µm (A) and 500µm (C).

Modification of apical orientation

We next addressed the question whether the initial formation dynamics in an EB could be described as a constant, not modifiable behavior, or whether they could be modified, such as defining the apical orientation of neuroepithelia in EBs. This could be of interest in many considerations: first, the event of secondary neural rosette formation is highly artificial as it involves rapid reorientation of neuroepithelia, which in that form was never reported to happen *in vivo*. Second, if the process of primary or secondary neural rosette formation could be altered, it could potentially also be modified with the aim of creating more neural tube invagination-like events.

For apical modifications, we first investigated the effects of the initial EB formation medium onto the apical orientation of neuroepithelial cells. When comparing different organoid protocols (Supplemental Table 1), it can be seen that the first cerebral organoid protocols usually started with a very similar medium composition based on DMEM/F12 or G-MEM and Knockout Serum Replacement (KOSR) and/or fetal bovine serum (FBS) (Lancaster et al. 2013; Kadoshima et al. 2014; Qian et al. 2016). These medium compositions were partially based on previous EB protocols, but also were of close formulation to the stem cell medium used for the cultivation of stem cells. Exemplarily, the hES medium used for initial EB formulation in the protocol by Lancaster et al. 2013 is also used for iPSC stem cell culture, whereas H9 embryonic stem cells are cultured in mTESR1 medium and then transferred to hES for EB formation. The initial medium formulations, however, introduced high levels of variability onto the EB formation of H9 cells, and particularly KOSR and FBS are reported to induce high levels of variability (Chaudhry et al. 2008). We therefore discussed that mTESR1 could be a promising replacement of hES medium, first to screen whether EBs actually form, but also for investigating the effects of a FBS free, but high protein environment on the apical orientation of neuroepithelia- mTESR1 contains BSA and has a total protein concentration of 13g/L (Ludwig et al. 2006; Hadley 2012). A further reductionist approach away from high-protein medium compositions can be found in a recent publication by Jo et al. 2016, where the EB formation medium was reduced to a composition very similar to the NI medium by Lancaster et al. 2013 (supplemental Table 1). Interestingly, the study by Jo et al. 2016 showed different morphology of EBs without recognizable pseudostratified layer on the outside of the EBs, and the depicted organoid structure was slightly different from what could be observed in organoids derived by Lancaster et al. 2013 protocol. The limited data on organoid structure which was shown in this study indicated a potentially different emergence of neuronal rosettes.

We therefore also decided to use NI medium for studying the effect of a KOSR/FBS free media on the apical orientation of cells. Following the logic of initial stem cell medium for EB formation, we also tried E8 medium without supplements. Notably, both NI and E8 medium compositions are of very similar composition and do not contain any protein source. The protein amount of E8 has been reported

to be approximately 0.03g/l, which means that its protein levels are reduced by the factor of 433x compared to mTESR1 (Hadley 2012). Summarizing, three different medium compositions for the replacement of hES were used (experimental outline: Figure 14A). All experiments were performed using H9 embryonic stem cells cultured in mTESR1 with regular protocol conditions.

As readouts, we preliminary focused on the IHC characterization of organoids before and after Matrigel embedding. However, as control for proper differentiation of potentially existing neuroepithelia towards (forebrain) neurons, IHC of ~30day old organoids and qPCR on ~50 day old organoids were performed. It has to be stated here that all the media besides the exact NI formulation were described to support the formation of EBs before (hES: Lancaster et al. 2013, E8: Lin & Chen 2014 and mTESR1: StemCellTechnologies 2015). For initial formulation of EBs, bFGF was added to the hES medium but to no other media. RI was added to all medium compositions for increased cell survivability, as commonly done for EB formation (Lancaster et al. 2013; Lin & Chen 2014). After day 5-6, the EBs were transferred on NI medium and proceeded following the Lancaster et al. 2013 protocol.

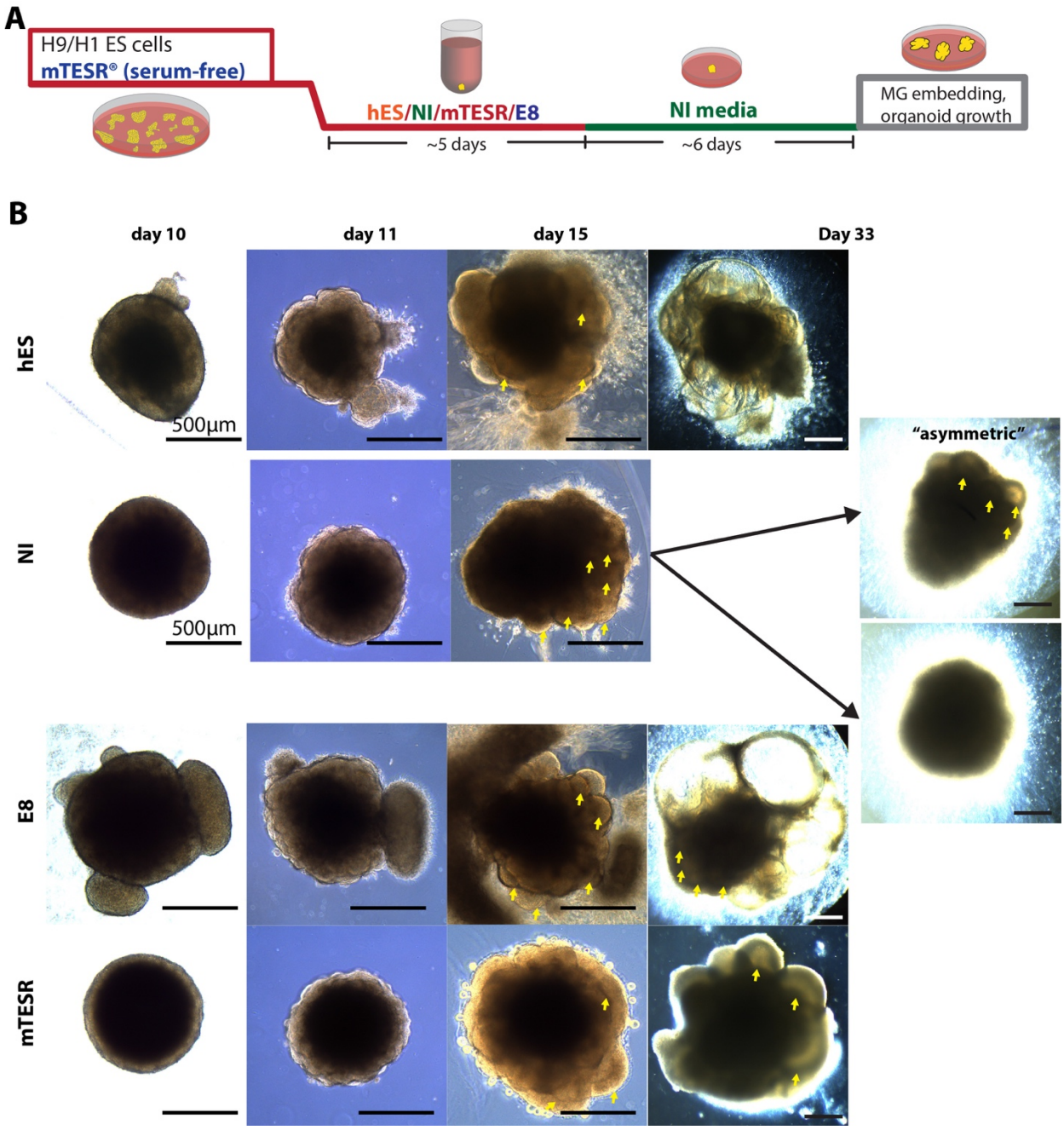

Figure 14: Experimental setup and EB morphology
A) Experimental outline of the following hES medium exchange experiment. hES was replaced with NI, mTESR or E8 medium. After day 5-6, the EBs were cultured in NI medium and the protocol was proceeded as usual. B) Representative development of hES, NI, E8 and mTESR-derived organoids. hES, NI, E8 and mTESR derived EBs/organoids show significant differences in their emergence. hES-derived EBs did show expanded neuroepithelia on day 10 and stereotypic budding after Matrigel embedding (yellow arrows on day 15). However, on day 33 all previously observed rosette-like structures differentiated into cyst structures and no neuronal rosettes were observed. NI-derived EBs did not show a pseudostratified structure before Matrigel embedding and did also not show strong morphological changes after Matrigel embedding. However, on day 15 neuronal rosettes were observable (yellow arrows). NI-derived EBs in multiple batches showed the emergence of 2 different groups of organoids. While one group remained small and developed high levels of processes into the Matrigel, the other group depicted asymmetric organoids with one side with big rosettes (yellow arrows) and the other side looking similar to the first group, or developing cysts. Quantifications showed an almost 50:50 split between polarized (22 organoids) and unpolarized organoids (24) in 2 independent batches of 46 NI-derived organoids. E8 derived EBs showed bud outgrowth of the

EB before Matrigel embedding. After Matrigel embedding, morphological changes were observable but on similar levels to NI-derived EBs. Later, neuronal rosettes were observable, and on day 33 many organoids were depicting big cyst structures and only few rosettes (yellow arrow). mTESR-derived EBs showed a thin, transparent layer without observable pseudostratified structure on the outside before Matrigel embedding. After Matrigel embedding, morphological changes were also not as observable as in hES-derived EBs. However, on day 15 massive lumen-like buds were observable. On day 33, many regions of big cortical plates could be observed (yellow arrows). Scale bars are 500µm.

Morphological differences from hES, NI, mTESR and E8 derived EBs

As initial readout of proper EB formation, brightfield live imaging of EBs was performed to investigate morphological differences. Strikingly, EB morphology varied tremendously across differently used medium compositions (Figure 14B). While hES derived EBs strongly produced the stereotypic structure of an EB with expanding neuroepithelia on day 10, NI derived EBs never formed this structure. Instead, NI derived EBs developed into a partially transparent EB without observable pseudostratified structure. However, from day 3 on, lumen-like structures were visible in the developing EB (supplemental Figure 6A), and they could faintly be observed also in later EBs. Stainings for n-Cadherin indicated strong epithelization on day 6 old NI-derived EBs and showed many neuronal rosettes in the developing EB (supplemental Figure 6B). E8 derived EBs on day 10 did show similar behavior to NI-derived EBs, but showed high numbers of outside bud formation as well (Figure 14B). Early lumen-like structures could be observed from day 3 on as well (supplemental Figure 6A). mTESR1-derived EBs on day 10 had a slim ring of transparent tissue without pseudostratified structure on the outside of the EB, but were, despite to this ring, completely non-transparent.
After Matrigel embedding, hES-derived EBs showed high levels of budding, as described before (Figure 14B). NI, E8 and mTESR-derived EBs also showed morphological changes after 24h, however they were by far not as strong as in hES-derived EBs. Thus, morphological differences were observable in all medium compositions but were strongest in hES-derived EBs.

Media-dependent orientation of neuroepithelia

Given the big morphological differences in early EB morphology, it was therefore interesting to observe on an immunohistochemistry level whether the EBs of different medium compositions were of neuronal identity, and whether the use of serum-free medium would have an impact on the apical orientation of neuroepithelial cells, if existent. For IHC analysis, we focused on the general neural linage identity marker Nestin, the neural crest marker SOX10 and the apical marker aPKCζ.

Using this marker setup revealed tremendous differences dependent on the medium used. hES showed the classical structure as observed in multiple batches of iPSC and H9 hES-derived EBs (Figure 15A, see also Figure 12A, B). Remarkably, NI-derived EBs before Matrigel embedding did not have

any expression of apical marker aPKCζ on the outside of the organoid (Figure 15B). However, the organoids contained a remarkable number of big primary rosettes which were filling almost the whole EB. Thus, almost the whole EB was highly Nestin positive and of neuronal identity. Interestingly, the organoids did not show high levels of SOX10 positive cells in the inside of the organoid, but very often had a ring of SOX10 positive cells on the outside of the EB. E8 derived EBs showed in parts a similar morphology to NI derived EBs, however the size of their primary rosettes was smaller and they showed large SOX10 positive buds on the outside of the EBs (Figure 15C). mTESR-derived EBs had a ring of Nestin on the outside of the organoid which was comparable to hES-derived EBs, however the ring was thicker than in observable hES-derived EBs. Remarkably, mTESR-derived EBs did neither show primary rosette formation nor a pseudostratified layer of neuroepithelia on the outside. Some aPKCζ expression in the Nestin-positive layer was observable, however much less structured than in the other media derived EBs. mTESR-derived EBs did also not show any SOX10 positive cells.

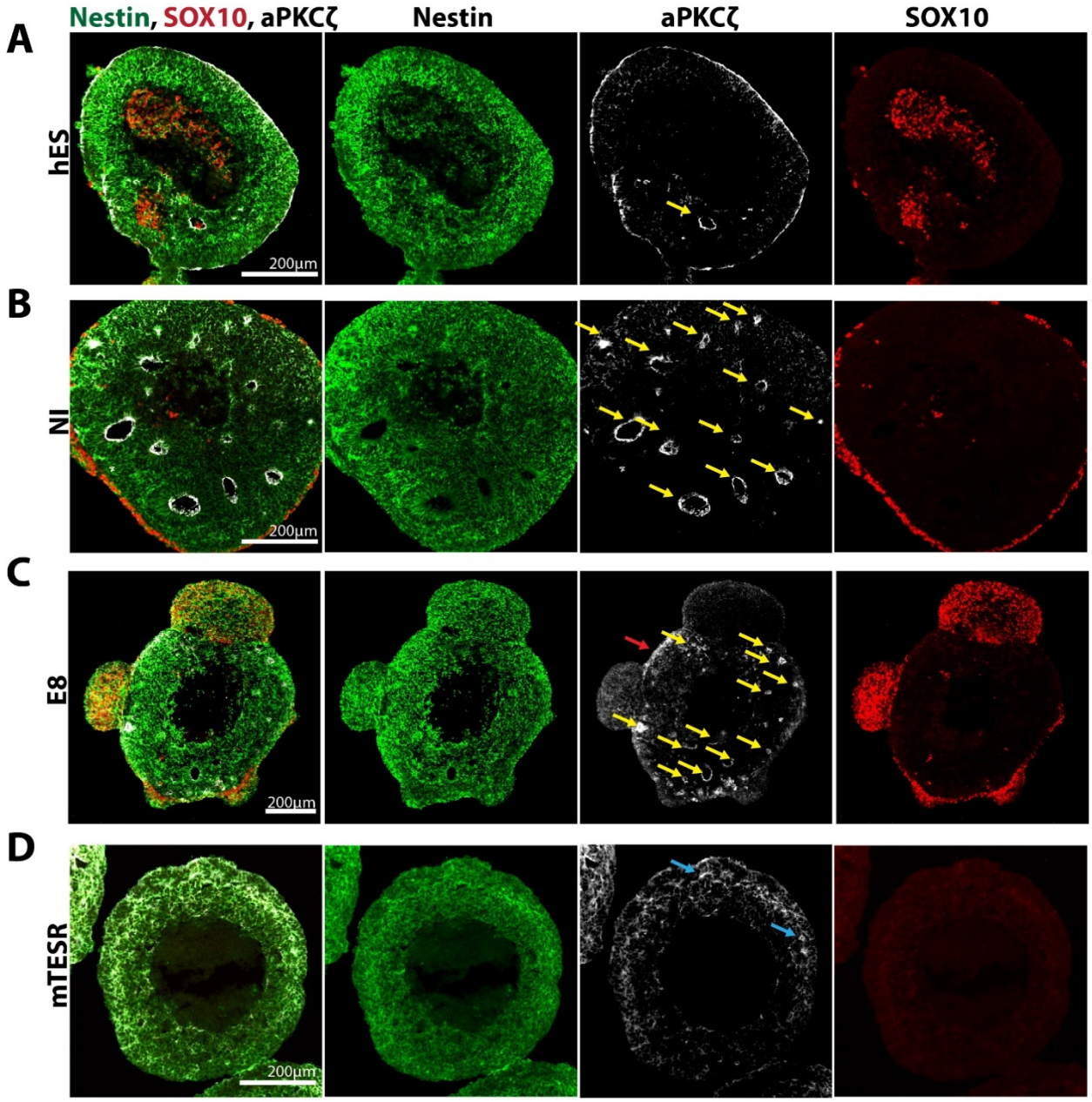

Figure 15: Morphology of hES and NI-derived EBs before Matrigel embedding
A)-D) Confocal spinning disk images of IHC labeled cryosections of H9 EBs on day 10 before Matrigel embedding. Stainings were the neuronal marker Nestin, the neural crest marker SOX10 and the apical marker aPKCζ. and EBs were grown with the regular method (A, hES) or with NI (B), E8 (C) or mTESR (D) as a replacement for the initial hES step. Note that C) E8 was recorded with a 10x and not 20x objective due to the high diameter of the EBs with tissue buds and cropped, but has a different scale bar. N>20 EBs of 2 independent replicates for hES, NI and mTESR and n=10 in one batch of E8-derived EBs. A) hES-derived EBs showed morphology as described before with one primary rosette inside of the EB (yellow arrow). B) NI-derived EBs did not show apical orientation towards the outside of the EB. However, they showed inside rosette formation with radialized Nestin^{+} cells with apical signal (yellow arrows in aPKCζ staining). Additionally, SOX10^{+} neural crest cells were mostly not situated in the inside of the EB, but on the outside. C) E8 derived EBs showed internal rosette formation in the inside of the EB (yellow arrows in aPKCζ staining). Interestingly, aPKCζ signal could also be observed close to the outside of the EB (red arrow), but aPKCζ was less organized in these regions and no pseudostratified/radial structure could be observed in Nestin stainings. Generally, E8 derived EBs had high levels of SOX10^{+} buds on the outside of the EB. D) mTESR-derived EBs did not show hES or NI&E8 stereotypic structures. mTESR-derived EBs had a thick, Nestin^{+} ring on the outside of the EB. However, no radial structure or rosette formation could be observed, and aPKCζ stainings indicated a mesh

of aPKCζ^{+} regions in the Nestin^{+} ring with some centers of higher expression (blue arrows), but no higher organized structure. SOX10^{+} cells were completely absent in mTESR-derived EBs. Scale bars are 200µm.

Media-dependent orientation of neuroepithelia in EBs 24h after Matrigel embedding

After Matrigel embedding, all medium compositions showed a different morphological phenotype again. hES derived organoids showed the stereotypical budding of the neuroepithelial ring and the development of neural rosettes (Figure 16A, see also Figure 13A, B). In contrast, E8 and NI did not show that reorientation of neuroepithelia at all (Figure 16B, C). The only morphological change was the expansion of rosettes into the Matrigel. Interestingly, in both NI and E8 derived organoids, SOX10 signaling decreased after Matrigel embedding. This was the case for the outside SOX10 positive ring in NI derived organoids but could better be observed in the initially highly SOX10 positive buds of E8 derived organoids (Figure 15C), which almost completely lost SOX10 expression (Figure 16C). This could indicate additional effects of the Matrigel onto neural crest cells, but was not further analyzed.
The mTESR-derived organoids showed high numbers of tremendously size-increased lumen formation (Figure 16D). This was interesting as no apical structure with radialized/pseudostratified Nestin^{+} cells was observable before. Thus, Matrigel had a strong impact on the epithelialization of the Nestin-positive neuronal ring on the outside of the EB. Additionally, the lumen in the mTESR-derived organoids were, compared to hES, NI and E8, more continuous and had observable liquid-filled cavities (Figure 16D). This development was unlike the sometimes-occurring big neuronal rosettes in hES-derived organoids (Figure 16A, 13A), which normally did not include liquid-filled cavities 24h after Matrigel embedding.

These results indicate that there are different options for starting rosettes for cortical plate formation in cerebral organoids. The serum-free media NI and E8 promoted epithelialization and the formation of apical layers in the inside of the organoids, thus promoting the formation of primary rosettes very early in organoid development. These rosettes were observable as early as day 2-3 (supplemental Figure 6A) and thus could be a replacing quality control step for NI-derived EBs.
E8, interestingly, partially underwent alternative differentiation and showed high numbers of neural crest buds and thus was not an optimal medium composition. However, as stated before, the supplements of E8, namely FGF2 and TGFβ1, were left out. Both FGF2 and TGFβ1 on the one hand could introduce patterning effects, which was the reasoning for leaving them out, but are also known to have important functions in the expansion of neural stem cells (Israsena et al. 2004; Yun et al. 2008). mTESR-derived EBs showed an intermingled version of EB formation between NI and hES, with no clear apical structure but the classical Nestin-positive ring on the outside of the EB with a necrotic/apoptotic core. However, while in the state before Matrigel embedding no pseudostratified structure was observed, the developing neuroepithelial lumen after Matrigel embedding were by far the biggest compared to all other groups.

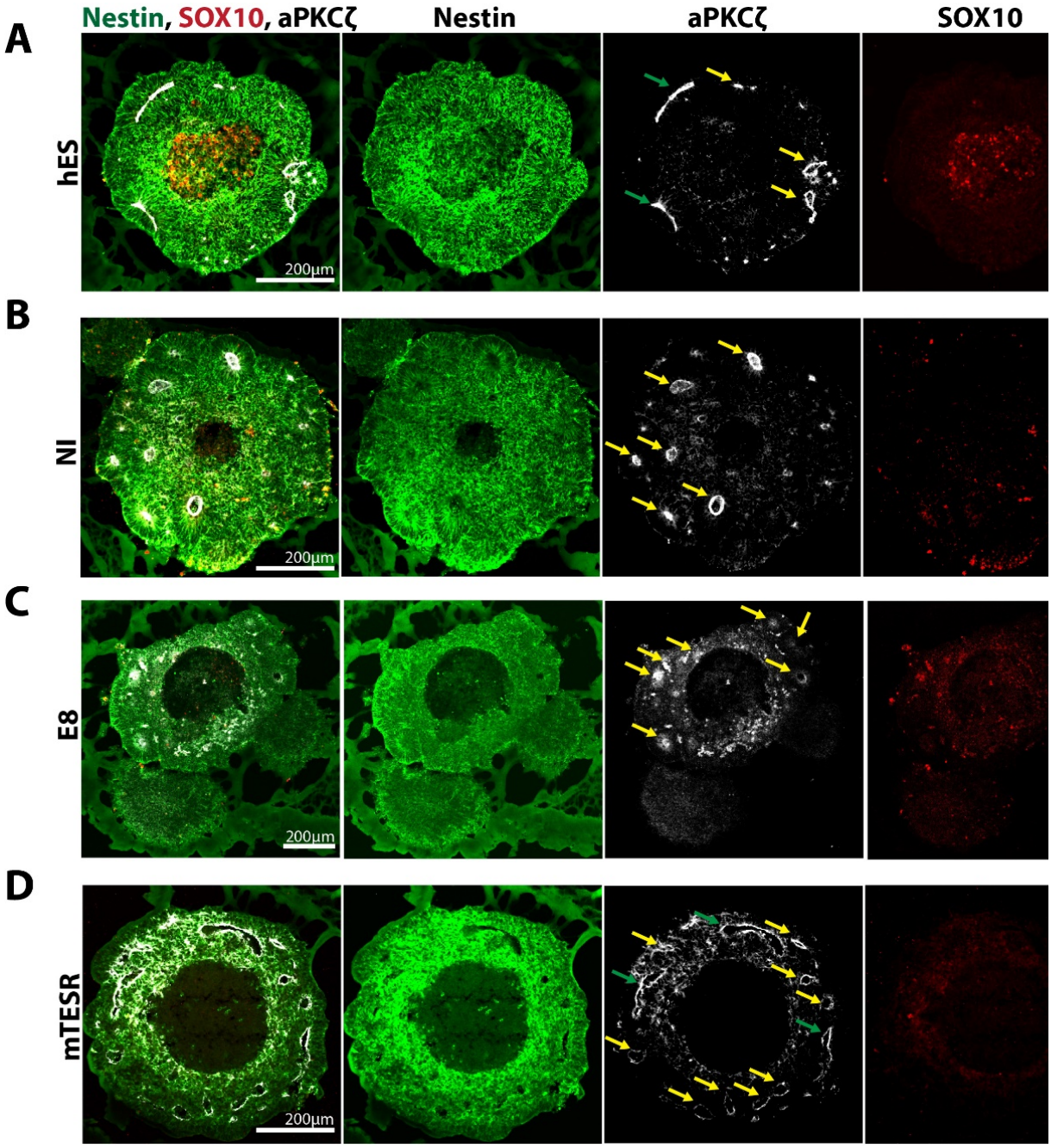

Figure 16: Morphology of hES, NI, E8 and mTESR-derived EBs 24h after Matrigel embedding
A)-D) Confocal spinning disk images of IHC labeled cryosections of H9 EBs on day 11, 24h after Matrigel embedding. EBs were grown with the regular method (A, hES) or with NI (B), E8 (C) or mTESR (D) as a replacement for the initial hES step. Note that E8 was recorded with a 10x and not 20x objective due to the high diameter of the EBs with tissue buds and cropped, but has a different scale bar. N>20 EBs of 2 independent replicates for hES, NI and mTESR and n=12 in one batch of E8. A) hES-derived EBs showed morphology as described before with the formation of neural rosettes (yellow arrows) with partially expanded apical orientation centers (green arrows). B) NI-derived EBs did not show morphological reorientations on both cellular organization (Nestin) or orientation of cells (aPKCζ). The only particular difference was the expansion of the neuronal rosettes into the Matrigel. SOX10 expression could be detected, but was significantly lower compared to EBs before Matrigel embedding, indicated by the non-round outside of the EB. Interestingly, SOX10 signaling was reduced in $SOX10^+$ cells compared to the $SOX10^+$ ring of cells before Matrigel embedding. C) E8-derived EBs were similar to NI-derived EBs. The already existing rosettes did slightly expand into the Matrigel. More strikingly, the initial $SOX10^+$ tissue buds on the outside of the EB completely loose SOX10

expression. Note the different scale bar for E8 derived EBs. D) mTESR-derived EBs underwent a significant morphological change towards a structured neuroepithelia with the formation of many rosettes (yellow arrows), some of them with elongated structure with a liquid-filled cavity (green arrows). $SOX10^+$ cells were absent in both mTESR-derived EBs before and after Matrigel embedding. Scale bars are 200µm.

Organoid development from hES, NI, E8 and mTESR-derived EBs

A limiting factor in interpreting different media-derived EBs is still the later readout, thus appropriate organoid development. Neuroepithelia is a broad term for the formation of multiple downstream neuronal linages, so the initial experimental setup could not indicate whether the medium-dependent production of EBs would also develop into forebrain organoids. A set of embedded organoids was grown to >30 days of culture using the standard Lancaster et al. 2013 organoid protocol, and then analyzed by IHC. Additionally, qPCR of ~50 day old organoids was performed.

On day 33, it was already observable by live imaging of all four used medium compositions, that the hES-derived organoid groups generally differentiated into different tissues (Figure 14B). Massive cyst structures on the outside of the organoid and no rosette-like morphology indicated that no neuronal rosettes were existent in these organoids. E8 derived organoids showed a similar phenotype, however some smaller rosettes were observable in most E8 derived organoids (Figure 14B). NI derived organoids showed two different types of organoids. Several organoids were developing into smaller organoids with many processes which invaded the Matrigel. In contrast, the other group of NI derived organoids developed into polarized organoids with one region containing big rosettes in the inside of the organoid, and another region which was either having no observable structure or cysts. Quantifications in brightfield indicated a polarized structure for 22 organoids and a non-polarized structure for 24 organoids out of 2 independent replicates of 46 organoids (Figure 14B).
mTESR-derived organoids showed massive bud outgrowth with observable, layered structure (Figure 14B). These buds were, unlike the NI derived organoid, mostly developing into the Matrigel.

A representative number of organoids was stained for the expression of forebrain marker FOXG1 and the pan-neuronal marker TUJ1 on day 33. In hES-derived organoids, no neuronal rosettes were observable in Brightfield live imaging (Figure 14B). Thus, H9 hES-derived organoids were excluded from IHC analysis, however they were included in later qPCR. NI derived organoids showed high numbers of FOXG1 positive rosettes in the organoid (Figure 17A). The depicted upper organoid was of polarized structure and showed small $FOXG1^+$ rosettes on the one side and size increased $FOXG1^+$ rosettes on the other side of the organoid. The second organoid shown did not show a polarized structure but showed comparable small $FOXG1^+$ rosette formation.
E8 derived organoids showed few FOXG1 positive rosettes, but overall many rosettes were FOXG1 negative (Figure 17A). Cysts were observable in all observed E8 derived organoids.

mTESR-derived organoids showed massive FOXG1-positive rosettes in multiple organoids (Figure 17A). The buds observable in WF from day 15 on (Figure 14B) were therefore neuroepithelial structures. We could observe rosettes with the size of up to 870µm diameter in mTESR-derived organoids.

Additionally, a qPCR of ~50 day old organoids for the markers FOXG1, TBR1, PAX6 and the ventral markers LHX6 and Nkx2.1 was performed. For E8, one replicate was used for analysis. For mTESR, two independent batches were used for analysis, and for hES and NI-derived organoids, 7 independent batches of organoids were analyzed. NI, mTESR and E8 had expression of FOXG1 as a forebrain marker compared to the multiple batches of hES derived organoids, where just one batch showed detectable FOXG1 expression. The, in combination with FOXG1, dorsal forebrain marker PAX6 was expressed in all groups, besides 2 NI-derived batches and one hES-derived batch of organoids. As hES-derived organoids did not show FOXG1 expression, other $PAX6^{+}$ regions such as cerebellum or optic cup could be represented in the hES-derived organoids. For NI-derived organoids, this could indicate a variability in ventral-dorsal forebrain patterning. Conclusive with that, TBR1, a dorsal forebrain marker was upregulated significantly in some NI derived organoid batches only. Some hES as well as mTESR and E8 derived organoids did also show upregulation of TBR1. The ventral forebrain MGE- marker Nkx2.1 was not be found upregulated in all groups, besides one NI-derived batch which showed strong expression. LHX6, another ventral forebrain marker, was significantly upregulated in some NI-derived organoid batches compared to hES. mTESR showed LHX6 expression in one of two batches, and the one batch of E8 derived organoids did not show expression.

Concluding this data, H9 hES-derived organoids overall showed very low expression of FOXG1, indicating non-forebrain patterning. NI-derived organoids produced forebrain organoids of varying dorsal or ventral forebrain identity. For mTESR and E8, numbers of batches are not high enough for broader classification, however the two batches of mTESR showed altering dorsal or ventral identity, and E8-derived organoids showed a dorsal forebrain-marker specific upregulation.

Thus, all medium compositions besides hES could show the ability of EB production for forebrain organoid formation, despite their varying EB morphology.

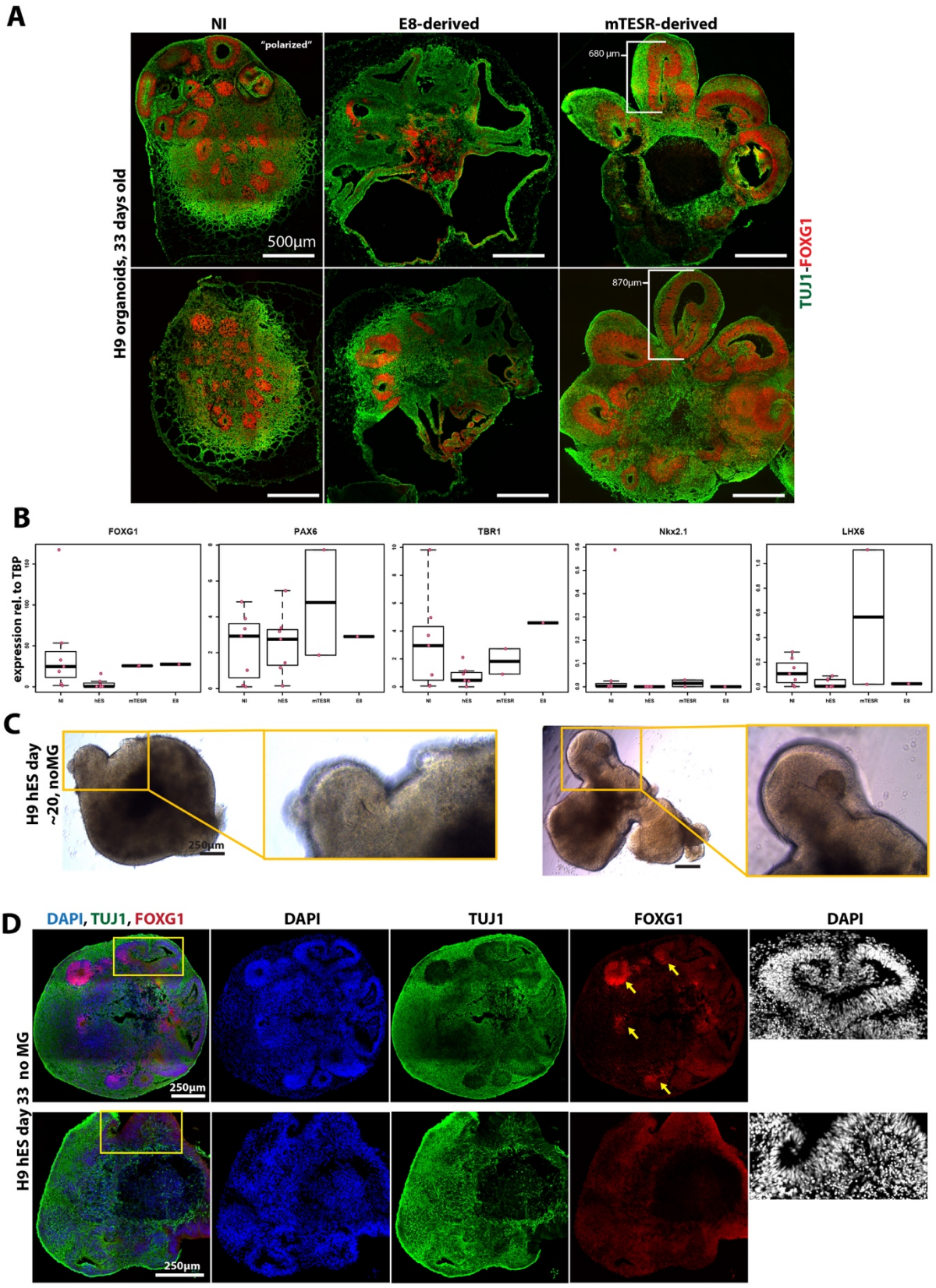

Figure 17: Organoid development on day 33 and ventral-dorsal qPCR characterization.
A) Confocal spinning disk tile scan images of IHC labeled cryosections of H9 EBs on day 33. Organoids were grown with NI (B), E8 (C) or mTESR (D) as a replacement for the initial hES step. Markers were TUJ1 as a pan-neuronal marker and FOXG1 as a forebrain marker. Notable are the high numbers of FOXG1 positive but

small rosettes in NI-derived organoids, with sometimes existent polarity in the organoids in rosette size. In contrast, E8 derived organoids did show cysts and low numbers of FOXG1 positive rosettes. However, $FOXG1^-$ rosettes could also be observed. mTESR-derived organoids showed tremendous buds of FOXG1-positive rosettes which filled out the inside of the emerged buds. Rosette sizes up to 870µm could be observed. B) qPCR of NI, hES, mTESR and E8 derived organoids between day 49 and 55 for dorsal (PAX6, TBR1) and ventral (Nkx2.1, LHX6) forebrain (FOXG1) marker expression. Data presented as relative to TBP expression. Each data point represents an independent organoid experiment with ~8 organoids collected. C) In hES-derived organoids without Matrigel embedding, infolding-like events could be observed on ~ day 20. 4 of 21 organoids of two independent replicates showed this infolding behavior. D) Confocal spinning disk tile scan images of IHC labeled 33 day old hES-derived organoids which were not embedded in Matrigel. Organoids were showing few $FOXG1^+$ rosettes (yellow arrows). However, multiple neuronal rosettes could be observed and infolding-like neural rosettes (DAPI) could be observed in 2 out of 10 organoid sections from 2 different experiments. Scale bars are 500µm (A) and 250µm (C, D)

Neural Rosette formation in Matrigel free Organoids

In none of the before reported primary or secondary rosettes, an invagination-like event could be observed. However, Kadoshima et al. 2014 reported invagination-like folding events in their organoid protocol which they termed “rounding morphogenesis” or “rolling epithelium”. One key difference in this protocol, particularly compared to Lancaster et al. 2013, is the addition of Matrigel as late as day 35 on, without any embedding step of the organoids.

Preliminary data of 12 day old hES-derived EBs showed the beginning of an incurling event in few organoids (Figure 12C), but this process would be disturbed by the step of Matrigel embedding through apical reorientation. To reproduce this rosette structure by Kadoshima et al., hES-derived organoids were not embedded but cultured further in 24well plates with medium exchanges every other day. We followed the standard Lancaster et al. 2013 protocol, but avoided shaking the organoids for reduced tissue damage. Remarkably, on day 20 infolding-like events could be observed in few organoids (Figure 17C). IHC analysis for TUJ1, FOXG1 and DAPI on day 33 revealed rosettes with a similar morphology as reported by Kadoshima et al., but in rosettes with no or just partially forebrain identity. Thus, a ventral-dorsal gradient with rounding morphogenesis in dorsal regions was not analyzed.

Parallel grown NI-derived organoids without Matrigel embedding did not show these rolling epithelium-rosettes (0 of 27 organoids of 2 independent replicates in whole mount live imaging on day 20) and did also not show rounding morphogenesis-like rosettes in IHC stainings (0 of 13 organoids of 2 independent replicates, 33 days old) (data not shown). As NI-derived EBs already have neuronal rosettes before Matrigel embedding, the formation of rolling epithelium is also not expected.

Concluding, folding events of rosettes as reported by Kadoshima et al. 2014 could also be observed in hES-derived organoids without Matrigel embedding.

Discussion

With this assessment of neural tube formation in cerebral organoids, multiple questions in the organoid field could be addressed. First, it was unknown how the rosettes in cerebral organoids emerge. Interestingly, two different origins of neural rosettes were observable: one type which was sometimes already existing in the inside of the EBs in the more frequently non-pseudostratified tissue, which we termed "primary neuronal rosettes" and the expanded outside rosettes originating from the remarkable level of morphogenesis due to Matrigel embedding. This process, however, can be seen more as an artificial process: the strong basal signaling of the extracellular matrix-based Matrigel induces the cells to undergo a tremendously fast change in their apical orientation and to re-form an expanded neuronal rosette on the outside of the EB. In this work, they will be termed "secondary neuronal rosettes". When comparing these two processes of neural rosette formation with the event of neural tube formation, it should be mentioned that especially the primary rosette formation showed more similarities to the event of secondary neurulation, where cells spontaneously accumulate to a neural tube-like structure – a process termed "canalization"- without any invagination-like events (Copp et al. 2014). This process occurs e.g. in mouse, and probably human, spinal cords from around somite 35 on and originates from pluripotent cells from the tail bud, which epithelialize (Gilbert 2000; Copp et al. 2014). As in fish, neural tube formation occurs completely through secondary neurulation (ibid, 2000), the formation of a tube/rosette-like structure could potentially be an intrinsic motivation or "ground state" of neural precursor cells or epithelial cells. We speculate that the reorientation of cells induces the search of cells for a new apical orientation, and the highest proximity for all cells of the neuroepithelia is approximately the middle of the neuroepithelia layer. However, further analysis with higher temporal resolution of the apical complex could provide deeper insights in the reorientation of cells, and the fundamental mechanisms involved in this process. The information of emergence of rosettes in cerebral organoids is of high importance for the question of neural tube closure in organoids which was speculated, and the characterizations before and after Matrigel embedding experiment together with time-lapse movies revealed that no such closure event happens in the protocol by Lancaster et al 2013.

We next addressed the question, whether the apical orientation of the apical-outside neuroepithelial ring could be modified. During neural tube formation, the neuroepithelia is comprised of a consistent apical-basal orientation which is initially also existent in the initial EBs, however the step of Matrigel embedding induces an artificial re-orientation. Contrary, primary rosettes were sometimes situated in the inside of the pseudostratified layer. An organoid comprised of only primary rosettes would be of interest in neural tube studies targeting the apical orientation of neuroepithelia, and where a re-orientation of apical orientation could be problematic. We speculated that low-protein, serum and serum-replacement free medium could have an impact in the apical orientation of neuroepithelia. With the usage of three different medium compositions for the first 5-6 days of EB formation we could show

the neural stem cells in an emerging EB are highly modifiable in their orientation, and that this orientation is set within the first days of EB emergence. Using NI and E8 without supplements, the initial formation of primary rosettes and no pseudostratified neuroepithelia with apical orientation towards the outside of the EB could be observed. Remarkably, lumen formation in NI and E8 derived organoids was observable on EBs already on day 3, which is earlier than any other EB-based neural rosette differentiation protocols. Thus, the neural rosette formation from NI and E8 derived organoids was determined in very early development and thus can be seen as consistent neural rosette structure even in later organoid developmental stages. Interestingly, on day 6 almost the whole EB was filled with neuroepithelial cells and only few Brachyury^{+} cells were observed, indicating an almost only neuroepithelial tissue. Further experiments will have to show, whether an NI-derived organoid is really undergoing the step of an embryoid body with all three germ layers, or if NI medium promotes a direct transition to neuroepithelia. In contrast, the usage of mTESR did not induce the formation of any neuroepithelial structure prior to the Matrigel embedding step. However, the remarkable size of the neuroepithelial rosettes are worth further investigations. Speculating here, the proceeded cultivation of stem cells in their initial medium could have proliferative effects on the EBs, which result in an expanded neuroepithelia and thus directly in increased neuroepithelial buds.

Of additional interest in the medium comparisons is the low-protein, defined composition of both NI and E8 medium. It has been reported before, that high KOSR levels significantly reduced EB yields (Chaudhry et al. 2008), and the high batch-to-batch variability in FBS with the problem of miss-differentiations lead to a big effort in finding defined serum replacements for cell culture (Tekkatte et al. 2011; Nestor et al. 2013). Both KOSR and FBS therefore may have implications in appropriate differentiation towards forebrain neurons, thus a sparing of these components could be useful. Removal of xenogeneic supplements may also have interesting applications particularly in medical applications: one of the main limitations in using differentiated tissues from embryonic or induced pluripotent stem cells is the addition of xenogeneic additives such as FBS and KOSR (Albumin), which can have implications in patients and thus is not allowed following GMP to produce e.g. cell therapies. Thus, removal of these xenogeneic ingredients is an important step towards usability of stem cells for therapeutic questions in humans.

It has to be mentioned that, besides protein levels and serum/serum replacement supplements, multiple different variables in medium compositions can have a function in proliferation, differentiation and orientation of cells. Particularly growth factors which are often added to stem cell medium, such as FGF2, TGF-β and insulin, may have an influence on the further differentiation of pluripotent stem cells. Medium compositions like mTESR1, which are a “black-box” without any possibility to modify the medium can in this consideration be a problem, as problematic factors cannot be left out. Because of this issue, it can be hard to impossible to narrow down a particular effect of a medium to a certain

component, which would be needed in the definition of a new medium. Thus, any of the previous experiments have to be seen as a first try to achieve the above-mentioned goals, but an interpretation of the function of certain factors – even to protein sources – is with the presented experimental setup, not possible. Further experiments to answer these questions could be e.g. the usage of NI and BSA/KOSR/FBS for further specification of the components impact on apical orientation of neuroepithelia.

As a second step, we also reproduced the folding-like rosettes reported by Kadoshima et al., 2014. While the event of Matrigel embedding in the original Lancaster et al. protocol induces artificial rosette formation, Kadoshima et al. 2014 could show that the step of Matrigel embedding in organoid development is not a necessity. In their organoid protocol, the apical-outside neuroepithelia can proliferate further and induces an infolding-like curling at the end of apical-outside rosettes. This effect is somewhat similar to neural tube formation on a cellular level, as Kadoshima et al. could even report that the infolding areas would be of dorsal identity, whereas the non-folding areas would be ventral – a cellular identity, which would remarkably depict the starting invagination structure *in vivo*. We could show that hES-derived organoids which were not Matrigel embedded showed this infolding-like behavior in a similar level to Kadoshima et al. 2014. However, as hES-derived organoids did develop forebrain identity rosettes at very low numbers, and none of them showed a folding-like event, the question of dorsal and ventral identity of cells was not addressed.

Summarized, two different states of consistent neural tube-like structures could be observed in cerebral organoids using protocol modifications: the emergence of primary neuronal rosettes in very early EB development which were contributing to later cortical plate development without structural rearrangement. These primary neuronal rosettes may be of similar mechanistical emergence as secondary neurulation structures, however further investigations would have to be done for this question. Secondly, invagination events in organoids can under certain conditions occur and may be considered as neural tube closure-like events with similar cellular proliferation profiles. The cellular identity of neuroepithelia in cerebral organoids is reported to be similar to neural tube neuroepithelia (Camp et al. 2015b) and thus could be used to study cellular behavior in a neural tube-like tissue complex. However, axial information (dorso-ventral, anterio-posterior) are just rudimentarily observed in rosettes in cerebral organoids (Renner et al. 2017), thus the limitation of studying neural tube closure in cerebral organoids must be clearly seen on cellular and organizational levels and on biological questions which address these elements.

Chapter III: Development of a scalable organoid platform

Author contributions

The hydrogel project originates from a collaboration of Tamás Kovács in the Knoblich lab with Nathalie Brandenberg and Silke Höhnel from the Lutolf Lab at EPFL, Swiss and was continued by the author after Tamás Kovács left IMBA.

Introduction

The cerebral organoid method is comparatively work intensive: a batch of initially 200 organoids will take roughly 10 hours or more work expenditure until the step of Matrigel embedding, without deeper screening of the growing EBs or later organoids and without proper quality controls. As many manual steps are needed, further scalability is hard to archive. We try to address these questions with the development of an all-in-one platform. The results of these experiments cannot be seen as finalized results, but just as intermediate steps towards a better usability of the organoid method and a faster, more reliable protocol. Due to this intermediate character, the extent of the experiments and of some conclusions may not be on a level which would be necessary for statements of fundamental evidence and can be considered as work in progress. Also, we will just discuss the current, positive results in this project and will not discuss the history of the project, which involved testing of multiple different well shapes, conditions and protocols and would go beyond the capacity of this thesis.
We were interested in developing a method for growing cerebral organoids which would allow to reduce the manual steps as far as possible. The most time-consuming steps in the organoid method are the making of EBs, the regular feeding of them, quality controls (dependent on batch quality) and the embedding in the Matrigel droplet (~4h) for a 2x 96well plate organoid batch. Together with the Lutolf laboratory in Switzerland (EPFL), we are trying to develop a system for organoid growth which improves this process in terms of speed, scalability and maintenance levels. In this project, we want to grow organoids on a defined polyethylenglycol (PEG) hydrogel structure which we want to introduce as an all-in-one platform for organoid cultivation. For this purpose, different requirements to structure and shape of the hydrogel must be considered:
a) easy seeding of cells
b) robust and homogenous EB growth
c) easy, reduced feeding maintenance of EBs
c) simplified Matrigel embedding step
d) handling of the organoids/ reduced feeding rhythm of later organoids

Additionally, a substrate which would allow modifications of structural stiffness and surface modifiability would be favored. The defined aim is the generation of a universal platform for organoid growth, which can be used in the steps of EB formation until the collection of organoids and should reduce working time by far. Additionally, it has been thought to implement patterning modifications at a later stage of this project, which would potentially allow the easy generation of brain region-specific organoids.

Results

PEG-derived wells support EB formation in hES and NI medium

As substrate material, we decided to use polyethylene glycol (PEG) based hydrogel. PEG is a biocompatible substance frequently used in bioengineering and is highly modifiable in stiffness, temporal stability and derivatization such as covalently attaching proteins onto the matrix (Hwang et al. 2009; Gjorevski et al. 2016; Lindborg et al. 2016). Initially, we investigated whether organoids can develop from a PEG hydrogel platform. To address this question, very small wells in hydrogel structures were used for organoid growth. Initially, very similar to approaches using microwells for upscaled EB growth were tried out (Hwang et al. 2009; Pettinato et al. 2015). However, this was not very successful as the small structures did not hold the EBs in place properly and they were easily washed out even when carefully moving these plates (data not shown). This was a particular problem as EBs for cerebral organoid development have to be hold in place for up to 13 days; a time period which was also not achieved by any microwell solution. We therefore tried to enlarge the well size to a diameter of 3mm and increased the well walls, which would a) allow longer cultivation of the EBs and b) would avoid the EB from floating. The resulting structure is somewhat complex, containing 7 wells in a PEG dome with a stabilizing PDMS ring on the outside, positioned in a well of a 6well plate (Figure 17A, B).

In the first trial of this design, we tried out different protocols and growth conditions. It was known from previous plate designs, that hES and NI medium would be stable enough for cultivation more than the usually 2-3 days in 96well plates. Cells were seeded for the whole dome structure at once, containing 7x9000 cells in 200µl of medium. After cells were aggregated on the bottom of the well structure (~20min), EB formation medium was added to the wells. Generally, 7ml of medium per well were used. We tried a) the standard hES-derived organoid protocol, with an incubation in hES-medium for 6 days and subsequent cultivation in NI, without medium exchange until Matrigel embedding. Additionally, we tried to grow NI-derived EBs with b) medium exchange on day 6 and c) no medium exchange at all until Matrigel embedding. Thus, while in one group the NI medium was exchanged completely once, we also tried to not exchange the NI medium at all for 10 days of culture. After

Matrigel embedding, the organoids were proceeded to grow on 6cm plates to obtain a clear readout of EB formation capacities of the hydrogel wells.

As readouts, IHC of EBs before Matrigel embedding and IHC of organoids on day 33 were performed. The analysis of EBs before Matrigel embedding should provide a precise morphological readout of EB formation, and a similar marker set as in chapter 2 for EB dynamics was used. The later readout was restricted to morphological (DAPI, TUJ1) and forebrain identity (FOXG1).

When comparing EBs using the regular protocol with hES medium or NI medium towards the hydrogel-derived EBs, moderate differences could be observed. While the 96well plate NI-derived EBs did show a transparent ring on the outside, the hydrogel-derived EBs were slightly bigger and differed mildly in their morphology (Figure 17C). However, they were similar to previously grown NI-derived EBs (Figure 14). hES-derived EBs grown on 96well-plates showed outgrowing buds from the EBs in quite high levels, which was not observable on hydrogel derived hES EBs. They showed a strongly transparent layer of neuroepithelia on the outside of the EB.

The IHC analysis is based on the early EB characterization described in chapter II. IHC of hydrogel derived NI and hES EBs showed a stereotypical formation of a $Nestin^+$ pseudostratified, apical ($aPKC\zeta^+$) outside neuroepithelia in hES-derived EBs with $SOX10^+$ cells inside of the EB, whereas the NI-derived EBs showed the formation of rosettes and had $SOX10^+$ cells on the outside of the EB (Figure 17D). N-Cadherin and β-catenin stainings confirmed this structural orientation (data not shown). The overall structure of both hydrogel hES-derived EBs as well as hydrogel NI-derived EBs did reassemble a hES and NI-stereotypical structure and thus passed the initial IHC quality control.

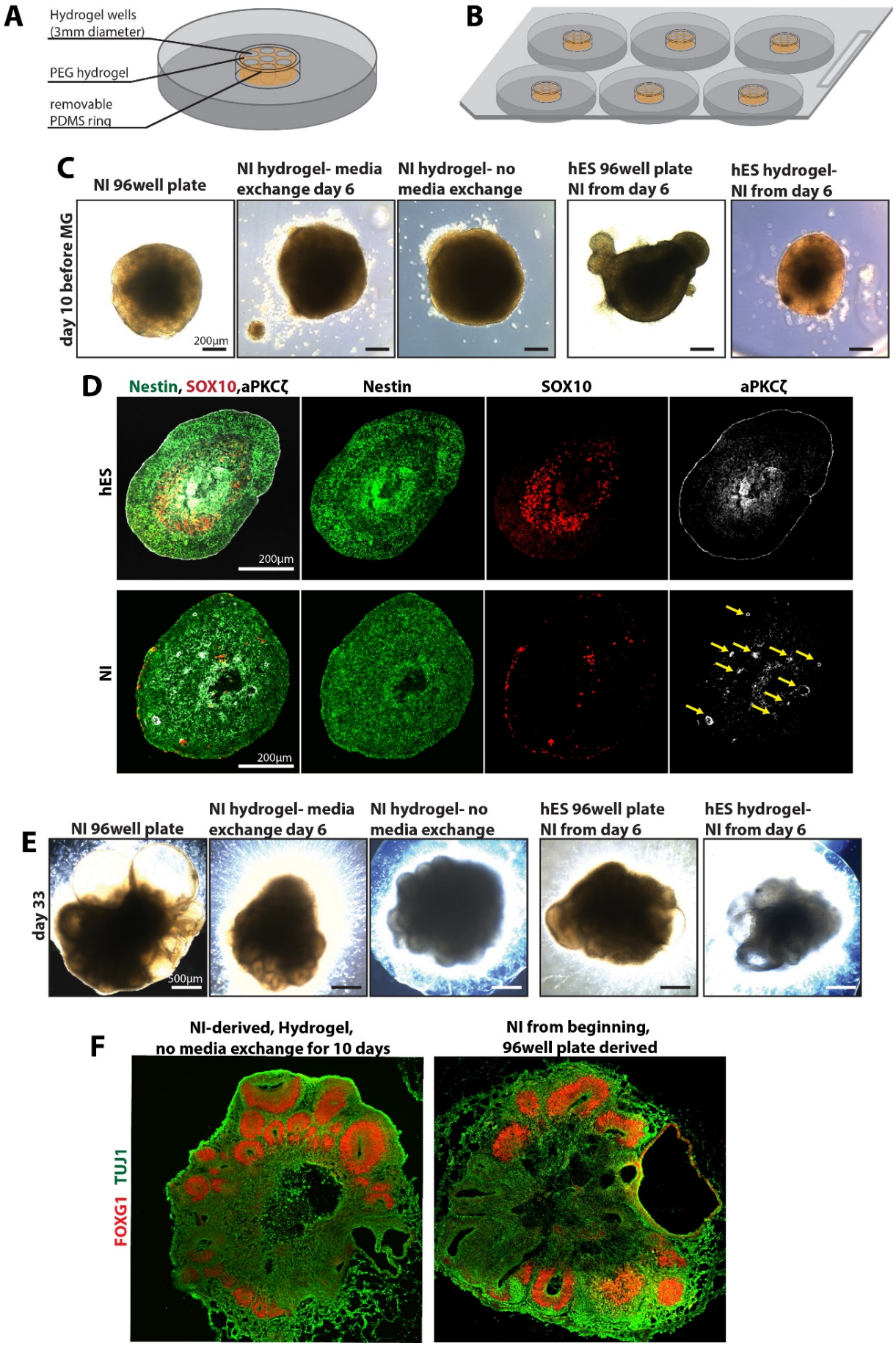
A
Hydrogel wells
(3mm diameter)
PEG hydrogel
removable
PDMS ring
B
C
NI 96well plate
NI hydrogel- media exchange day 6
NI hydrogel- no media exchange
hES 96well plate NI from day 6
hES hydrogel- NI from day 6
day 10 before MG
200µm
D
Nestin, SOX10,aPKCζ
Nestin
SOX10
aPKCζ
hES
NI
200µm
200µm
E
NI 96well plate
NI hydrogel- media exchange day 6
NI hydrogel- no media exchange
hES 96well plate NI from day 6
hES hydrogel- NI from day 6
day 33
500µm
F
NI-derived, Hydrogel, no media exchange for 10 days
NI from beginning, 96well plate derived
FOXG1 TUJ1

Figure 18: Hydrogel derived cerebral organoids
A) Well design for EB growth. A PEG Hydrogel dome has 7 wells of 3mm diameter situated in a circular structure in the middle of the plate. A (removable) PDMS ring stabilizes this structure. B) Plate design of a 6well plate for cerebral organoid growth. C) EBs from the standard method (hES 96 well), the NI-derived method (NI 96well) versus hydrogel-derived EBs, either cultured in NI with medium exchange on day 6 or without medium exchange until Matrigel embedding, or using hES medium for the first 6 days. D) IHC for Nestin, SOX10 and aPKCζ. hES-derived EBs showed a stereotypical radial pseudostratified neural stem cell layer on the outside of the EB, which was comparably thick. NI-derived EBs showed stereotypic inside rosette formation with radially organized cells around the aPKCζ^{+} lumen (yellow arrows in aPKCζ staining). Note that in the control batch, rosette number and size was as well smaller than in previously reported NI-derived organoids. E) Brightfield imaging of day 33 old control ("96well") vs. hydrogel derived organoids. NI derived organoids showed asymmetric as well as round organoid development. F) Representative IHC of hydrogel, NI-derived organoids for the pan-neuronal marker TUJ1 and the forebrain marker FOXG1. Scale bars are 200µm (C, D) and 500µm (E, F).

Hydrogel derived EBs produce organoids indistinguishable to control groups

After Matrigel embedding, the EBs were cultured in 6cm plates with medium changes every 3-4 days according to the regular protocol. 96well NI-derived organoids on day 33 showed cyst outgrowth in medium levels, while neural rosette formation was still observable (Figure 17E). The hydrogel plates did not show cyst development in both NI with medium exchange and NI without medium exchange, but showed the development of polarized and unpolarized organoids with observable neural rosettes. The 96well hES-derived organoids did show rosette formation in some organoids, which was also the case for hydrogel hES-derived organoids, however the overall number of these rosettes and the overall organoid morphology were not promising and an IHC analysis was not performed. IHC of NI-derived organoids from both the standard protocol and hydrogel-derived organoids showed indistinguishable development from both platforms (representative organoids in Figure 17F).

Summarized, we could show that using the hydrogel plates already fulfills several criteria which are necessities for upscaling. We could a) easily seed many EBs at once, b) allow robust and homogenous EB growth c) could on a preliminary level show that feeding of the EBs during the first 10 days may not be necessary and d) derive organoids from the hydrogel plates, which were non-discriminable from organoids grown with the regular Lancaster et al. 2013 cerebral organoid protocol.

Discussion

With the current developments in the hydrogel project, we could already address all required questions on the side of EB development. In a next step, we will address the question of embedding. For this, we also plan to design an artificial Matrigel composition (Lindborg et al. 2016; Gjorevski et al. 2016), consisting mainly of PEG, which would allow the organoid protocol to be running in a defined environment and hopefully make the embedding step easier and up-scalable. A big advantage of the

current design is, that the numbers of wells in the PEG dome can be increased dependent on plate size and also well numbers above 10 per dome should be easily possible. These steps would reduce especially the EB making and feeding process, which, together with new method enhancements (see results chapter 1.3), would reduce working costs further. Another advantage of the current design would be its all-in-one platform, which makes the multiple platform changes (96well plate, 24well plate, 6cm or 10cm plates) obsolete and, on top of that, could potentially also increase oxygen supply which is thought to be an issue particularly in 96well plates (unpublished data).

Material & Methods

Protocol: The cerebral organoid method based on Lancaster et al. 2013

Low FGF hES media		
250ml	**500ml**	
200ml	400ml	**DMEM/F12**
50ml	100ml	**KOSR**
7.5ml	15ml	**ES-quality FBS**
2.5ml	5ml	**GlutaMAX**
2.5ml	5ml	**MEM-NEAA**
1.75µl	3.5µl	**2-Mercaptoethanol**
Filtered using 22µm filter bottles		
Store at 4˚C up to 2 weeks		
Variations:		
-hES media **+ in house FGF2** for stem cells (add 1:1000 FGF2 just before use)		
-hES media **+bFGF** (Peprotech) (1:2500) and **Rock Inhibitor Y-27632** (**RI**, 1:100) for EB formation (add just before use!). RI working solution: 5mg on 2.96ml H_2O.		
-hES media w/o additional supplements for EB growth before NI		

MEF media		
250ml	**500ml**	
225ml	450ml	**DMEM *(No F12!)***
25ml	50ml	**FBS (stem cell ("SC") quality)**
2.5ml	5ml	**GlutaMAX**
Filtered using 22µm filter bottles		
Store at 4˚C up to 2 weeks		
MEF feeders:		
MEF CF-1 IRR from GlobalStem® Mouse Embryo Fibroblasts		

mTESR	
400ml	**mTESR 1 Basal Medium (4˚C)**
100ml	**mTESR 1 5X Supplement (-20˚C)**
Filtered using 22µm filter bottles	
Aliquot in 40ml and freeze until use.	

Improved NeuroDMEM-A		
250ml	**500ml**	
125ml	250ml	**DMEM/F12**
125ml	250ml	**Neurobasal4**
1.25ml	2.5ml	**N2 supplement**
5ml	**10ml**	**B27 - vitamin A supplement**
62.5µl	125µl	**Insulin**
87.5µl	175µl	**1:100 (!!) 2ME in DMEM/F12**
2.5ml	5ml	**Glutamax**
1.25ml	2.5ml	**MEM-NEAA**
2.5ml	5ml	**Penicillin+Streptomycin (P/S)**
Filtered using 22µm filter bottles		
Store at 4˚C up to 2 weeks		

Improved NeuroDMEM+A		
250ml	**500ml**	
125ml	250ml	**DMEM/F12**
125ml	250ml	**Neurobasal**
1.25ml	2.5ml	**N2 supplement**
5ml	**10ml**	**B27 + vitamin A supplement**
62.5µl	125µl	**Insulin**
87.5µl	175µl	**1:100 (!!) 2ME in DMEM/F12**
2.5ml	5ml	**Glutamax**
1.25ml	2.5ml	**MEM-NEAA**
2.5ml	5ml	**Penicillin+Streptomycin (P/S)**
0.745g	1.49g	HEPES (in DMEM?)
2.5ml	5ml	Vitamin C solution (40mM stock)
Filtered using 22µm filter bottles		
Store at 4˚C up to 2 weeks		

Special Media:

Colagenase IV solution		
50ml	**100ml**	
50mg	100mg	**Collagenase IV**
50ml	100ml	**DMEM/F12**
Filtered using 22µm filter bottles		
Store at 4˚C up to 2 weeks or -20˚C for 6months		

Gelatin coating solution		
250ml	**500ml**	
0.25g	0.5g	**Gelatin**
250ml	500ml	**sterile water for tissue culture**
Filtered using 22µm filter bottles		
Store at 4˚C up to 1 year		

Differentiation (Diff) media		
250ml	**500ml**	
125ml	250ml	**DMEM/F12**
125ml	250ml	**Neurobasal**
1.25ml	2.5ml	**N2 supplement**
2.5ml	5ml	**B27 +/- vitamin A supplement**
62.5µl	125µl	**Insulin**
87.5µl	175µl	**1:100 (!!) 2ME in DMEM/F12**
2.5ml	5ml	**GlutaMAX**
1.25ml	2.5ml	**MEM-NEAA**
2.5ml	5ml	**Penicillin+Streptomycin (P/S)**
Filtered using 22µm filter bottles		
Store at 4˚C up to 2 weeks		
Variations:		
Diff-A and Diff+A (choose correct B27 supplement!) Improved Diff-A and Diff+A: see next page		

Neural Induction (NI) media		
250ml	**500ml**	
250ml	500ml	**DMEM/F12**
2.5ml	5ml	**N2 supplement**
2.5ml	5ml	**GlutaMAX**
2.5ml	5ml	**MEM-NEAA**
250µl	500µl	**Heparin solution**
Filtered using 22µm filter bottles		
Store at 4˚C up to 2 weeks		

MEF freezing media		
10ml	**50ml**	
5ml	25ml	**DMEM/F12**
4ml	20ml	**FBS (stem cell ("SC") quality)**
1ml	5ml	**DMSO**
Filtered using 22µm filter bottles		
Store at 4˚C up to 2 weeks or -20˚C for 6months		

2x iPS Freezing Media		
10ml	**50ml**	
8ml	40ml	**FBS (stem cell ("SC") quality)**
2ml	10ml	**DMSO**
Filtered using 22µm filter bottles		
Store at -20˚C up to 6 months		

2x ES Freezing Media		
10ml	**50ml**	
6ml	30ml	**FBS (stem cell ("SC") quality)**
2ml	10ml	**hES media**
2ml	10ml	**DMSO**
Filtered using 22µm filter bottles		
Store at -20˚C up to 6 months		

Dispase solution		
50ml	**100ml**	
25mg	50mg	**Dispase**
50ml	100ml	**DMEM/F12**
Filtered using 22µm filter bottles		
Store at 4˚C up to 2 weeks or -20˚C for 6months		

Reagent list

mTeSR1 medium: (Stem Cell Technologies, cat. no. 05850) DMEM/F12: (Invitrogen, cat. no. 31330-038) Knockout serum replacement (KOSR): (Invitrogen, cat. no. 10828-028) GlutaMAX: (Invitrogen, cat. no. 35050-038) Sterile PBS (DPBS without Ca2+/Mg2+; Thermo Fisher Scientific, cat. no. 14190-169) Sterile H2O (Water for Injection (WFI) for Cell Culture; Thermo Fisher Scientific, cat. no. A1287301) Penicillin/Streptomycin (P/S): (Sigma, cat. no. P0781) Minimal essential medium non-essential amino acids (MEM-NEAA): (Sigma cat. no. M7145 2-Mercaptoethanol (2-ME): (Merck, cat. no. 8057400005) bFGF: (FGF2; Peprotech, cat. no. 100-18B) Collagenase Type IV: (Gibco, cat. no. 17104-019) hESC-quality FBS (it should be tested for compatibility with hESCs; Gibco, cat. no. 10270-106)	Heparin: (Sigma, cat. no. H3149) Rock inhibitor Y27632: (Millipore, cat. no. SCM075) N2 supplement: (Invitrogen, cat. no. 17502048) B27 without vitamin A supplement (- Vit. A): (Invitrogen, cat. no. 12587010) B27 with vitamin A supplement (+Vit. A): (Invitrogen, cat. no. 17504044) Neurobasal medium: (Invitrogen, cat. no. 21103049) Insulin solution: (Sigma, cat. no. I9278-5ML) Matrigel, hESC-Qualified: (Corning, cat. no. 354277) Matrigel: (Corning, cat. no. 354234) EDTA: (Sigma-Aldrich, cat. no. E6758) IWP-2 (IWP2): (Sigma, cat. no. I0536) Smoothened agonist (SAG): (Millipore, cat. no. 566660) Cyclopamine A (CycA): (Calbiochem, cat. no. 239803) In house bFGF for stem cell culture (hES medium)

Equipment list

Incubators: New Brunswick, model Galaxy 170s Biological safety cabinet: Faster Safefast Premium 212 6-well tissue culture dishes: Eppendorf, cat. no. 0030720113 Filter pipette tips (P1250, P300, P20 P10): Biozym, cat. no. VT0270, VT0250, VT0220 Tubes: 1.5-ml size; Fisher Scientific, cat. no. 05-408-129 Stericup 0.2-µm filter unit (500 and 250 ml): Millipore, cat. no. SCGVU02RE& SCGVU05RE) Steriflip 50 mL filter: Millipore, SCGP00525 U-bottom ultra-low attachment plates, 96 well: Corning, cat. no. 7007 Conical tubes, 15 ml: Greiner Cell Star, cat. no. 188271 Parafilm: Sigma-Aldrich, cat. no. P7793 Tissue culture dish, 60 mm: Eppendorf, cat. no. 00307701119 Tissue culture dish, 100 mm: Eppendorf, cat. no. 0030702115 Orbital shaker: Infors Celltron orbital shaker, cat. no. INF-69222	2 mL Aspiration pipettes: Falcon, cat. no. 35755 Serological pipettes, 5, 10, 25 ml: BD Falcon, cat. no. 357543, 357551, 357525 Water bath, 37 °C: Fisher Scientific, Isotemp water bath, model 2333, cat. no. 15-462-21Q Inverted tissue culture microscope: Zeiss, model Axio Vert.A1 Cell counter: Invitrogen, Countess II together with: Countess Cell Counting Chamber Slides, Thermo Fisher Scientific, cat. no. C10228 (package includes Tryphan blue) Sterile standard forceps: Fine Science Tools, cat. no. 11000 Vacuum pump: Integra, Vacusafe Tissue embedding mold: Thermo Fisher Scientific, cat. no. 1220 Low-melt agarose: Biozym, cat. no. 850080 Glass bottom dishes: ibidi 35µm, high µ-Dish, cat.no.81158

Cell lines used

- iPSCs: Feeder-dependent human induced pluripotent stem cells (hiPSCs) were ordered from Systems Biosciences, cat. SC101A-1) including pluripotency verification and contamination-free.
- MEF feeder cells used are from MTI-GlobalStem, cat.6001G.
- H9 feeder free (FF) human embryonic stem cells (hESCs) were obtained from WiCell with verified normal caryotype and contamination-free. Cells and organoids were cultured in a 37°C incubator with humidity control and 5% CO_2.

Routine maintenance and feeding of iPSCs

1. Feed cells daily by replacing medium with 2ml fresh hES +FGF2 (1:1000).
2. When colonies are small, double feeding (4ml of medium per well) to skip one day of feeding can be performed. Avoid frequent double feeding!
3. When colonies get bigger, differentiation of cells can be reduced by either adding more hES+FGF2 medium (up to 4ml) or increase the feeding frequency to up to 2x every day.
4. If colonies or colony-centers are differentiated, they must be removed to avoid loss of pluripotency of other colonies.
5. Perform mycoplasma tests (PCR+ MycoAlert assays) regularly.

Routine maintenance and feeding of H9 cells

1. Feed cells daily by replacing medium with 2ml fresh mTESR medium. Thaw mTESR medium 1 day in advance at 4°C and acclimatize at RT for ~15min before usage. Do not heat mTESR in the water bath unless all medium is consumed the same day.
2. When colonies are small, double feeding (4ml of medium per well) can be performed to skip one day of feeding. Avoid frequent double feeding or double feeding when plates are close to confluency.

3. When colonies get bigger, add more mTESR (up to 4ml) or increase the feeding frequency to up to 2x every day.
4. If colonies or colony-centers are differentiated, they must be removed to avoid loss of pluripotency of other colonies.
5. Perform mycoplasma tests (PCR+ MycoAlert assays) regularly (~every month).

Routine passaging of hiPS cells (without making EBs)

If many colonies show differentiation, follow "Making embryoid bodies" protocol for selection of undifferentiated colonies!

1. Prepare an appropriate number of wells in 6-well plate with MEFs.
2. If colony size of the hIPSCs is sufficient, split into new wells (usually, every ~5 days).
3. If colonies or colony-centers are differentiated, they must be removed to avoid loss of pluripotency of other colonies.
4. Wash cells with room temperature D-PBS w/o Ca and Mg.
5. Add 1ml Collagenase IV solution and incubate at 37˚C for 10min.
6. Remove Collagenase IV solution and add 1ml hES medium (no FGF2 needed here and in the following steps).
7. Use a cell lifter to scrape the colonies off the well.
8. Transfer the colonies into a 15ml conical tube. Wash well with 1ml of hES medium.
9. Spin at 200g for 2min.
10. Wash MEF cells with warm D-PBS with Ca and Mg and add 1ml hES.
11. Remove supernatant of iPSCs and add 1ml hES medium.
12. With a P1000 pipet, break the colonies in medium-small fragments. The fragments should still be visible and should not form 3D aggregations of cells (they result in 3D colonies with differentiation), but also should not be too small.
13. One well of cultured iPSCs can be split in a range of 1:3 to 1:10, depending on the colony density and the estimated time of use of the cells. Usually, a regular-density well is split 1:6.
14. Take the adequate volume (for 3 wells and 1:6 ratio, take 500µl of cells) of colony fragments and transfer in new tube. Add additional medium, so that 1ml of medium goes into each new well. For the example given, add another 2.5ml of medium.
15. Transfer 1ml of the colony fragments into each new well. Add 1µl FGF2 per ml medium to the wells.
16. Shake carefully and not circular, but in a 90˚ angle, to equally distribute the colonies. Shakers and frequent opening and closing of the incubator may position the colony fragments in the middle of the well and lead to an unequal distribution of colonies.
17. Feed every day with 2ml hES+FGF2. If colonies get bigger, increasing the medium volume or decreasing the feeding time helps to avoid differentiation.

Routine passaging of feeder free H9 (without making EBs)

1. Position a Matrigel-coated well into the incubator for 10-20min. Remove MG suspension and add 2ml of warm mTESR.
2. Wash cells 2x with 600µl EDTA working solution (50µl of 0.5M EDTA stock into 50ml $PBS^{-/-}$.
3. Add another 600µl of EDTA and incubate at 37˚C for approx. 5min. The colonies are ready when cells in the middle of the colonies start to detach from each other.

4. Suck off EDTA and carefully wash off colonies off with 500µl mTESR. Multiple rounds of washing can be performed, by adding new 500µl to the plate each washing step. The colonies should not be broken up into too small pieces.
5. Breaking colonies into smaller pieces may be useful for subsequent colony picking e.g. in case of differentiation, but a higher dilution for splitting has to be used and cells will need longer for growing back to normal colony size.
6. Use an appropriate dilution (usually 1:10-1:30) for plating on the Matrigel coated plates +mTESR.
7. Shake carefully to equally distribute the colonies. Shakers and frequent opening and closing of the incubator may position the colony fragments in the middle of the well and lead to an unequal distribution of colonies.

Making embryoid bodies with feeder dependent iPSC

1. Prepare an appropriate number of wells with MEFs in 6-well plate, if cells should be passaged.
2. Thaw Collagenase IV solution, Dispase solution, Trypsin, Trypsin inhibitor, Rock Inhibitor (RI) and bFGF. Warm up hES medium to room temperature.
3. Remove medium from cells and wash 2x with RT D-PBS w/o Ca and Mg.
4. Add 1ml warm Collagenase IV solution per well. Incubate for 10min at 37˚C.
5. Add another 1ml of warm Dispase solution on top of the Collagenase IV solution. Incubate at 37˚C until undifferentiated colonies have detached. Check regularly, as detachment time may vary between 15 and 50 min and a too long incubation may lead to the release of differentiating colonies. Differentiated colonies can be recognized by having granule, slightly colored structures in the middle of the colonies, single cells are visible and the border of the colony is not smooth but spicy. Undifferentiated colonies should have a uniform surface with no single cells visible, and a smooth border.
6. Carefully tilt the plate and transfer medium with detached colonies in a 15ml conical tube using a P1000 pipet. Do not harshly move the plate to avoid detachment of undifferentiated colonies!
7. Let the colonies sink in the tube, then carefully suck off most of the supernatant medium. Wash 3x with 1ml hES medium to remove detached MEF cells from colonies. After each washing step, let the colonies sink to the bottom again for 1-2min (dependent on colony size).
8. **Splitting:** Bring the colonies back in suspension in the last washing step. Remove an appropriate aliquot for splitting in a 15ml conical tube. For splitting colonies of one well into 3 wells in a 1:6 ratio, half of the medium must be transferred. Add medium to get 1ml of volume. Use a P1000 tip and break the colonies in medium-small fragments. From here, follow "Routine passaging of hIPS cells" from step 12 on.

As the following steps of making EBs are very time crucial, the colonies for this step can be kept in 1ml medium until EBs are made. Do NOT break the colonies apart before using them.

9. Add 1ml of Trypsin/EDTA and incubate exactly 2min in a 37˚C water bath. Directly add 1ml Trypsin inhibitor on top and pipette up and down 7-10 times to make a single cell suspension.
10. Add 1ml hES medium and spin down cells at 200g for 4min.
11. Immediately remove supernatant and resuspend cells in 1-2ml hES medium + RI. The cells can remain in single cell suspension in medium +RI for some time, but will die fast without RI.
12. Cell counting: mix 6µl of cell suspension and 6µl of trypan blue on a counting slide and use a cell counter for counting (being quick is crucial for cell viability in this step). Live cell count and cells alive (in %) are the important values for further proceeding and should be noted. If

cell viability is far below 90%, the cells should not be used for growing organoids. Reasons for low viability can be slow or wrong handling of the cells.

13. Per EB, 9000 cells in 150µl hES+ bFGF (1:2500) +RI (1:100) are needed. Add the appropriate volume of hES medium to the cells and directly add RI and bFGF (1:2500).
14. Pipet 150µl of medium in each well of a 96well ultra low attachment plate. Carefully shake cells before pipetting to avoid inhomogeneous cell distribution.

Making embryoid bodies with feeder free H9 cells

1. When hESCs colonies are ready for splitting, wash colonies with D-PBS w/o Ca. The colonies should be used for making EBs when the colonies are small enough to not touch each other and show no signs of differentiation (e.g. spicy cells outside of the colonies, dark spot in the middle of the colony).

   Variant: Additional passaging of H9

   When H9 are subsequently used for passaging, rinse 2x with EDTA working solution instead of washing with D-PBS$^{-/-}$. Then add 600µl EDTA working solution and incubate at 37˚C for approx. 5min. Suck off EDTA carefully. Wash appropriate amount of cells (e.g. 1/8 of the plate) off with warm mTESR for further plating. Plate appropriate amount (usually a range between 1:10 to 1:30) to a Matrigel-coated well (see "routine passaging of H9").
2. Suck off PBS or EDTA. Add 600µl of Accutase solution on the cells and incubate 3-4 minutes @37˚C. The colonies should easily go off by tapping the plate on the side. Remove colonies by spraying with 2x 1ml mTESR, pipet medium and cells up and down 5 times and transfer to a 15-ml conical tube. Centrifuge for 3min at 150rpm @RT. Carefully remove supernatant and resuspend cells in 1-2ml hES medium +RI.
3. Cell counting: mix 6µl of cell suspension and 6µl of trypan blue on a counting slide and use a cell counter for counting (being quick is crucial for cell viability in this step). A high cell survival rate (%) is crucial for further processing. If cell viability is far below 90, the cells should not be used for growing organoids. Reasons for low viability can be slow or wrong handling of the cells. Add RI to increase cell survivability.
4. Add appropriate volume of hES medium +1:100 Rock inhibitor +1:2500 bFGF. Use 9000 live cells in 150ul/well.
5. Pipet 150ul in each well of a low attachment 96-well plate. Carefully shake cell suspension before and during pipetting to avoid sinking of cells or fibers.
6. Change the medium after 3 and 5 days, using hES medium **without** RI and bFGF.

Growing Organoids (iPSC and H9)

1. Feed EBs on day 3 and day 5 with 150µl hESC without bFGF or RI. Suck off as much as possible from the medium before adding new medium.
2. EB quality check: The EBs should form a clear defined round ball (disk-shaped in Z axis) with defined borders after 2 days. The middle of the EB should be dark, the outside more transparent.
3. At size 500-600µm (usually between day 5 and 6), EBs which pass quality controls are set on neural induction. Prefill a 24 well ultra-low attachment plate (one EB each well) with NI medium (drugs for patterning may already be added here). EBs which did not form, are too small or misshaped should not be used further (Quality control 1). EBs which are fail quality

criteria (not round, fiber, no dark spot and shiny edge, too small or too big, wrong structure) are trashed.

Alternative: Keep cells in 96well plate and exchange hES medium with NI medium. No differences in EB or organoid growth could be observed with this method.

4. For transferring the EBs in the 24well plate, cut a 200µl tip 2-3mm above the end in an aslope manner. Suck in the EB with the tip without damaging the EB. Let the EB sink down in the tip and then transfer just the EB without the medium into the 24 well plate.
5. Feed the EBs on NI every other day. After 3 feedings (approx. day 11), the EBs should have a very shiny, radially striped band on the outside of the EB. On day 10-13, all EBs which have these structures can be used further for embedding. Any kind of outgrowth from the EB and misshaped EBs should not be used further (Quality control 2).
6. For embedding, thaw Matrigel (MG) on ice with water, or at 4˚C in ice overnight.
7. Prepare Parafilm: Cut Parafilm in a size that fits in the plate you want to grow the organoids in. Work as sterile as possible. Press the Parafilm with the paper side up against the holes of a 200µl tip box to create little molds (approx. 5mm diameter).
8. Remove paper and position Parafilm in the dish.
9. Position 6-8 EBs at once in the Parafilm molds and suck off medium.
10. Use a P200 pipette for pipetting about 30µl (one droplet) of MG onto each EB. Keep the MG on ice during pipetting as it solidifies fast at RT.
11. Position the EBs in the middle of the droplet using a pipette tip.
12. Put the Matrigel droplets in an incubator for 20-30min.
13. Add corresponding volume of Diff-A (alternative: Improved-A) medium (6cm plate: 5-7ml, 10cm plate: 20-30ml) to the side of the dish. If MG droplets do not fall off the Parafilm, use a P1000 pipette and carefully wash the droplets from the Parafilm.
14. Remove the Parafilm with forceps and put the dish in an incubator.
15. After 2-7 days (dependent on medium volume, number and size of organoids), the medium has to be changed (indicated by changing color of the medium, from red to yellow). Remove the medium and add new medium carefully. MG easily breaks apart when pipetting too fast, so add the medium dropwise or carefully to the side of the plate.
16. After the first feeding, position the plates on a shaker to guarantee better nutrient accessibility.
17. In each feeding step, organoids which are too small, develop into cysts or where the Matrigel breaks apart, should be sucked off together with the medium to increase consistency. (Quality control 3).
18. When the organoids grow out of Matrigel (usually, around day 40), add 1% MG to the medium.
19. From day 20 on, use Diff+A and not Diff-A (**alternative**: Improved+A subsequent to Improved-A) for feeding.

Related protocols

Prepare commercial MEF feeders

1) Store the commercial vials of MEFs in liquid nitrogen tanks. For thawing, remove a vial and thaw in a 37˚C water bath until a sliver of ice remains.
2) While thawing, prepare a 50ml tube containing 10ml MEF medium.
3) Pipette the MEFs from the vial into the 50ml tube. Centrifuge at 270g for 5min.

4) If MEF cells should be used directly for plating, resuspend the cells in 1ml MEF medium and take an appropriate aliquot. One commercial vial contains approx. 4 million cells. For one well of a 6well plate, 110,000 cells are needed. For the remaining cells, continue with step 5.
5) Resuspend cells in 30ml MEF medium. Plate the cells on three 10cm^2 plates using 10ml each plate. Incubate overnight.
6) Next day: Wash cells with warm PBS w/o Ca and Mg. Add 5ml of trypsin on each plate and incubate 5min. Transfer the cells in a 50ml vial and wash plates 2x with MEF medium.
7) Centrifuge cells at 270g for 5min. Remove supernatant and resuspend in 1ml MEF medium.
8) For freezing: for each well of a 6well plate, use 130.000 theoretical cells (do not count the cells but assume the 4mio cells are still intact). Therefore, if one vial for 2 wells and one for 6 wells should be frozen, take 260.000 and 780.000 cells in the corresponding volume.
9) For freezing, usually 0.5-1ml per cryotube are used. Resuspend cells in ½ of that volume- the other half of the medium will be MEF freezing medium.
10) Prepare a Mr. Frosty with correct labeling.
11) Add the MEF freezing medium, mix and pipet into the cryotubes. Position the cryotubes in the Mr. Frosty and quickly (within 3min) transfer the MEFs into a -80˚C freezer.

Thaw MEF cryotubes

1. Coat an appropriate number of wells with 0.1% Gelatin for at least 30min at 37˚C.
2. Position the cryotube in a 37˚C water bath until a sliver of ice remains.
3. Pipet the MEFs in a 15ml tube containing 10ml MEF medium.
4. Centrifuge at 270g for 5min.
5. Remove supernatant
6.
    a. **Slow method:**
    Resuspend cells in 1ml MEF medium for each well. Put 1ml of MEFs in each gelatin coated plate. Let MEFs grow over night before use, so that they can attach to the plate.
    b. **Fast method:**
    Resuspend cells in 1ml hES medium for each well. Add FGF2 (1:1000) and pipet 1ml of MEFs in each well. The MEFs are ready to use and iPSCs can be pipetted on top of them.

Thawing human iPSCs& H9 feeder free embryonic stem cells

iPSC:

1. Prepare an appropriate number of wells in 6-well plate with MEFs. Use slow MEF method for better viability of iPSCs.
2. Wash MEFs with RT PBS with Ca and Mg.
3. Add 2ml hES medium + RI (1:100).

iPSC and H9:

4. Prepare 2x 50ml conical tubes, tube 1 containing 1ml (hES/mTESR)+RI and tube 2 containing 9ml (hES/mTESR)+RI. Use mTESR for H9 and hES medium for iPSC cells.
5. Thaw vile of iPSCs&H9 in the water bath until just a sliver of ice remains.
6. Transfer 1ml of hES+RI (iPSC) or mTESR+RI (H9) from tube 2 carefully (dropwise!) on the cells. Then, transfer the cells carefully to tube 1.
7. Transfer the remaining 8ml medium from tube 2 dropwise and carefully on the cells. Use a 1ml pipet for extra care and carefully shake the tube for better distribution of the new medium.

8. Spin 200g for 2min.
9. Remove the supernatant and add 1ml (hES/mTESR) + RI to the pellet. Carefully resuspend by pipetting slowly 1-2 times. Do NOT break up colonies!
10. Transfer the resuspended cells onto the prepared MEF well/ a Matrigel coated well.
11. Change 2ml of the medium after 36-48 hours, not before. Change to medium still containing RI!
12. Then, normal feeding routine of iPSCs/H9 can be maintained.

Matrigel coating for feeder free H9 cells

1. MG Aliquots for coating (different to embedding MG!) can be stored at -20°C. Be careful to not heat up the Matrigel in any of the following steps. The number on the MG tubes corresponds to the number of wells of a 6well plate which can be coated.
2. Store the MG on ice. Put a 15ml falcon on ice as well and add the same volume (in ml) of **cold** DMEM-F12 in the falcon as has been written on the MG tube (e.g. 12ml).
3. Add 1ml of medium from the tube with a P1000 onto the frozen Matrigel and retransfer it immediately into the 15ml tube. Repeat until all Matrigel is dissolved. Mix medium in the 15ml tube to create a homogenous solution of MG in medium.
4. Use the following volumes for coating:
   96well plate: 50µl
   24well plate: 250µl
   12well plate: 500µl
   6well plate: 1ml
   6cm plate: 2.5ml
   10cm plate: 6ml
5. Seal plates with Parafilm and store in the fridge (up to 2 weeks should be fine). If used directly after coating, incubate for 20min @37˚C. For usage out of the fridge, 10min @37˚C are sufficient.

Variants of the cerebral organoid protocol used in this work:

1. Fusing the cerebral organoids:
   Instead of fusing the cerebral organoids separately, two patterned organoids were positioned into one Matrigel droplet in close proximity. See also (Bagley, Reumann & Knoblich 2017).
2. Replacing of hES medium for apical modifications:
   The EBs were produced as in the original protocol, despite the resuspension of cells and the further dilution. For resuspension in 1-2ml of medium for cell counting, mTESR was used. For the final dilution, the corresponding medium (NI, hES, E8$^{-supplements}$, mTESR) were used.
3. Hydrogel plates (Hydrogel domes):
   7x9000= 63.000 cells were diluted in 200µl of medium and pipetted on the top of the dome. After ~20min the cells were settled appropriately and 7ml of culture medium (either hES+ bFGF+RI or NI+RI) were added onto the wells.
   hES medium was exchanged on day 6 to NI medium without intermediate medium changes.
   NI medium was either changed on day 6 to renewed NI, or the EBs were kept in NI without medium exchange for the whole 10 days. After 10 days, the EBs were conservatively embedded using the regular protocol, and incubated in 6cm dishes.

   For chapter I, the previously described Diff-A and Diff+A medium was used for further organoid growth. For Chapter II and III, improved –A and improved +A was used.

Protocol: IHC analysis of cerebral organoid tissue

Fixing organoids in OCT:

1. Put organoids in a 15ml tube and remove medium. Rinse 3x with PBS.
2. Replace with 12ml 4% PFA in PBS without methanol (if low levels of fluorophores need to be quenched, 4% PFA containing Methanol can be used) and fix for 30min-2hours at RT on a rotator or shaker. Alternatively, incubate in a 15ml tube over night at 4˚C. Fixation time is dependent on organoid size.
3. Rinse 3x with PBS to remove PFA. If organoids are large, washing for 3x 5-10min increases PFA removal.
4. Remove PBS and replace it with 30% sterile-filtrated sucrose (in PBS) solution over night at 4˚C on a rotator/rocker. The organoids are saturated with sucrose when they sink into the sucrose solution instead of floating around.
5. Variant A: Remove sucrose solution and replace with a 50:50 mix of 30% sucrose (in PBS) and OCT. Incubate at RT for at least 2-4 hours on a rotator to allow OCT to enter the organoids. To prepare this mix, add 30% sucrose (in PBS) and OCT, mix in a 50ml tube and centrifuge down to remove air bubble.
   Variant B: Transfer organoids in a 3cm dish and add OCT. Move organoids with a pipet tip to completely encompass them in OCT and let them sit for 10 minutes. This variant is recommended particularly for small EBs and embedded young organoids.
6. Transfer organoids with a cut P1000 pipet tip (make sure the organoids fit easily through the pipet tip without damaging them) and put them into a cryomold. If variant A in step 5 was used, remove as much of the OCT-Sucrose mix as possible and replace with a small amount of fresh 100% OCT. Use no more OCT than is required to cover organoids so they remain positioned flat on the bottom of the cryomold. Position organoids in their final desired orientation. EBs from 3cm dishes can be transferred using a p200 pipet tip and can precisely be positioned in the middle of the cryomold.
   Note: Avoid air bubbles in the OCT! To guarantee good cutting quality, position the organoids in the middle of the cryomold and keep at least 3mm space to the borders of the cryomold.
7. For freezing, put a flat piece of metal (e.g. a metal Eppendorf cooler rack) on a plate of dry ice and allow to cool. When cooled, reposition the metal surface to a horizontal, non-tilted position. Place the cryomold containing the organoids in OCT onto the cold metal surface, and allow OCT/tissue to start freezing. As the block begins to freeze, the organoids will be fixed into position. At this point, more OCT can be added to completely fill the cryomold and create an additional layer on top. This layer will be used for fixing the block in the cryostat and should therefore approximately have the diameter of the cryostat holder (~2cm). Store the embedded organoids within the cryomolds at -80 degree wrapped in a plastic bag to avoid drying out of the specimen.

Sectioning of fixed organoid tissue:

1. Remove tissue from the -80˚C freezer and transport on dry ice. Equilibrate the tissue block in the cryostat for at least 10min.
2. Setting the cryostat cutting temperature: specimen= -13˚C, blade/room= -15˚C.

This temperature is a starting point, but the temperature must be adjusted according to the behavior of the tissue. In general, the blade temperature should be 2-3 degrees colder than the specimen. If the OCT-embedding sections are curling heavily, the temperature is too cold. If the tissue is sticking to the blade or brushes which are used for section rearrangement, the temperature is too warm.

3. Remove frozen OCT tissue block from the cryomold and fix with some OCT onto the cryostat holder plate. It is advisable to adjust the surface of the OCT block by adding a thin layer of OCT on top to test for an optimal sectioning angle and temperature prior to sectioning of the specimen.
4. Once the tissue block is fixed to the cryostat holder, mount the holder on the cryostat sectioning block. Trim the specimen (50µm sections first, then ~20µm when tissue becomes visible in the tissue block) until the tissue of the organoid is visible when collected on a slide. A cutting thickness of around 20µm is recommended, but could be further reduced for smaller organoids (→more sections). Rolling of slices can be prevented by using two brushes simultaneously.
5. For collecting tissue, a section thickness of around 20µm is recommended. Use 2 brushes to avoid rolling of the slides. Collect the tissue sections on Superfrost ultra-plus slides (DO NOT touch the surface of the slides with ungloved hands!). Initially begin with 10 slides and collect each consecutive section on a different slide such that a single slide contains a series of every 10^{th} section. To transfer tissue onto the slide, position the slide slowly above the specimen and then lower the slide just until touching the tissue. The tissue will attach to the warmer slide and thaw. The slide is usually a little bit charged, which causes the tissue section to "jump" on the slide. If the slide is charged too much and the jumping is not controllable, touch the slide to a metal object or an ungloved hand to remove the charge. If using an ungloved hand, make sure to not touch any surface where tissue will be fixed.
6. Let slides dry overnight at RT in a carton slide holder, then store in slide boxes at -20˚C.

Immunostaining of OCT-embedded cryosections

DO NOT let the slides dry out once rehydrated!

1. Thaw slides containing tissue sections and allow to dry at RT for at least 30min.
2. (Optional): Use a pap-pen or a liquid blocker pen to draw a border around the sections on the slide and allow to dry.
3. Put slides in a slide holder and place into PBS until the water-soluble OCT is not visible any more (approximately 10 minutes). Rinse 2x times with PBS.
4. **(Optional) Post-fixation on slide:**

Put slides in a humidified, light-protected staining box. Add 4%PFA (approximately 300µl, all slices need to be covered) for 5 minutes. Then, wash 3x 15min in PBS.

Post-fixation may be necessary when **(1)** fixation was not complete and **(2)** fluorescence of proteins could not completely be removed (in this case, take PFA+ Methanol). **Note**: Post-fixation with 4%PFA + methanol might make it necessary to perform antigen-retrieval.

5. Put slides back in the staining box. Permeabilize and block with 0.3% Triton X 100 (TX100) and 5% BSA with 0.05% NaN for at least 30min at RT (up to 2 hours should be fine). Use 300-500ul solution per slide. Once permeabilization/blocking is complete, shake the solution off the slide.
6. Add the primary antibody solution (5% BSA, 0.1% TX100, 0.05% NaN in PBS +primary antibodies). Prepare 200µl of antibody solution per slide. Add antibody solution to the slides in the humidified staining chamber. Do NOT move the staining box after addition of the antibody solution. Incubate at 4˚C over night.
7. Rinse 3x with PBS. Then, wash 3x for 15min with PBS-T (PBS+0,01% TX100).
8. Stain with 300µl of diluted secondary antibody (normally 1:500) in antibody solution for 2 hours in a humidified staining box at RT.
9. Shake off liquid from the slide and add 300-500µl 1x DAPI (diluted 1:1000 of stock 2mg/ml). Incubate 3-10min (usually, 5min is sufficient).
10. Rinse 3x with PBS, then wash 2x 15min with PBS-T and 1x 15min with PBS (the final wash should NOT contain TX100).
11. Shake off remaining PBS from the slides.

    Variant A: Mount with a cover glass using DAKO mounting medium. Use approximately 4 drops (150ul) medium to one side of the slide. Put on coverslip on one side and gently let it sink on the slide. Avoid air bubbles! Use a pipet to apply DAKO medium onto the slide to avoid air bubbles.

    Let the mounting medium harden by incubating the slides at RT for several hours or overnight. The slides can be used for microscopy approximately 30min after mounting if careful, but as the DAKO medium is not fixed the coverslip may be movable. Using immersion objectives is not advisable.

    Variant B: Use Vectashield antifade solution instead of DAKO in same volumes, put on coverslip and seal slide with nail polish. These slides are ready to go directly after nail polish has hardened.

List of primary antibodies used:

Species	Antibody	Provider	Catalog nr.	Dilution used	Species	Antibody	Provider	Catalog nr.	Dilution used
Ms	PAX6	Abcam	ab78545	1:100	Gt	DCX	Santa Cruz	sc-8066	1:200
Rb	FoxG1	Abcam	ab18259	1:200	Ms	NeuN	Millipore	MAB377	1:100
Rb	PV	Swant	PV27	1:1000	Rat	SST	Millipore	MAB354	1:200
Rb	Calbindin	Swant	CD38a D-28K	1:1000	Ms	Nkx2.1	Dako	M3575	1:50
Ms	Calretinin	Swant	?	1:1000	Rb	Nkx2.1	Epitomics	6594-1	1:1000
Ms	GAD67	Millipore	MAB5406	1:800	Rb	CXCR4	Abcam	ab124824	1:500
Rb	VGAT	Synaptic Systems	131 013	1:500	Rb	RFP/tdtomato	Abcam	ab62341	1:100
Ms	Nestin	BD	611658	1:200	Gt	Brachyury	R&D Systems	AF2085	10mg/ml
Ms	TUJ1	Sigma-Aldrich	T8578-100UL	1:500	Gt	DLX2	Santa Cruz	sc-18140	1:100
Ms	n-cadherin	BD	610920	1:500	Rb	GSX2	Millipore	ABN162	1:500
Rb	beta-Catenin	Sigma-Aldrich	1:1000	1:1000	Rb	LHX6	Abcam	ab22885	1:200
Gt	SOX10 N-20	Santa Cruz	sc-17342	1:200	Ms IgG1	Ki67	BD	550609	1:100
Gt	SOX1	R&D Systems	AF3389	1:500	Ms	MAP2 clone Ap20	Millipore	MAB3418	1:500
Ms	aPKCzeta (H1)	Santa Cruz	SC-17781	1:200	Ms IgG2b	HuC/D	Abcam	ab21271	1:200
Rb	SOX9	Millipore	AB5535	1:500	Chk	GFP	Aves lab/swant	GFP-1020	1:500
Chk	GFP	Abcam	ab13970	1:1000	Rb	APKC zeta	Santa Cruz	SC-216	1:200
Rb	NPY	Abcam	ab30914	1:1000	Rb	vGAT	Synaptic Systems	131 013	1:2000
Ms	Reelin	Millipore	MAB5366	1:200	Gt	Sp8	Santa Cruz	sc-104661	1:300
Rb	SOX6	Abcam	ab30455	1:500	Rb	VIP	Immunostar	20077	1:750
Ms	COUP-TFII	Perseus Proteomics	PP-H7147-00	1:300					

List of secondary antibodies used:

Species	Recognizes	Fluorophore	Provider	Catalog nr.	Dilution used
Dk	rabbit	AlexaFluor 568	Invitrogen	A10042	1:500
Dk	rabbit	AlexaFluor 647	Invitrogen	A31573	1:500
Dk	Mouse IgG	Alexa Fluor 568	Invitrogen	A10036	1:500
Dk	Mouse IgG	Alexa Fluor 647	Invitrogen	A31571	1:500
Dk	chicken	AlexaFluor 488	Jackson Immuno	703-605-155	1:500
Dk	goat	Alexaflour 647	Invitrogen	A21447	1:500
Dk	rat	AlexaFluor 647	Jackson Immuno	712-605-150	1:500
Gt	MsIgG1	AlexaFluor 568	Invitrogen	A21124	1:500
Gt	MsIgG2b	AlexaFluor 568	Invitrogen	A21144	1:500

Microscopy

Cell culture imaging (Fluorescent and Brightfield) was performed with a Zeiss Axio Vert.A1 (Zeiss, Zeiss GmbH) widefield microscope with an Axiocam ERc 5s camera (Zeiss, Zeiss GmbH) with 2.5x, 5x and 10x objectives. For overlaying of fluorescence, both RFP and GFP channels were recorded separately in grey, then pseudocolored and merged using Fiji.

Widefield imaging of IHC stainings was performed using an AxioImager Z2 (Zeiss, Zeiss GmbH) with a Sola SM2 illumination source, 5x 0.15 plan-neofluar, 10x 0.3 plan-neofluar or 20x 0.5 plan-neofluar objectives and images were obtained with a Hamamatsu Orca Flash 4 camera. Filters used were: Ex360/40nm- Em 445/50nm, Ex480/40nm-Em 535/50nm and Ex560/55nm-Em 645/75nm.

Confocal imaging was done on a Zeiss LSM700 AxioImager (Zeiss, Zeiss GmbH) with a 20x 0.8 plan-apochromat dry objective using Zeiss Zen software. Lasers used were 405nm(5mW), 488nm (10mW), 555nm(10mW) and 639nm(5mW) together with the filter sets SP490, SP555, SP640 and LP490, LP560 and LP640. For whole organoid tile scans using the attached scanning stage the Zeiss Zen implemented stitching algorithm was used. For fluorescent colocalization imaging, Z-scans were performed (1µm).

Spinning disk imaging was performed on a Yokogawa W1 spinning disk confocal microscope (VisiScope, Visitron Systems GmbH, Puchheim, Germany) mounted on the Eclipse Ti-E microscope (Nikon, Nikon Instruments BV) using VisiView software. Lasers used were 405nm (120mW), 488nm (200mW), 561nm (150mW), 640nm (150mW) together with the filters DAPI 640/50, GFP 525/50, mCherry 609/54 and Cy5 700/75. Objectives used were CFI plan Apo lambda 20x 0.75 air and CFI plan Apo lamda 40x 0.95 air together with 1x and 2x lens switches (2x lens switch: 2x magnification). Cameras used for recording were either the Andor Ixon Ultra 888 EMCCD camera (13µm pixel size, 1024x1024pixel) or the PCO edge 4.2m sCMOS camera (6.5µm pixel, 2028x2028pix). For live imaging, the attached incubation chamber with heating, CO_2 and humidity setup was used. 5-6 EBs were mounted with low melting agarose in 35mm µ-Dishes (Ibidi, cat. No. 80136).
Acquired tile scans on the VisiScope were stitched using Fiji Grid/Collection stitching (Preibisch et al., Bioinformatics, 2009) or the VisiView implemented OverView stitching function.

qPCR

For each sample group, 8-12 organoids were collected at day 30-40 into RNAse-free tubes. The tubes were kept on ice throughout the whole procedure. Before RNA-extraction, the organoids were washed 3x in cold PBS and Matrigel was removed by incubation in Cell Recovery Solution (Corning, cat.354253) for 1 hour at 4°C. Then, the organoids were rinsed again by rinsing 3x with cold PBS. RNA extraction was performed using the RNeasy mini kit (Quiagen, cat.74104). cDNA synthesis was performed using 2µg of the RNA (measured with a Nanodrop®) and the Superscript enzyme (Invitrogen) according to the manufacturer protocols.
qPCR reactions were performed using the Sybr Green master mix (Promega) on a CXF384 BioRad machine. Following protocol was used: 1) 95°C 3min 2) 85°C 10sec 3) 62°C 10sec 4) 72°C 40sec 5) goto2, 40cycles 6) 95°C 1min 7) 50°C 10sec.

Quantification was performed by calculating the ΔCt value using TBP as a reference gene. Data is presented as expression level ($2^{-\Delta Ct}$) relative to TBP.

qPCR primers:

Gene	Primer 1	Primer 2
FOXG1	TGGCCCATGTCGCCCTTCCT	GCCGACGTGGTGCCGTTGTA
TBR1	CTCAGTTCATCGCCGTCACC	AGCCGGTGTAGATCGTGTCATA
DLX2	ACGTCCCTTACTCCGCCAAG	AGTAGATGGTGCGGGGTTTCC
GSX2	CACCGCCACCACCTACAAC	CAGGAGTTGCGTGCTAGTGA
NKX2.1	GCCGTACCAGGACACCATG	ATGTTCTTGCTCACGTCCCC
LHX6	CCGTCTGCAGGCAAGAACAT	GACACACGGAGCACTCGAG
PAX6	CTGGTTGGTATCCGGGGACT	TCGCATTTGAGCCTCATCTGA

Statistics

Statistics were performed using Prism 7 (Graphpad). For the comparison of 2 groups, an unpaired two-tailed Student's t-test was performed. For comparing multiple groups, a one-way ANOVA with posthoc Tukey's test was used.

References

I endeavored to ascertain the copyright holders of all illustrations and secure their consent to the utilization of their illustrations in the present paper. If, in spite of my efforts, a copyright infringement should have occurred, I kindly request the relevant parties to contact me.

Abranches, E. et al., 2009. Neural Differentiation of Embryonic Stem Cells In Vitro: A Road Map to Neurogenesis in the Embryo. *PLOS ONE*, 4(7), p.e6286. Available at: https://doi.org/10.1371/journal.pone.0006286.

Astashkina, A. & Grainger, D.W., 2014. Critical analysis of 3-D organoid in vitro cell culture models for high-throughput drug candidate toxicity assessments. *Advanced Drug Delivery Reviews*, 69–70, pp.1–18. Available at: http://dx.doi.org/10.1016/j.addr.2014.02.008.

Bagley, J.A., Reumann, D., Bian, S., et al., 2017. Fused cerebral organoids model interactions between brain regions. *Nature Methods*, 12(10). Available at: http://www.nature.com/doifinder/10.1038/nmeth.4304.

Bagley, J.A., Reumann, D. & Knoblich, J.A., 2017. Detailed Cerebral Organoid Fusion Method. Available at: http://dx.doi.org/10.1038/protex.2017.064.

Barber, M. & Pierani, A., 2015. Tangential migration of glutamatergic neurons and cortical patterning during development: Lessons from Cajal-Retzius cells. *Developmental Neurobiology*, 76(8), pp.847–881. Available at: http://doi.wiley.com/10.1002/dneu.22363.

Bartolini, G., Ciceri, G. & Marín, O., 2013. Integration of GABAergic Interneurons into Cortical Cell Assemblies: Lessons from Embryos and Adults. *Neuron*, 79(5), pp.849–864.

Batista-Brito, R. et al., 2009. The Cell-Intrinsic Requirement of Sox6 for Cortical Interneuron Development. *Neuron*, 63(4), pp.466–481.

Bear, M.F., Connors, B.W. & Paradiso, M.A., 2007. *Neuroscience- Exploring the Brain* third Edit., Philadelphia: Lippincott Williams& Wilkins.

ten Berge, D. et al., 2008. Wnt Signaling Mediates Self-Organization and Axis Formation in Embryoid Bodies. *Cell Stem Cell*, 3(5), pp.508–518. Available at: http://dx.doi.org/10.1016/j.stem.2008.09.013.

Bershteyn, M. et al., 2017. Human iPSC-Derived Cerebral Organoids Model Cellular Features of Lissencephaly and Reveal Prolonged Mitosis of Outer Radial Glia. *Cell Stem Cell*, 20, pp.1–15. Available at: http://linkinghub.elsevier.com/retrieve/pii/S1934590916304635.

Birey, F. et al., 2017. Assembly of functionally integrated human forebrain spheroids. *Nature*. Available at: http://www.nature.com/doifinder/10.1038/nature22330.

Bortone, D. & Polleux, F., 2009. KCC2 expression promotes the termination of cortical interneuron migration in a voltage-sensitive calcium-dependent manner. *Neuron*, 62(1), pp.53–71.

Brady, S.T. et al., 2012. *Basic Neurochemistry: Principles of Molecular, Cellular and Medical Neurobiology* Eigth Edit. R. W. Albers & D. L. Price, eds., Oxford.

Britanova, O. et al., 2006. A novel mode of tangential migration of cortical projection neurons. *Developmental Biology*, 298(1), pp.299–311.

Brown, M.T.C. et al., 2012. Ventral tegmental area GABA projections pause accumbal cholinergic interneurons to enhance associative learning. *Nature*, 492(7429), pp.452–456. Available at: http://www.nature.com/doifinder/10.1038/nature11657.

Busskamp, V. et al., 2014. Rapid neurogenesis through transcriptional activation in human stem cells. *Molecular Systems Biology*, 10(11), p.760. Available at: http://msb.embopress.org/cgi/doi/10.15252/msb.20145508.

Buzsáki, G. & Draguhn, A., 2004. Neuronal oscillations in cortical networks. *Science*, 304(June), pp.1926–1929. Available at: http://www.sciencemag.org/content/304/5679/1926.short.

Camp, J.G. et al., 2015a. Human cerebral organoids recapitulate gene expression programs of fetal neocortex development. *Proceedings of the National Academy of Sciences of the United States of America*, 112(51), pp.15672–7. Available at: http://www.pubmedcentral.nih.gov/articlerender.fcgi?artid=4697386&tool=pmcentrez&rendertype=abstract.

Camp, J.G. et al., 2015b. Human cerebral organoids recapitulate gene expression programs of fetal neocortex development. *Proceedings of the National Academy of Sciences of the United States of America*, 112(51), pp.15672–7.

Cauli, B. et al., 2014. Revisiting enigmatic cortical calretinin-expressing interneurons. *Frontiers in neuroanatomy*, 8(June), p.52. Available at: http://www.pubmedcentral.nih.gov/articlerender.fcgi?artid=4067953&tool=pmcentrez&rendertype=abstract.

Chaudhry, M.A. et al., 2008. Basal medium composition and serum or serum replacement concentration influences on the maintenance of murine embryonic stem cells. *Cytotechnology*, 58(3), pp.173–179.

Church, G.M., 2017. Youtube: The future of genetic codes and BRAIN codes, accessed 03.05.2017. Available at: https://www.youtube.com/watch?v=p2TcAA7VqmM&t=1474s.

Clevers, H., 2016. Modeling Development and Disease with Organoids. *Cell*, 165(7), pp.1586–1597. Available at: http://dx.doi.org/10.1016/j.cell.2016.05.082.

Copp, A.J., Stanier, P. & Greene, N.D.E., 2014. Neural tube defects – recent advances , unsolved questions and controversies. *Lancet Neurology*, 12(8), pp.799–810.

Cummings, B.S., Wills, L.P. & Schnellmann, R.G., 2004. Measurement of Cell Death in Mammalian Cells. *Curr Protoc Phamacol*, 1(Lemasters 1999), pp.1–30.

Denaxa, M. et al., 2001. The adhesion molecule TAG-1 mediates the migration of cortical interneurons from the ganglionic eminence along the corticofugal fiber system. *Development (Cambridge, England)*, 128, pp.4635–4644.

Dennis, E.A. & Bradshaw, R.A., 2011. *Intercellular Signaling in Development and Disease: Cell*

Signaling Collection, San Diego: Academic Press (Elsevier).

Dhara, S. & Stice, S., 2008. Neural differentiation of human embryonic stem cells. *Journal of cellular biochemistry*, 105(3), pp.633–640. Available at: http://onlinelibrary.wiley.com/doi/10.1002/jcb.21891/full.

Douglas, R.J. et al., 1995. Recurrent excitation in neocortical circuits. *Science*, 269(5226), pp.1–5. Available at: http://www.ncbi.nlm.nih.gov/pubmed/7638624%5Cnhttp://www.sciencemag.org/content/269/5226/981.short.

Le Dréau, G. & Martí, E., 2012. Dorsal-ventral patterning of the neural tube: A tale of three signals. *Developmental Neurobiology*, 72(12), pp.1471–1481.

Elkabetz, Y. et al., 2008. Human ES cell-derived neural rosettes reveal a functionally distinct early neural stem cell stage. *Genes and Development*, 22(2), pp.152–165.

Erlander, M.G. et al., 1991. Two genes encode distinct glutamate decarboxylases. *Neuron*, 7(1), pp.91–100. Available at: http://eutils.ncbi.nlm.nih.gov/entrez/eutils/elink.fcgi?dbfrom=pubmed&id=2069816&retmode=ref&cmd=prlinks%5Cnpapers2://publication/uuid/7EF7D56C-AA8C-4EB8-B93C-4F0CB5BACF3D.

Fatehullah, A., Tan, S.H. & Barker, N., 2016. Organoids as an in vitro model of human development and disease. *Nature cell biology*, 18(3), pp.246–54. Available at: http://dx.doi.org/10.1038/ncb3312%5Cnhttp://www.ncbi.nlm.nih.gov/pubmed/26911908.

Fernández, V., Llinares Benadero, C. & Borrell, V., 2016. Cerebral cortex expansion and folding: what have we learned? *The EMBO Journal*, 35(10), pp.1021–1044. Available at: http://emboj.embopress.org/lookup/doi/10.15252/embj.201593701.

Flames, N. et al., 2004. Short- and Long-Range Attraction of Cortical GABAergic Interneurons by Neuregulin-1. *Neuron*, 44(2), pp.251–261. Available at: http://linkinghub.elsevier.com/retrieve/pii/S0896627304006373.

Florio, M. & Huttner, W.B., 2014a. Neural progenitors, neurogenesis and the evolution of the neocortex. *Development (Cambridge, England)*, 141(11), pp.2182–94. Available at: http://dev.biologists.org/content/141/11/2182.

Florio, M. & Huttner, W.B., 2014b. Neural progenitors, neurogenesis and the evolution of the neocortex. *Development (Cambridge, England)*, 141(11), pp.2182–2194. Available at: http://dev.biologists.org/content/141/11/2182.

Gelman, D.M., Marin, O. & Rubenstein, J.L.R., 2012. *The Generation of Cortical Interneurons. In: Noebels JL, Avoli M, Rogawski MA, etal., editors. Jasper's Basic Mechanisms of the Epilepsies [Internet]. 4th edition. Bethesda (MD): National Center for Biotechnology Information (US); 2012.*, Available at: http://www.ncbi.nlm.nih.gov/books/NBK98190/pdf/Bookshelf_NBK98190.pdf.

Gilbert, S., 2000. *Developmental Biology. 6th edition. Sunderland (MA): Sinauer Associates; 2000. Formation of the Neural Tube. Available from: https://www.ncbi.nlm.nih.gov/books/NBK10080/. Accessed 06.03.2016*,

Gjorevski, N. et al., 2016. Designer matrices for intestinal stem cell and organoid culture. *Nature Publishing Group*, 539.

Guo, J. & Anton, E.S., 2014. Decision making during interneuron migration in the developing cerebral cortex. *Trends in Cell Biology*, 24(6), pp.342–351.

Hadley, E., 2012. The Role of Albumin in Feeder-Free Culture Media. Available at: https://www.stemcell.com/role-of-albumin-in-feeder-free-culture-media.html [Accessed May 21, 2017].

Haider, B. et al., 2006. Neocortical Network Activity In Vivo Is Generated through a Dynamic Balance of Excitation and Inhibition. *Journal of Neuroscience*, 26(17), pp.4535–4545.

Harland, R. & Gerhart, J., 1997. Formation and Function of Spemann ' S Organizer. *Annual Reviews of Cellular andDevelopmental Biology*, 13, pp.611–667.

Hevner, R.F. et al., 2003. Cajal-Retzius cells in the mouse: Transcription factors, neurotransmitters, and birthdays suggest a pallial origin. *Developmental Brain Research*, 141(1–2), pp.39–53.

Hikasa, H. & Sokol, S.Y., 2017. Wnt Signaling in Vertebrate Axis Specification. , (Sokol 2011).

Hong, L.E. et al., 2012. Mismatch negativity and low frequency oscillations in schizophrenia families. *Clinical Neurophysiology*, 123(10), pp.1980–1988.

Huch, M. & Koo, B.K., 2015. Modeling mouse and human development using organoid cultures. *Development*, 142(18), pp.3113–3125. Available at: http://dev.biologists.org/cgi/doi/10.1242/dev.118570.

Hwang, Y.-S. et al., 2009. Microwell-mediated control of embryoid body size regulates embryonic stem cell fate via differential expression of WNT5a and WNT11. *Proceedings of the National Academy of Sciences*, 106(40), pp.16978–16983. Available at: http://www.pnas.org/cgi/doi/10.1073/pnas.0905550106.

Israsena, N. et al., 2004. The presence of FGF2 signaling determines whether beta-catenin exerts effects on proliferation or neuronal differentiation of neural stem cells. *Developmental Biology*, 268(1), pp.220–231. Available at: http://www.nature.com/doifinder/10.1038/nmeth902.

Jo, J. et al., 2016. Midbrain-like Organoids from Human Pluripotent Stem Cells Contain Functional Dopaminergic and Neuromelanin-Producing Neurons. *Stem Cell*, pp.1–11. Available at: http://dx.doi.org/10.1016/j.stem.2016.07.005.

Jones, E.G., 2009. The origins of cortical interneurons: Mouse versus monkey and human. *Cerebral Cortex*, 19(9), pp.1953–1956.

Kadoshima, T. et al., 2014. Self-organization of axial polarity, inside-out layer pattern, and species-specific progenitor dynamics in human ES cell–derived neocortex. *Proceedings of the National Academy of Sciences*, 111(20), pp.7498–7498. Available at: http://www.pnas.org/cgi/doi/10.1073/pnas.1407159111.

Kelsom, C. & Lu, W., 2013. Development and specification of GABAergic cortical interneurons. *Cell & Bioscience*, 3(1), p.19. Available at: http://cellandbioscience.biomedcentral.com/articles/10.1186/2045-3701-3-19.

Kepecs, A. & Fishell, G., 2014. Interneuron cell types are fit to function. *Nature*, 505(7483), pp.318–326. Available at: http://www.nature.com/doifinder/10.1038/nature12983.

Kessaris, N. et al., 2014. Genetic programs controlling cortical interneuron fate. *Current Opinion in Neurobiology*, 26, pp.79–87. Available at: http://dx.doi.org/10.1016/j.conb.2013.12.012.

Kowalczyk, T. et al., 2009. Intermediate neuronal progenitors (basal progenitors) produce pyramidal-projection neurons for all layers of cerebral cortex. *Cerebral Cortex*, 19(10), pp.2439–2450.

Lancaster, M.A. et al., 2013. Cerebral organoids model human brain development and microcephaly. *Nature*, 501(7467), pp.373–379. Available at: http://dx.doi.org/10.1038/nature12517.

Lancaster, M.A. & Knoblich, J.A., 2014. Generation of cerebral organoids from human pluripotent stem cells. *Nature Protocols*, 9(10), pp.2329–2340. Available at: http://www.nature.com/doifinder/10.1038/nprot.2014.158.

Lancaster, M.A. & Knoblich, J.A., 2014. Organogenesis in a dish: Modeling development and disease using organoid technologies. *Science*, 345(6194), p.1247125. Available at: http://www.sciencemag.org/cgi/doi/10.1126/science.1247125.

Lee, S. et al., 2010. The largest group of superficial neocortical GABAergic interneurons expresses ionotropic serotonin receptors SooHyun. *Journal of Neuroscience*, 30(50), pp.16796–16808.

Lewis, D.A., Hashimoto, T. & Volk, D.W., 2005. Cortical inhibitory neurons and schizophrenia. *Nature Reviews Neuroscience*, 6(4), pp.312–324. Available at: http://www.nature.com/doifinder/10.1038/nrn1648.

Li, Y. et al., 2017. Induction of Expansion and Folding in Human Cerebral Organoids. *Cell Stem Cell*, 20(3), p.385–396.e3. Available at: http://linkinghub.elsevier.com/retrieve/pii/S1934590916304532.

Liddle, E.B. et al., 2016. Abnormal salience signaling in schizophrenia: The role of integrative beta oscillations. *Human Brain Mapping*, 37(4), pp.1361–1374.

Lin, Y. & Chen, G., 2014. Embryoid body formation from human pluripotent stem cells in chemically defined E8 media. *Stembook.Org*, pp.1–4. Available at: http://www.stembook.org/sites/default/files/protocols/Embryoid-body-formation-from-human-pluripotent-stem-cells-in-chemically-defined-E8-media.pdf.

Lindborg, B.A. et al., 2016. Rapid Induction of Cerebral Organoids From Human Induced Pluripotent Stem Cells Using a Chemically Defined Hydrogel and Defined Cell Culture Medium. *Stem Cells Translational Medicine*, pp.1–10. Available at: http://stemcellstm.alphamedpress.org/cgi/doi/10.5966/sctm.2015-0305.

Liu, Y. et al., 2013. Directed differentiation of forebrain GABA interneurons from human pluripotent stem cells. *Nature protocols*, 8(9), pp.1670–9. Available at: http://www.pubmedcentral.nih.gov/articlerender.fcgi?artid=4121169&tool=pmcentrez&rendertype=abstract.

Lledo, P.M., Merkle, F.T. & Alvarez-Buylla, A., 2008. Origin and function of olfactory bulb interneuron diversity. *Trends in Neurosciences*, 31(8), pp.392–400.

Ludwig, T.E. et al., 2006. Feeder-independent culture of human embryonic stem cells. *Nature*

Methods, 3(8), pp.637–646. Available at: http://www.nature.com/doifinder/10.1038/nmeth902.

Ma, T. et al., 2013. Subcortical origins of human and monkey neocortical interneurons. *Nature Neuroscience*, 16(11), pp.1588–1599.

Le Magueresse, C. & Monyer, H., 2013. GABAergic Interneurons Shape the Functional Maturation of the Cortex. *Neuron*, 77(3), pp.388–405. Available at: http://dx.doi.org/10.1016/j.neuron.2013.01.011.

Marin, O., 2012. Interneuron dysfunction in psychiatric disorders. *Nature Reviews Neuroscience*, pp.1–14. Available at: http://www.nature.com/doifinder/10.1038/nrn3155.

Marín, O. et al., 2010. Guiding Neuronal Cell Migrations. *Cold Spring Harbor Perspectives in Biology*, 2(2), pp.1–21.

Marín, O. & Rubenstein, J.L., 2001. A long, remarkable journey: tangential migration in the telencephalon. *Nature reviews. Neuroscience*, 2(11), pp.780–90. Available at: http://www.ncbi.nlm.nih.gov/pubmed/11715055.

Markram, H. et al., 2004. Interneurons of the neocortical inhibitory system. *Nature Reviews Neuroscience*, 5(10), pp.793–807. Available at: http://www.nature.com/doifinder/10.1038/nrn1519.

Maroof, A.M. et al., 2013. Directed Differentiation and Functional Maturation of Cortical Interneurons from Human Embryonic Stem Cells. *Stem Cell*, 12(5), pp.559–572. Available at: http://dx.doi.org/10.1016/j.stem.2013.04.008.

Marques, I. et al., 2015. Unraveling the pathogenesis of ARX polyalanine tract variants using a clinical and molecular interfacing approach. *Molecular genetics & genomic medicine*, 3(3), pp.203–14. Available at: http://www.pubmedcentral.nih.gov/articlerender.fcgi?artid=4444162&tool=pmcentrez&rendertype=abstract [Accessed March 15, 2016].

Martin, G.R., 1981. Isolation of a pluripotent cell line from early mouse embryos cultured in medium conditioned by teratocarcinoma stem cells. *Proceedings of the National Academy of Sciences*, 78(12), pp.7634–7638. Available at: http://www.pnas.org/cgi/doi/10.1073/pnas.78.12.7634.

Meinhardt, A. et al., 2014. 3D reconstitution of the patterned neural tube from embryonic stem cells. *Stem Cell Reports*, 3(6), pp.987–999.

Miyoshi, G. et al., 2010. Genetic fate mapping reveals that the caudal ganglionic eminence produces a large and diverse population of superficial cortical interneurons. *Journal of Neuroscience*, 30(5), pp.1582–1594.

Miyoshi, G. et al., 2007. Physiologically distinct temporal cohorts of cortical interneurons arise from telencephalic Olig2-expressing precursors. *The Journal of neuroscience : the official journal of the Society for Neuroscience*, 27(29), pp.7786–7798.

Mota, B. & Herculano-Houzel, S., 2012. How the Cortex Gets Its Folds: An Inside-Out, Connectivity-Driven Model for the Scaling of Mammalian Cortical Folding. *Frontiers in Neuroanatomy*, 6(February), pp.1–14.

Muguruma, K. et al., 2015. Self-organization of polarized cerebellar tissue in 3D culture of human

pluripotent stem cells. *Cell Reports*, 10(4), pp.537–550. Available at: http://dx.doi.org/10.1016/j.celrep.2014.12.051.

Nakano, T. et al., 2012. Self-formation of optic cups and storable stratified neural retina from human ESCs. *Cell Stem Cell*, 10(6), pp.771–785. Available at: http://dx.doi.org/10.1016/j.stem.2012.05.009.

Nestor, M.W. et al., 2013. Differentiation of serum-free embryoid bodies from human induced pluripotent stem cells into networks. *Stem Cell Research*, 10(3), pp.454–463. Available at: http://dx.doi.org/10.1016/j.scr.2013.02.001.

Nicholas, C.R. et al., 2013. Functional Maturation of hPSC-Derived Forebrain Interneurons Requires an Extended Timeline and Mimics Human Neural Development. *Stem Cell*, 12(5), pp.573–586. Available at: http://dx.doi.org/10.1016/j.stem.2013.04.005.

Nóbrega-pereira, S. et al., 2008. Postmitotic Nkx2-1 controls the migration of telencephalic interneurons by direct repression of guidance receptors Sandrina. *Neuron*, 59(5), pp.733–745.

Oikari, L.E. et al., 2016. Data defining markers of human neural stem cell lineage potential. *Data in Brief*, 7, pp.206–215.

Olivetti, P.R. & Noebels, J.L., 2012. Interneuron, interrupted: molecular pathogenesis of ARX mutations and X-linked infantile spasms. *Current Opinion in Neurobiology*, 22(5), pp.859–865. Available at: http://dx.doi.org/10.1016/j.conb.2012.04.006.

Paredes, M.F. et al., 2016. Extensive migration of young neurons into the infant human frontal lobe. *Science*, 354(6308), p.aaf7073-aaf7073. Available at: http://www.sciencemag.org/cgi/doi/10.1126/science.aaf7073.

Pekkanen-Mattila, M. et al., 2010. Spatial and temporal expression pattern of germ layer markers during human embryonic stem cell differentiation in embryoid bodies. *Histochemistry and Cell Biology*, 133(5), pp.595–606.

Pettinato, G., Wen, X. & Zhang, N., 2015. Engineering Strategies for the Formation of Embryoid Bodies from Human Pluripotent Stem Cells. *Stem cells and development*, 24(14), pp.1595–609. Available at: http://www.ncbi.nlm.nih.gov/pubmed/25900308.

Qian, X. et al., 2016. Brain-Region-Specific Organoids Using Mini-bioreactors for Modeling ZIKV Exposure. *Cell*, 165(5), pp.1238–1254. Available at: http://dx.doi.org/10.1016/j.cell.2016.04.032.

Rakic, P., 2009. Evolution of the neocortex: a perspective from developmental biology. *Nature Reviews Neuroscience*, 10(10), pp.724–735. Available at: http://dx.doi.org/10.1038/nrn2719%5Cnpapers2://publication/doi/10.1038/nrn2719.

Renner, M. et al., 2017. Self- organized developmental patterning and differentiation in cerebral organoids. *The EMBO Journal*, p.e201694700. Available at: http://emboj.embopress.org/lookup/doi/10.15252/embj.201694700.

Rudy, B. et al., 2010. Three groups of interneurons account for nearly 100% of neocortical GABAergic neurons C. J. McBain & G. Fishell, eds. *Developmental Neurobiology*, 71(1), pp.45–61. Available at: http://doi.wiley.com/10.1002/dneu.20853.

Sakaguchi, H. et al., 2015. Generation of functional hippocampal neurons from self-organizing human

embryonic stem cell-derived dorsomedial telencephalic tissue. *Nat Commun.*, 6, p.8896. Available at: http://www.nature.com/doifinder/10.1038/ncomms9896%5Cnhttp://www.ncbi.nlm.nih.gov/pubmed/26573335%5Cnhttp://www.pubmedcentral.nih.gov/articlerender.fcgi?artid=PMC4660208.

Sasai, Y., 2013. Next-Generation Regenerative Medicine: Organogenesis from Stem Cells in 3D Culture. *Stem Cell*, 12(5), pp.520–530. Available at: http://dx.doi.org/10.1016/j.stem.2013.04.009.

Sato, H. et al., 2016. Microfabric Vessels for Embryoid Body Formation and Rapid Differentiation of Pluripotent Stem Cells. *Nature Publishing Group*, pp.1–13. Available at: http://dx.doi.org/10.1038/srep31063.

Schulz, T.C. et al., 2003. Directed neuronal differentiation of human embryonic stem cells. *BMC neuroscience*, 4(1), p.27. Available at: http://www.biomedcentral.com/1471-2202/4/27.

Selby, L., Zhang, C. & Sun, Q.-Q., 2007. Major defects in neocortical GABAergic inhibitory circuits in mice lacking the fragile X mental retardation protein. *Neuroscience Letters*, 412(3), pp.227–232. Available at: http://linkinghub.elsevier.com/retrieve/pii/S030439400601202X.

Seshadri, S. et al., 2015. Interneuronal DISC1 regulates NRG1-ErbB4 signalling and excitatory-inhibitory synapse formation in the mature cortex. *Nature communications*, 6, p.10118. Available at: http://www.nature.com/doifinder/10.1038/ncomms10118.

Sineva, G.S. & Pospelov, V.A., 2014. *β-catenin in pluripotency. Adhering to self-renewal or wnting to differentiate?* 1st ed., Elsevier Inc. Available at: http://dx.doi.org/10.1016/B978-0-12-800178-3.00002-6.

StemCellTechnologies, 2015. Reproducible and Uniform Embryoid Bodies Using AggreWell(TM) Plates, Stemcell(TM)Technologies, Version 3.1.0 document #29146.

Stenman, J., Toresson, H. & Campbell, K., 2003. Identification of two distinct progenitor populations in the lateral ganglionic eminence: implications for striatal and olfactory bulb neurogenesis. *The Journal of neuroscience : the official journal of the Society for Neuroscience*, 23(1), pp.167–174.

Sultan, K.T., Shi, S.-H. & Brown, K.N., 2013. Production and organization of neocortical interneurons. *Frontiers in cellular neuroscience*, 7, pp.1–14. Available at: papers3://publication/doi/10.3389/fncel.2013.00221/abstract.

Sun, G.J. et al., 2015. Tangential migration of neuronal precursors of glutamatergic neurons in the adult mammalian brain. *Proc Natl Acad Sci U S A*, 112(30), pp.9484–9489. Available at: http://www.ncbi.nlm.nih.gov/pubmed/26170290%5Cnhttp://www.pnas.org/content/112/30/9484.full.pdf.

Sun, T. & Hevner, R.F., 2014. Growth and folding of the mammalian cerebral cortex: from molecules to malformations. *Nature reviews. Neuroscience*, 15(4), pp.217–32. Available at: http://www.ncbi.nlm.nih.gov/pubmed/24646670.

Sussel, L. et al., 1999. Loss of Nkx2.1 homeobox gene function results in a ventral to dorsal molecular respecification within the basal telencephalon: evidence for a transformation of the pallidum into the striatum. *Development*, 126(15), pp.3359–3370. Available at: http://www.ncbi.nlm.nih.gov/pubmed/10393115.

Tamamaki, N., 2002. Radial glias and radial fibers: what is the function of radial fibers? Development of the radial glia. *N. Tamamaki Anatomical Science International*, 77, pp.2–11.

Tekkatte, C. et al., 2011. "Humanized" Stem Cell Culture Techniques: The Animal Serum Controversy. *Stem Cells International*, 2011, pp.1–14. Available at: http://www.hindawi.com/journals/sci/2011/504723/.

Théveneau, E., Duband, J.L. & Altabef, M., 2007. Ets-1 confers cranial features on neural crest delamination. *PLoS ONE*, 2(11), p.e1142.

Turrigiano, G., 2011. Too many cooks? Intrinsic and synaptic homeostatic mechanisms in cortical circuit refinement. *Annual review of neuroscience*, 34, pp.89–103.

Vazin, T. et al., 2014. Efficient derivation of cortical glutamatergic neurons from human pluripotent stem cells: A model system to study neurotoxicity in Alzheimer's disease. *Neurobiology of Disease*, 62, pp.62–72. Available at: http://www.sciencedirect.com/science/article/pii/S0969996113002490 [Accessed May 15, 2017].

Vogels, T.P. & Abbott, L.F., 2009. Gating Multiple Signals through Detailed Balance of Excitation and Inhibition in Spiking Networks. *Nature neuroscience*, 12(4), pp.483–91.

Walsh, T. et al., 2008. Rare Structural Variants Disrupt Multiple Genes in Neurodevelopmental Pathways in Schizophrenia. *Science*, 320, pp.539–543. Available at: papers3://publication/uuid/05EF08F4-FE69-4441-BAFB-9AFA2E5D705D.

Wilson, P.G. & Stice, S.S., 2006. Development and differentiation of neural rosettes derived from human embryonic stem cells. *Stem Cell Reviews*, 2(1), pp.67–77. Available at: http://link.springer.com/10.1007/s12015-006-0011-1.

Wonders, C.P. & Anderson, S., 2006. The origin and specification of cortical interneurons. *Nature Neuroscience*, 7, pp.687–696.

Woodruff, A. & Yuste, R., 2008. Of mice and men, and chandeliers. *PLoS Biology*, 6(9), pp.1833–1836.

Wu, Z. et al., 2015. GABAergic Projections from Lateral Hypothalamus to Paraventricular Hypothalamic Nucleus Promote Feeding. *Journal of Neuroscience*, 35(8), pp.3312–3318. Available at: http://www.jneurosci.org/cgi/doi/10.1523/JNEUROSCI.3720-14.2015.

Yozu, M. et al., 2008. COUP-TFII is preferentially expressed in the caudal ganglionic eminence and is involved in the caudal migratory stream. *Journal of Neuroscience*, 28(50), pp.13582–13591. Available at: http://www.ncbi.nlm.nih.gov/pubmed/19074032.

Yu, X. & Zecevic, N., 2011. Dorsal radial glial cells have the potential to generate cortical interneurons in human but not in mouse brain. *The Journal of neuroscience : the official journal of the Society for Neuroscience*, 31(7), pp.2413–20. Available at: http://www.pubmedcentral.nih.gov/articlerender.fcgi?artid=3079257&tool=pmcentrez&rendertype=abstract.

Yun, C. et al., 2008. TGF-beta signaling in neuronal stem cells. *Disease markers*, 24(4–5), pp.251–255.

Zecevic, N., Hu, F. & Jakovcevski, I., 2012. Cortical interneurons in the developing human neocortex.

, 71(1), pp.18–33.

Zhang, M., Schöler, H.R. & Greber, B., 2013. Rapid and efficient generation of neurons from human pluripotent stem cells in a multititre plate format. *Journal of visualized experiments : JoVE*, (73), p.e4335. Available at: http://www.ncbi.nlm.nih.gov/pubmed/23486189.

Zijlmans, M. et al., 2012. High-frequency oscillations as a new biomarker in epilepsy. *Annals of Neurology*, 71(2), pp.169–178.

Acknowledgements

I would like to thank everybody that supported me during my Master studies!

I am deeply grateful to Jürgen Knoblich for giving me the great opportunity to work in his laboratory, for his support throughout my studies, and particularly for his belief in me and my work, which was highly encouraging.

I also want to thank Josh for his supervision throughout my thesis, his constant support and unlimited discussions about science, the brain and craft beer. Without his support, this thesis would not have been possible – keep on rocking science!

A big thank also goes to all the members of the Knoblich lab& translational unit. It was an absolutely amazing opportunity for me to not just get an organoid and cell culture biased insight into science, but also to have an experienced field of Drosophila research as a paradigm. And also outside of the science frame, you have been an amazing environment which I highly enjoyed being part of. I am absolutely looking forward to the next years in this lab, it is going to be awesome!

I also want to thank Nathalie Brandenberg and Sylke Höhnel from the Lutolf Lab @EPFL, I was always looking forward to our meetings for solving some more science- it has been highly motivating to work with you!

Special thanks also go to the outstanding scientific support facilities! I want to particularly thank Tobias Müller from BioOptics, who is the master of microscopy bug/problem solving, and Pawel for all the cool introductions to the world of microscopes! I also want to thank the HistoPathology for their helpful support for all the problems one can have from fixing over sectioning to staining tissues. I also want to thank Krzysztof Chylinski from the Protein Facilities for his amazing CRISPR/Cas9 support in the generation of cell lines- this support did not make it into this thesis, but was highly useful for later research!

Thanks also to the many people from IMBA/IMP/MFPL for all the coffee breaks and insights into other scientific fields, from sponges over zebrafish to beating hearth cells.

Thanks also go to my family and friends outside of the scientific world, which helped me in remembering that there is a live outside of science, and for all the cool trips in the last years!

And last but not least- thank you, Nina, for being on my side and tolerating my grumpy side, when a long day in science did not turn out to be successful. My work would not have been possible without your support, and I will never forget that!

Supplemental material

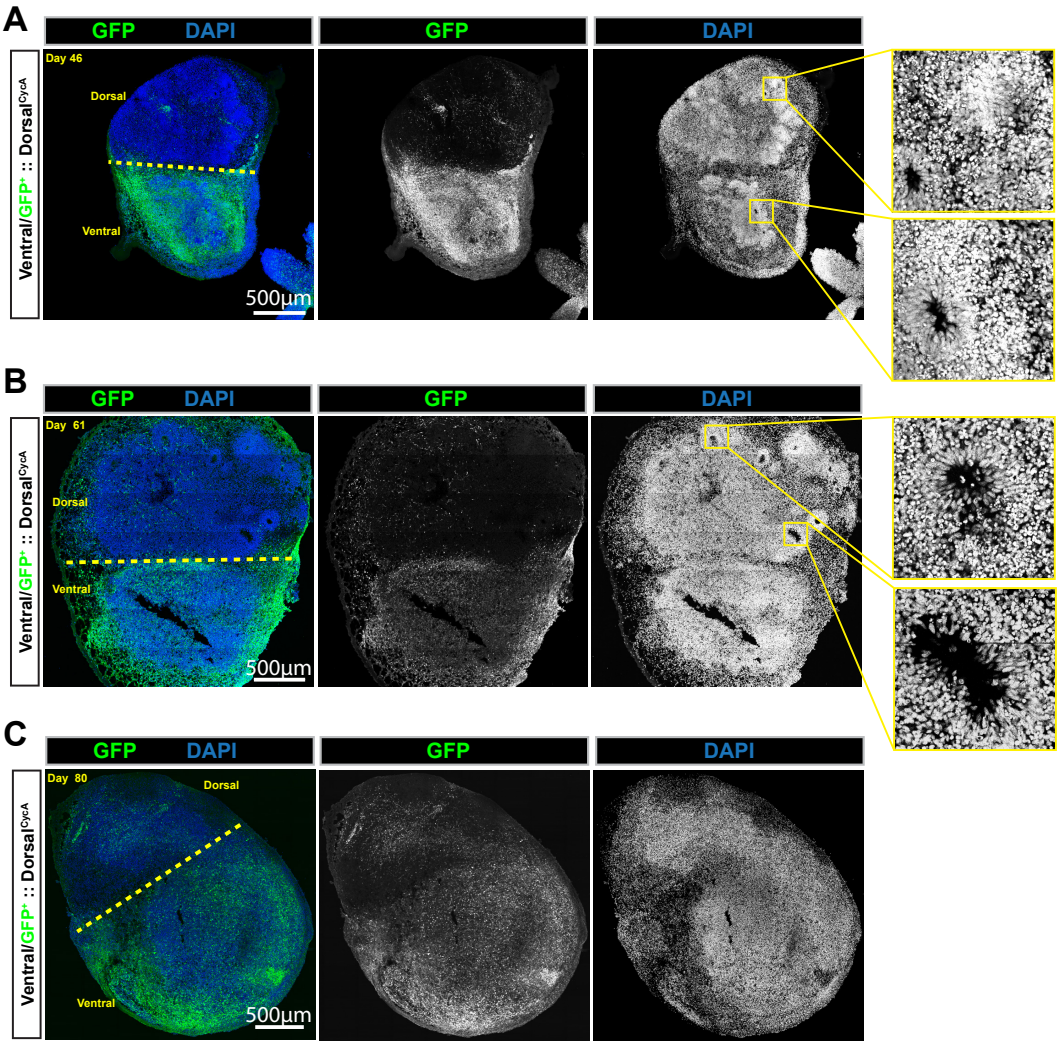

Supplemental Figure 1: Morphology and appearance of fused ventral-dorsal^{CycA} organoids changes over time and neuronal rosettes disappear.
A) & B) 46 and 61 day old ventral-dorsal^{CycA} fusions contain VZ-like progenitor regions (insets). C) Older, >80 day old organoids contained less or no VZ-like progenitor regions. Scale bars are 500µm. Figure adapted from (Bagley et al. 2017).

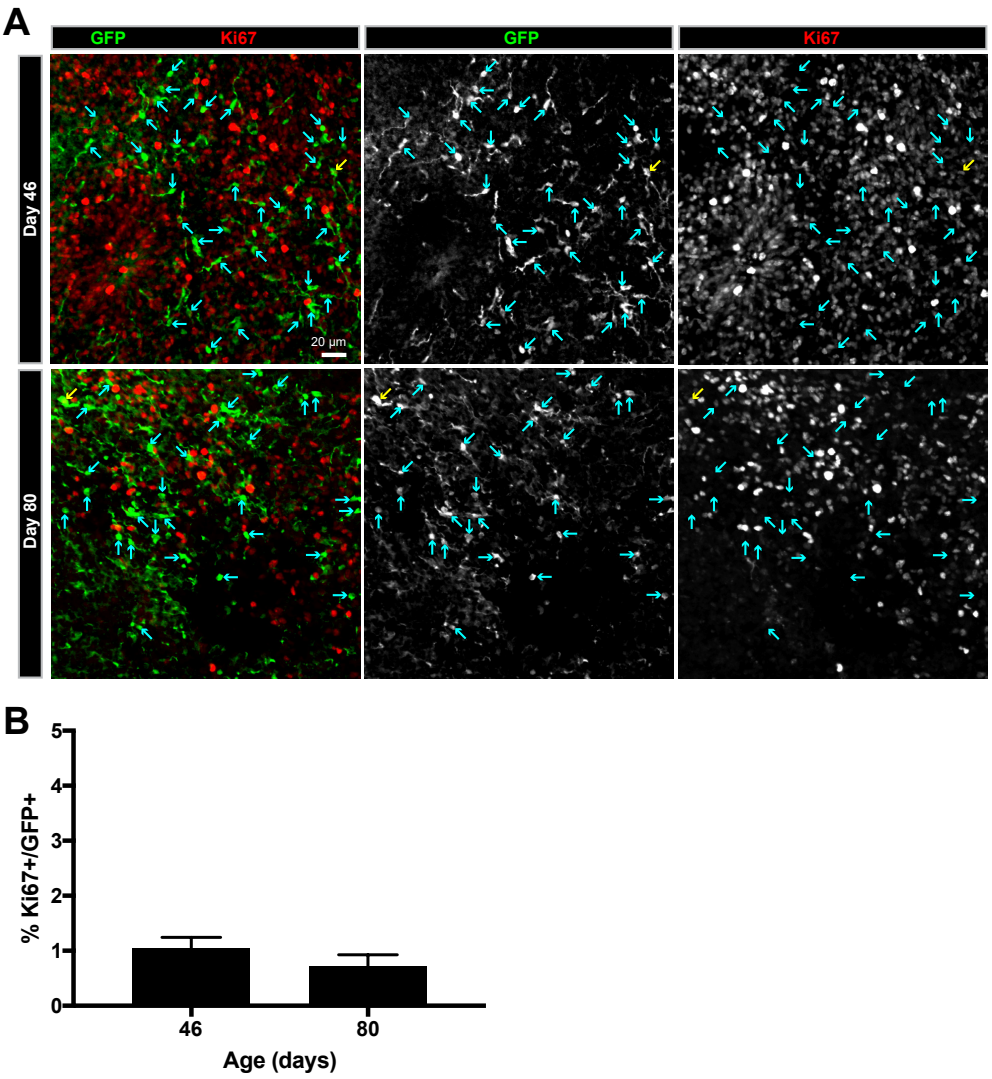

Supplemental Figure 2: Migrating GFP^{+} cells are highly non-proliferative.
A) Confocal images of GFP-Ki67 immunostained fused ventral-dorsal^{CycA} organoids in the dorsal section of 46 and 80 day old cerebral organoids. Very few cells coexpressed GFP and Ki67 (yellow arrows) and most were negative for Ki67 (blue arrows). B) Quantification of % positive cells (mean±SD) of GFP^{+} migrated cells expressing Ki67 from 46 day old (1.1±0.2%, 2420 cells, sections from n=4 organoids) and 80 day old (0.7%±0.2%, 3067 cells counted from n=4 organoids) fusions. Scale bar is 20µm. Figure adapted from (Bagley et al. 2017).

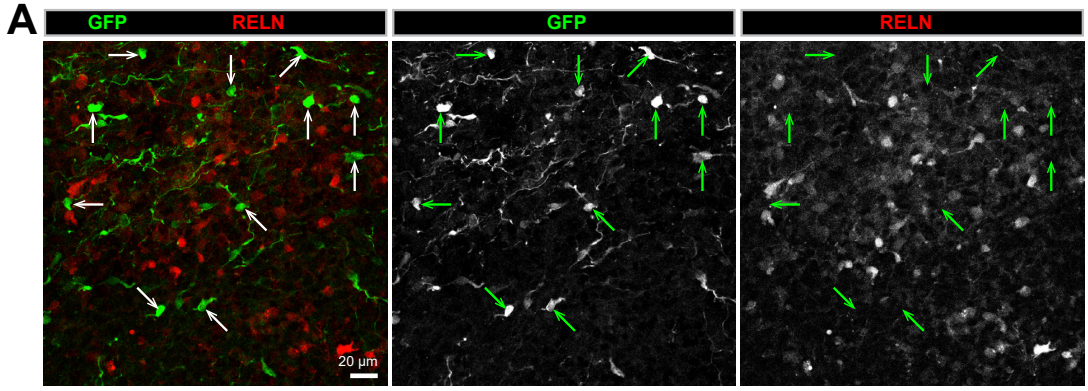

Supplemental Figure 3: GFP^{+} cells which migrated from ventral into dorsal^{CycA} did not express RELN. A) Confocal image of GFP-RELN immunostaining in the dorsal region of an 80 day old ventral-dorsal^{CycA} organoid fusion. No double-positive cells could be observed (green arrows), although many dorsal^{CycA} cells were positive for RELN. Scale bar is 20µm. Figure adapted from (Bagley et al. 2017).

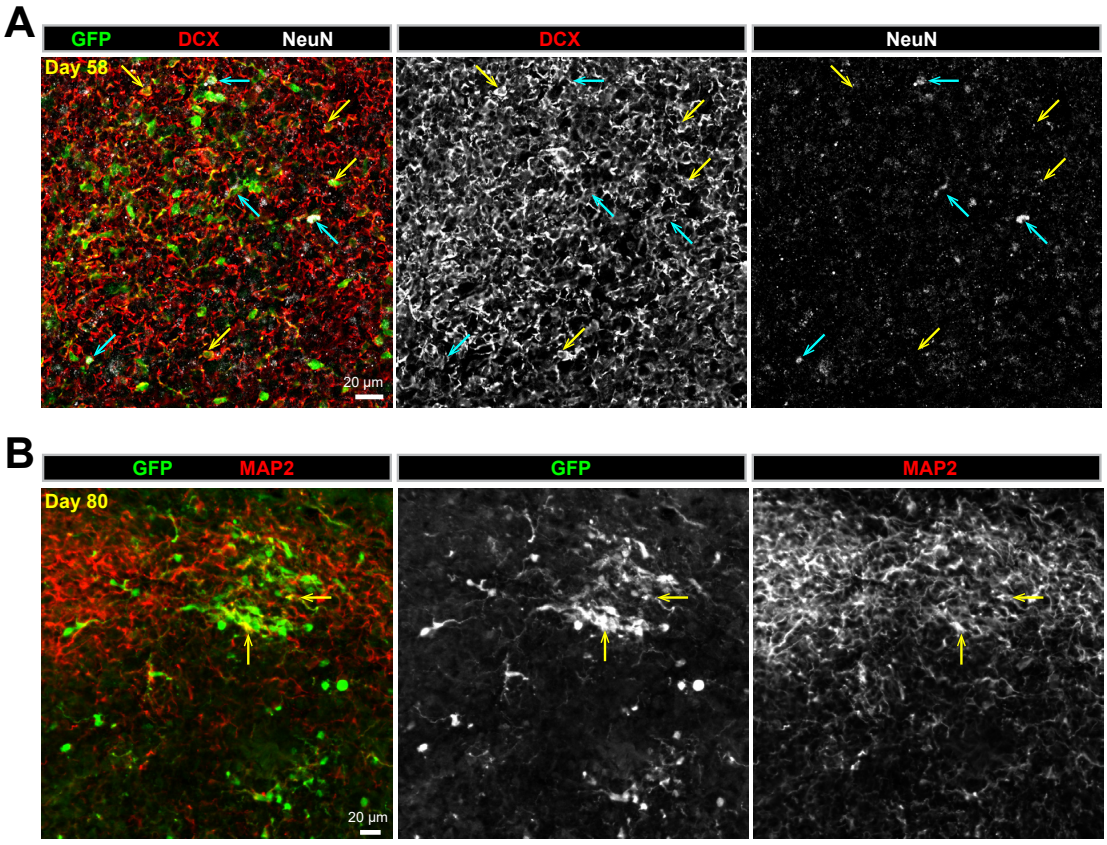

Supplemental Figure 4: Migrating GFP^{+} cells express immature and mature neuronal markers.
A) Confocal image of GFP/DCX/NeuN immunostaining in the dorsal region of a 58 day old ventral-dorsal^{CycA} fusion. GFP^{+} cells are DCX^{+} and thus immature neurons (yellow arrows). Some GFP^{+} cells start to express mature (DCX^{+}/NeuN^{+}) markers (blue arrows). B) Confocal image of GFP-MAP2 immunostaining in the dorsal region of an 80 day old ventral-dorsal^{CycA} organoid fusion. Some GFP^{+} cells were expressing the mature marker MAP2 (yellow arrows). Scale bars are 20µm. Figure adapted from (Bagley et al. 2017).

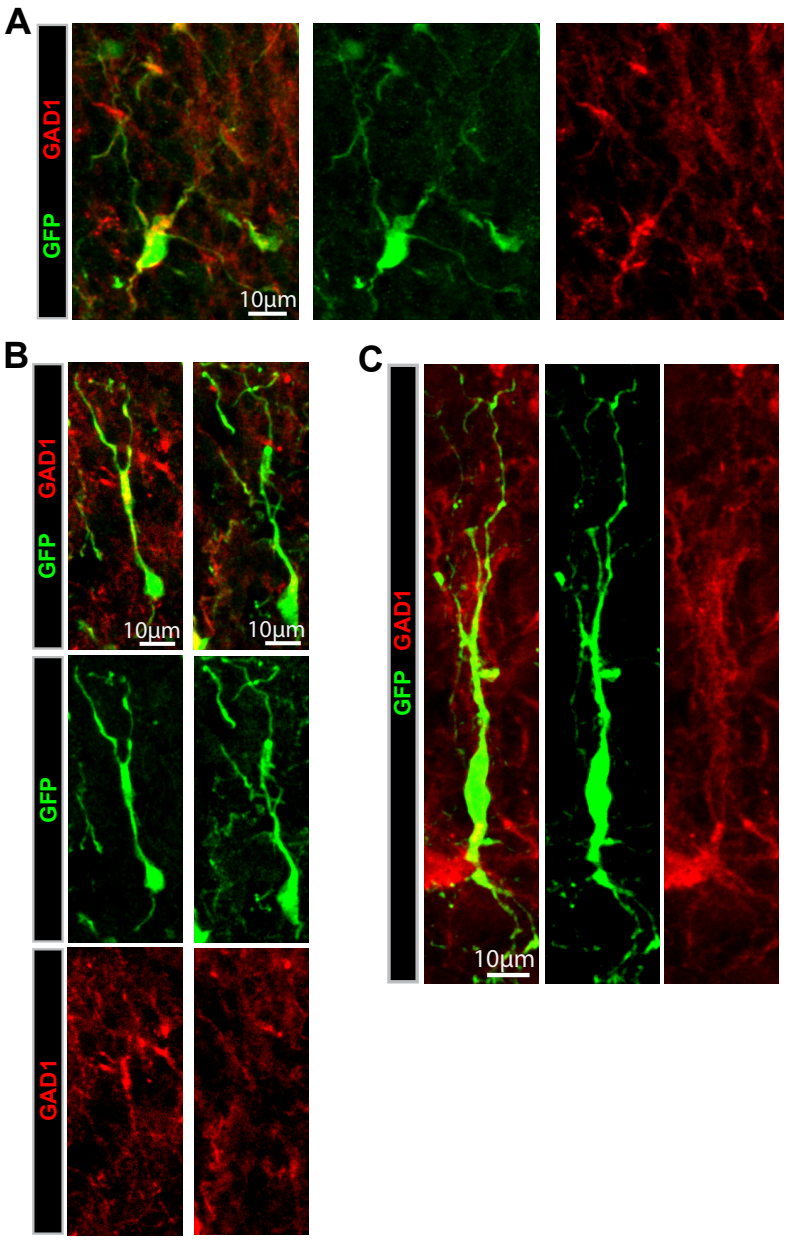

Supplemental Figure 5: Morphology of GFP^{+} migrated cells.
A)-C) Cropped z-projections of 80x spinning disk z-stacks of GFP^{+} cells in the dorsal section of a ventral dorsal^{CycA} cerebral organoid fusion. A) A GFP^{+}, GAD1^{+} interneuron which already developed a branched morphology. Branchings developed in many directions and the cell body is large and round. B) GFP^{+} GAD1^{+} interneurons with migratory morphology, as observed as well in timelapse movies in (Bagley et al. 2017). Cells had an elongated cell body and a branched leading process as well as a trailing process. C) GFP^{+} GAD1^{+} interneuron with a leading process with 3 branches and a bifurcated trailing process. Scale bars are 10µm. Figure adapted from (Bagley et al. 2017).

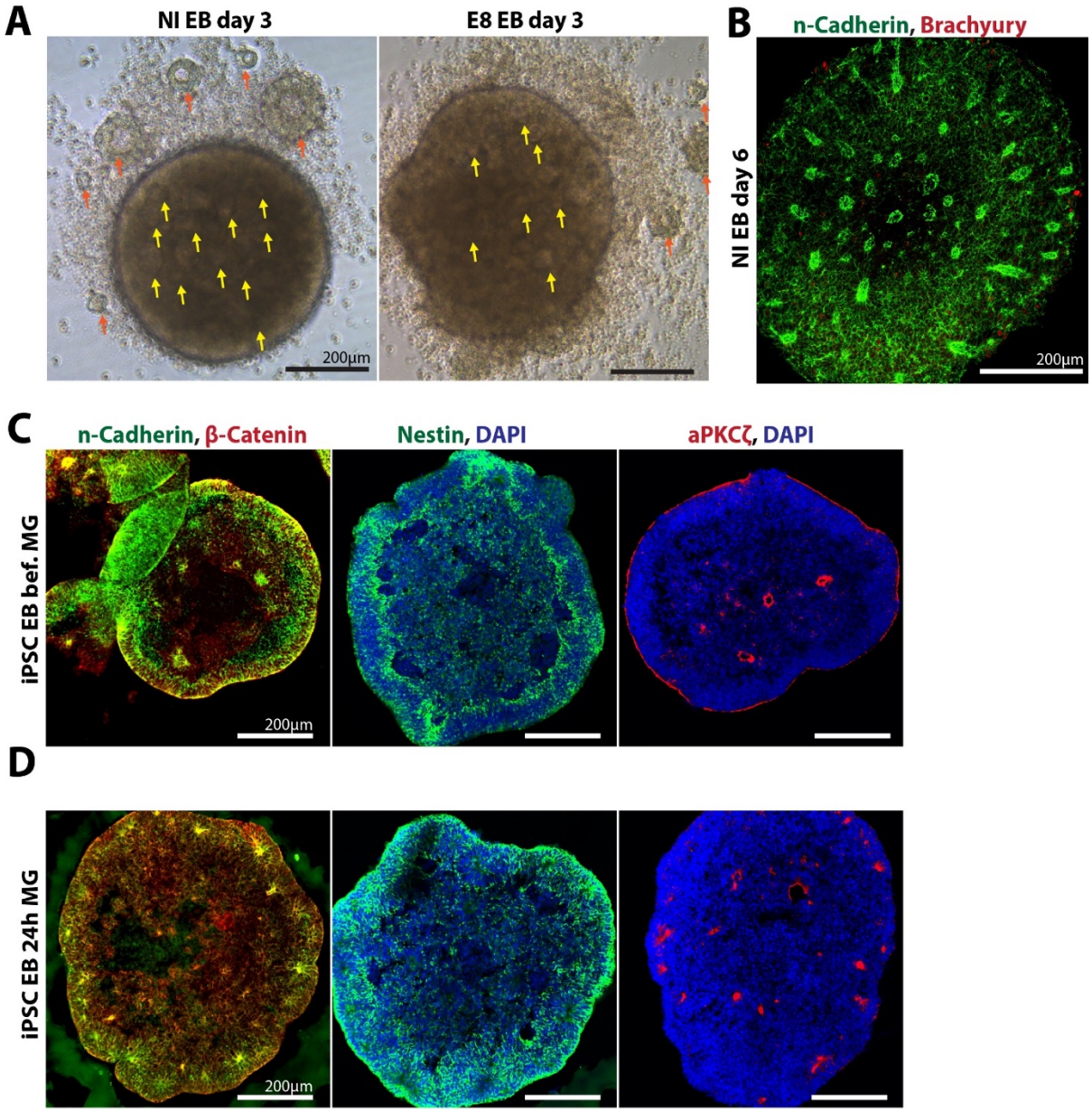

Supplemental Figure 6: iPSC hES-derived EBs show a similar phenotype as H9 hES-derived EBs.
A) Brightfield image of an NI- and E8-derived EB with observable lumen formation as a sign of epithelization. n=12 (NI) and n=13 (E8). B) Confocal image of an IHC section stained for n-Cadherin and Brachyury. Observable neuronal rosette formation is observed throughout all imaged EBs (n=4) with few Brachyury/T^{+} cells. C) Confocal images of iPSC hES-derived EBs on day 11 before Matrigel embedding. Stainings for n-Cadherin, β-Catenin (first panel), Nestin-DAPI (second panel) and aPKCζ-DAPI (third panel) indicate a neuroectoderm layer on the outside of EBs with apical orientation towards the outside. D) Confocal images of iPSC hES-derived EBs on day 12, 24h after Matrigel embedding for the same markers as in A). The neuroectoderm on the outside has re-oriented to form neuronal rosettes and apical (aPKCζ)-outside signal is lost. N=8-16 EBs for panel C and D. Scale bars are 200µm.

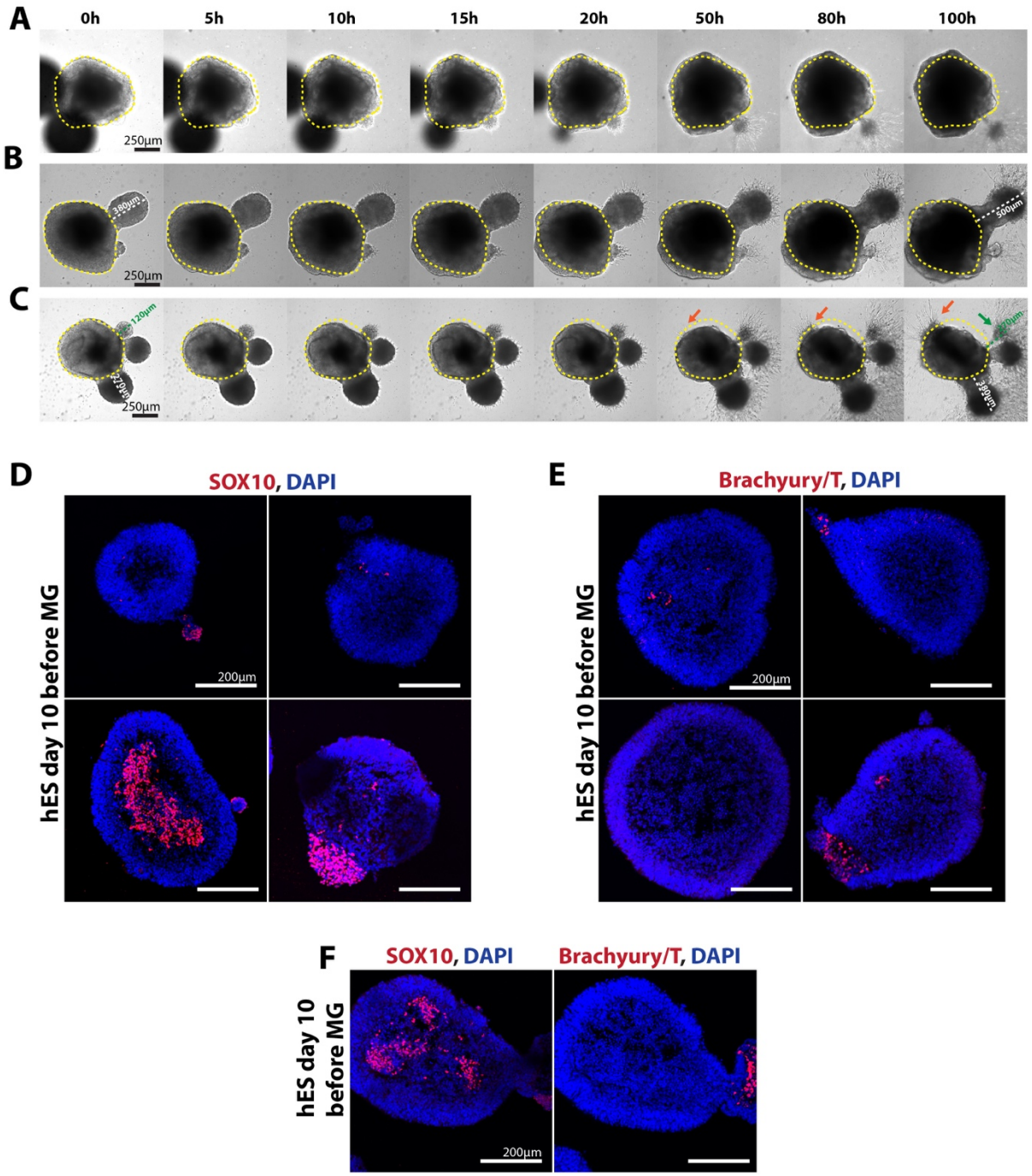

Supplemental Figure 7: Early budding tissue on EBs can disrupt organoid development and is frequently positive for neural crest marker SOX10 and Mesoderm marker Brachyury/T.
A)-C) Brightfield time-lapse recordings of H9 hES-derived EBs which were embedded in Matrigel on 0h. A) An EB with no respectively mild outgrowth of tissue buds showed expansion into the Matrigel over 100h from its starting area (yellow dashed line). B) An EB with one tissue bud showed EB/ organoid growth into Matrigel, but an observable tension of the highly migratory tissue bud was created onto the organoid as the tissue bud was migrating 120µm into the Matrigel (1.3x starting distance). C) An EB which would not pass quality control criteria for an organoid. Noteworthy are the less developed pseudostratified layer on the outside and the three tissue buds on the outside of the EB. While the biggest bud (white dashed line) migrates 1.4x its original distance into the Matrigel, a smaller bud (green dashed line) more than doubled its distance from the organoid (2.25x) from 120µm to 270µm distance. Additionally, the embedded EB elongates over time in the direction of the migratory tissue buds. D) Confocal SOX10-DAPI IHC images of H9 hES-derived EBs on day 10 before Matrigel embedding, indicating that many but not all (right upper panel) tissue buds were of neural crest identity. E)

Confocal Brachyury/T-DAPI IHC images of H9 hES-derived EBs on day 10 before Matrigel embedding. Many EBs did show Brachyury/T cells either on low or on no observable level (left side), however some EBs showed Brachyury/T positive cells on the outside of EBs on tissue buds. F) Serial section of a SOX10-DAPI and Brachyury/T-DAPI staining of the same experiment. Note the SOX10/Brachyury double positive tissue bud on the right side of the EB. Scale bars are 250µm (A-C) and 200µm (D-F).

Protocols: Published cerebral organoid methods

Lancaster et al 2013 original protocol/ Improved — 48well low attachment plate, Corning — MG EMBEDDING+ transfer to 6 or 10cm plate on shaker

0 1 2 3 4 5 6 7 8 9 10 11 12 13 14 15 16 17 18 ---------- 40 ---------->

cell lines: hES media | NI media | Differentiation media

iPSC H9 9000 cells

hES media: +bFGF, RI (80 DMEM/F12, 20 KOSR, 3 ES-quality FBS, 1 GlutaMAX, 1 MEM-NEAA, 3.5µl 2-ME)

-bFGF, RI

Corning U-bottom ultra low attachment 96well plate
150-200ul per well

NI media: 100 DMEM/F12, 1 N2 supplement, 1 GlutaMAX, 1 MEM-NEAA, 500µl Heparin solution

keep in 96 well plate or transfer:
Corning 48well flat bottom low attachment

Differentiation media: *-vitA* (50 DMEM/F12, 50 Neurobasal, 0.5 N2, 1 B27 -vitA, 125µl insulin, 175µl 1:100 2-ME in DMEM/F12, 1 GlutaMAX, 0.5 MEM-NAA, 1 P/S)

Improved NeuroDMEM-A (draft): same media, but exchange: 2 B27 -vitA

Diff +vitA change: B27 + vitA

Improved NeuroDMEM+A (draft): *same media, but exchange/add:* 2 B27 +vitA, 1.49g/500ml HEPES, 5ml Vitamin C 40mM stock

add 1% MG to media

Kadoshima et al (+Sasai), "new" method 2014 — Transfer to 9cm petridish (noncell adhesive)

0 1 2 3 4 5 6 7 8 9 10 11 12 13 14 15 16 17 18 19 20 21 ---------- 35 ---------- 56 ---------- 70 ---------->

cell lines: Cortical differentiation medium: | 2nd media: | 2nd media+extras | 2nd media: suppl. #2

KhES-1 9000 cells TrypLE Expr. (Invitrogen) +Dnase I + Y.27632

Cortical differentiation medium: 80 G-MEM, 20 KOSR, 1mM Pyruvate, 0.2mM 2-ME, 100U/ml P/S, 20µM Y-27632, 3µM IWR1e, 5µM SB43542

Sumitomo Bakelite low-cell-adhesion 96well plates V-bottomed conical
100µl per well

Some rosettes keep apical towards the outsided as there is no MG embedding step.

2nd media: 100 DMEM/F12, N2 supplement, CD Lipid concentrate, 0.25mg/ Fungizone, 100U/m P/S

40% O2, 5% CO2
no orbital shakers needed?

2nd media+extras: added from day 35 on: 10 FBS, 2.5g/50(Heparin, 1 Matrigel (low growth-factor)

Change to a lumox dish on dy56 (enhances gas exchange)

2nd media: suppl. #2: 2% MG, +B27 supplement

Rosettes observable in >90dy old organoids

"To prevent cell death in the central portions of large aggregates, the aggregates were cut into half-size with fine forceps under a dissecting micro- scope every 2 wk after day 35 and were cultured using a lumox dish (SARSTEDT; high O2 penetration) after day 56. From day 70, the concentration of Matrigel was increased [final 2% (vol/vol)] and B27 supplement (Invitrogen) was also added to the medium."

Muguruma et al (+Sasai), Cerebellum organoids (2015) — Transfer to 9cm petridish (noncell adhesive)

0 1 2 3 4 5 6 7 8 9 10 11 12 13 14 15 16 17 18 19 20 21 ---------->

cell lines: Differentiation medium (gfCDM) + Insulin | Differentiation media -Y-27632, -SB-431542 | Media 2

KhES-1 6000 cells TrypLE Expr. (Invitrogen)

Differentiation medium (gfCDM) + Insulin: 100 Isocove's modified DMEM+F12, 1 chemically defined lipid conc., 450µM monothioglycerol, 15µg/ml apo-transferrin, 5mg/ml crystallization-purified BSA, 1x P/S, 7µg/ml insulin, 10µM Y-27632, 10µM SB431542, +FGF2 (50ng/ml) from day 2

Sumitomo Bakelite low-cell-adhesion 96well plates V-bottomed conical
100µl per well

"One-third dilution (removal of one-third volume of the medium and addition of the same volume of fresh medium) and full-volume replacement (replacement of the whole medium with fresh medium) with gfCDM supplemented insulin were performed on day 7 and 14, respectively."
(RI and SB were just added at the beginning and get diluted out)

Cerebellum is derived by FGF2-treated cultures of hESC, and FGF19 and SDF1 promote the self-formation of polarized neural-tube like structures and a "continuous cerebellar plate neuroepithelium and rhombic-lip-like structure at one end and a three-layer cytoarchitecture similar to the embryonic cerebellum."
FGF19, SDF1 and FGF2 treatment timings are not mentioned in Material&Methods
Usage of cyclopamine A for enhanced CP specification

Media 2: 100 Neurobasal, 1 Glutamax, 1 N2, 1 P/S

standard 5% CO2 incubator setup.
48-144 organoids per dish!
Full-volume media replacement: every 7 days
no orbital shakers mentioned?

Sakaguchi et al. (+Sasai), Neocortical and choroid plexus organoids (2015) — Transfer to 9cm petridish (noncell adhesive)

0 1 2 3 4 5 6 7 8 9 10 11 12 13 14 15 16 17 18 19 20 21 ---------->

cell lines: Differentiation media | Neocortical induction/Choroid plexus induction

KhES-1 9000 cells TrypLE Expr. (Invitrogen)

Differentiation media: 80 G-MEM, 20 KOSR, 0.1mM NEAA, 1mM Pyruvate, 0.1mM 2-ME, 100U P/S, 3µM IWR1e, 5µM SB431542 (TGFbeta inh.)

Sumitomo Bakelite low-cell-adhesion 96well plates V-bottomed conical
100µl per well

Neocortical induction media: 100 DMEM/F12, 1 GlutaMAX, 1 N-2, 1 Chem. defined lip., 0.25mg/ml fungizone, 100U P/S

Choroid plexus induction media: 90 DMEM/F12, 1 N-2, 1 Chem. defined lip., 10 FBS, 3µM CHIR 99021, 0.5nM BMP4

Both protocols: 40% O2 incubator!
Feed every 3 days

Sakaguchi et al. (+Sasai), Medial pallium organoids (2015)

	0	1	2	3	4	5	6	7	8	9	10	11	12	13	14	15	16	17	18	19	20	21	27	35	50
cell lines:	Choroid/Pallium induction media																					Media 2	Long term culture media		cut aggregates into half
KhES-1	90	DMEM/F12																				90	DMEM/F12	90	Neurobasal	
9000 cells	1%	N-2																				10	FBS	10	FBS	
TrypLE Expr.	1	Chem. defined lip.																				1	GlutaMAX	1	B27 w/o vitA	
(Invitrogen)	10	FBS																				1	N2	2mM	L-glutamine	transfer on Lumox dish
	3µM	CHIR 99021																				1	Chem. defined lip	100U	Penicillin	(high oxigen penetration)
	0.5nM	BMP4																						100ug/ml	Streptomycin	from day 50 on
	40% O2, same media as choroid plexus induction media																							0.25mg/ml	Fungizone	
	media changes every 3 days																									

Nakano et al. (+Sasai), Optic cup (neural retina) organoids (2011)

	0	1	2	3	4	5	6	7	8	9	10	11	12	13	14	15	16	17	18	19	20	21	27	35	50
cell lines:	Diff media		+1% Matrigel (growth factor reduced) from day 2																neural retina culture media						
hES	70	G-MEM											removal of IWR1e		+3µM CHIR99021 to media				100	DMEM/F12					
9000 cells	20	KOSR											from the media		OR: 40ng/ml Wnt3A (R&D)				1	GlutaMAX					
TrypLE Expr.	10	FBS													(just for 3 days)				1	N2					
(Invitrogen)	0.1mM	NEAA																							
	1mM	Pyruvate																							
	0.1mM	2-ME																							
	100U	P/S																							
	3µM	IWR1e																							
	100nM	SAG																							
	+1% Matrigel (growth factor reduced) from day 2- day 18																								

Qian et al 2016 (Guo-Li Ming): spinning bio reactor forebrain organoids — Matrigel embedding — Transfer to a well of a 12-well spinning bioreactor

	0	1	2	3	4	5	6	7	8	9	10	11	12	13	14	15	16	17	18	19	20	21	71	>110
cell lines:	Stem cell media:				Induction media										Differentiation media								Maturation medium	
hiPSCs	80	DMEM/F12	transfer to an		100	DMEM/F12									100	DMEM/F12							100	Neurobasal
feeder-dep.	20	KOSR	ultra-low		1	N2									1	N2							1	B27
	1	NEAA	attachment		5g/500m	Heparin									1	B27							1	P/S
	1	P/S	6-well plate		1	P/S									1	P/S							1	2-ME
	1	2-ME	(Corning)		1	NEAA									1	2-ME							0.2mM	Ascorbic Acid
	1	Glutamax	with 3ml stem		1	Glutamax									1	NEAA							20ng/ml	BDNF
	10ng/ml	FGF-2	cell media		4ng/ml	WNT-3A									2.5µg/m	Insulin							20ng/ml	GDNF
Collagenase IV for 1h			WITHOUT		1µM	CHIR99021									Mechanical disassociation from Matrigel								1ng/ml	TGFbeta
wash colonies			FGF-2		1µM	SB-431542									with a pipet								0.5mM	cAMP
			but with:		(only half of the stem cell																			
Culture colonies in a 15ml			2µM Dorsomorphine		media gets replaced										*Media has to be changed every other day!*									
conical tube for 1 day			2µM A83-01		with Induction media)																			

Quian et al. 2016 (Guo-Li Ming) midbrain organoid protocol: — Transfer to a well of a 12-well spinning bioreactor

	0	1	2	3	4	5	6	7	8	9	10	11	12	13	14	15	16	17	18	19	20	21
cell lines:	Stem cell media:		EB media:		SHH medium			Induction medium							Differentiation media							
hiPSCs	80	DMEM/F12	85	DMEM/F12	100	DMEM/F12		100	DMEM/F12						100	Neurobasal						
feeder-dep.	20	KOSR	15	KOSR	1	N2		1	N2						1	B27						
	1	NEAA	1	2-ME	1	Glutamax		1	Glutamax						1	Glutamax						
	1	P/S	1	Glutamax	100nM	LDN-193189		100nM	LDN-193189						1	2-ME						
	1	2-ME	100nM	LDN-193189	3µM	CHIR99021		3µM	CHIR99021						20ng/ml	BDNF						
	1	Glutamax	10µM	SB-431542	100ng/ml	SHH									20ng/ml	GDNF						
	10ng/ml	FGF-2	100ng/ml	SHH (Peprotech)	2µM	Purmorphamine									0.2mM	Ascorbic acid						
Collagenase IV for 1h			2µM	Purmorphamine	100ng/ml	FGF-8									1ng/ml	TGFbeta						
wash colonies			100ng/ml	FGF-8	(gradual switch from EB										0.5mM	cAMP						
					to SHH media)																	
	Culture colonies in a 15ml																					
	conical tube for 1 day							No matrigel embedding in this protocol!														

Xuyu et al. 2016 (Guo-Li Ming) Hypothalamus Organoids: — Transfer to a well of a 12-well spinning bioreactor

	0	1	2	3	4	5	6	7	8	9	10	11	12	13	14	15	16	17	18	19	20	21
cell lines:	Stem cell media:		Induction media A		Induction media B			Differentiation media														
hiPSCs	80	DMEM/F12	90	DMEM/F12	90	DMEM/F12		50	DMEM/F12													
feeder-dep.	20	KOSR	10	KOSR	10	KOSR		50	Neurobasal													
	1	NEAA	1	NEAA	1	NEAA		1	B27													
	1	P/S	1	P/S	1	P/S		1	NEAA													
	1	2-ME	1	2-ME	1	Glutamax		1	P/S													
	1	Glutamax	1	Glutamax	1	N2		1	Glutamax													
	10ng/ml	FGF-2	2.5µM	LDN-193189	10ng/ml	Wnt-3A		10ng/ml	FGF-2													
Collagenase IV for 1h			3µM	SB-431542	20ng/ml	SHH		10ng/ml	CTNF													
wash colonies			450µM	1-Thioglycerol	2µM	Purmorphamine																
								Media has to be changed every other day.														
Culture colonies in a 15ml																						
conical tube for 1 day								No matrigel embedding in this protocol.														

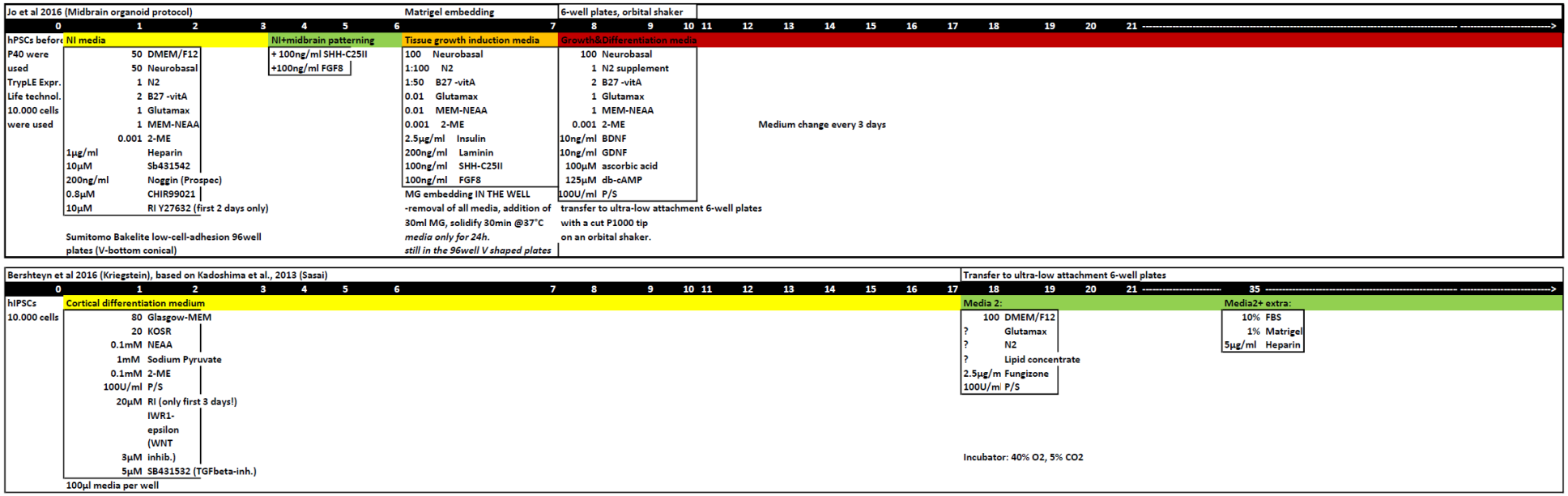
Jo et al 2016 (Midbrain organoid protocol)
Matrigel embedding
6-well plates, orbital shaker
0 1 2 3 4 5 6 7 8 9 10 11 12 13 14 15 16 17 18 19 20 21
hPSCs before P40 were used TrypLE Expr. Life technol. 10.000 cells were used
NI media
50 DMEM/F12
50 Neurobasal
1 N2
2 B27 -vitA
1 Glutamax
1 MEM-NEAA
0.001 2-ME
1µg/ml Heparin
10µM Sb431542
200ng/ml Noggin (Prospec)
0.8µM CHIR99021
10µM RI Y27632 (first 2 days only)
Sumitomo Bakelite low-cell-adhesion 96well plates (V-bottom conical)
NI+midbrain patterning
+ 100ng/ml SHH-C25II
+100ng/ml FGF8
Tissue growth induction media
100 Neurobasal
1:100 N2
1:50 B27 -vitA
0.01 Glutamax
0.01 MEM-NEAA
0.001 2-ME
2.5µg/ml Insulin
200ng/ml Laminin
100ng/ml SHH-C25II
100ng/ml FGF8
MG embedding IN THE WELL
-removal of all media, addition of 30ml MG, solidify 30min @37°C
media only for 24h.
still in the 96well V shaped plates
Growth&Differentiation media
100 Neurobasal
1 N2 supplement
2 B27 -vitA
1 Glutamax
1 MEM-NEAA
0.001 2-ME
10ng/ml BDNF
10ng/ml GDNF
100µM ascorbic acid
125µM db-cAMP
100U/ml P/S
transfer to ultra-low attachment 6-well plates with a cut P1000 tip on an orbital shaker.
Medium change every 3 days
Bershteyn et al 2016 (Kriegstein), based on Kadoshima et al., 2013 (Sasai)
Transfer to ultra-low attachment 6-well plates
0 1 2 3 4 5 6 7 8 9 10 11 12 13 14 15 16 17 18 19 20 21 35
hIPSCs 10.000 cells
Cortical differentiation medium
80 Glasgow-MEM
20 KOSR
0.1mM NEAA
1mM Sodium Pyruvate
0.1mM 2-ME
100U/ml P/S
20µM RI (only first 3 days!)
IWR1-epsilon (WNT 3µM inhib.)
5µM SB431532 (TGFbeta-inh.)
100µl media per well
Media 2:
100 DMEM/F12
? Glutamax
? N2
? Lipid concentrate
2.5µg/m Fungizone
100U/ml P/S
Incubator: 40% O2, 5% CO2
Media2+ extra:
10% FBS
1% Matrigel
5µg/ml Heparin